FAST NEUTRON POLARIZATION STUDIES

Thesis

submitted by

HENRY DAVIE, B.Sc.

for the degree of

DOCTOR OF PHILOSOPHY

University of Edinburgh

September 1971

EX BIBL. UNIV. EDINBURGEN.

ABSTRACT OF THESIS

The design, construction and operation of a fast neutron polarimeter employed to study the neutrons emitted in the $^{2}H(d,n)^{3}He$ reaction at deuteron energies less than 1MeV is described. The polarimeter employs neutron scattering from a high pressure helium gas scintillator into two liquid scintillator neutron detectors, all three scintillators being mounted on a rotatable cradle to allow an interchange of the roles of the two neutron detectors and hence eliminate instrumental error arising from differences in their detection efficiences. In selecting an appropriate scattering angle consideration is given to the speed of data collection and the accuracy to which the analysing power of helium is known. A series of electronic units designed to operate with the polarimeter is described. Considerable use is made of both linear and digital integrated circuits in these units, and a modular racking system is used for their construction. The importance of recording the helium recoil spectra associated with the neutrons detected in coincidence between the neutron detectors and the gas scintillator is emphasised, experimental measurements and Monte-Carlo type calculations being performed to account for background tails present in

these spectra. Measurements of the polarization of the neutrons emitted in the $^{2}H(d,n)^{3}He$ reaction at a mean laboratory reaction angle of 46^{o} are reported for six mean deuteron energies in the range from $\sim$300keV to $\sim$ 800keV using a Ti-D target of 100keV stopping power. Programmes to allow semi-automated data handling by a small computer are described, as are Monte-Carlo type computations of the mean analysing power of the polarimeter. The results and experimental techniques of previous workers are critically examined, and proposals are made for the possible improvement of the polarimeter and for its use in further studies.

CONTENTS

CONTENTS (Continued).

CONTENTS (Continued).

CHAPTER 1.

FAST NEUTRON POLARIZATION STUDIES

Due to the strong spin-orbit coupling in nuclear interactions, nucleons emitted in a nuclear reaction at a fixed reaction angle will in general exhibit a polarization of their spin direction, such a polarization being perpendicular to the reaction plane for unpolarized reaction parent nuclei.

In 1949 Wolfenstein[1] first drew attention to such effects, referring specifically to the case of the D-D reaction. A technique for the measurement of the transverse polarization of fast neutrons had previously been proposed by Schwinger[2] in 1946. This involved measuring the azimuthal asymmetry of the neutrons after being elastically scattered by a light nucleus - hereafter called the analyser.

Among the first experimental observations of the polarization of neutrons produced in reactions were those of Huber and Baumgartner[3] and Ricamo[4], both groups publishing in 1953 their results on the $^{2}H(d,n)^{3}He$ reaction, using carbon as an analyser. Thereafter a considerable volume of work concerning the measurement of neutron polarization resulting from reactions and scattering has been published, as may be evidenced from the reviews of Haeberli[5] and Galloway[6]. The motivation behind such studies include the possibility, once accurate polarization measurement techniques have evolved, of determining spin and parity assignments of compound nuclear states, and of evaluating the effect

of spin-orbit forces in nuclear scattering of fast neutrons, as well as obtaining further details of the reaction mechanisms of neutron producing reactions.

1.1 The Neutrons from the $^{2}H(d,n)^{3}He$ Reaction

The $^{2}H(d,n)^{3}He$ reaction has probably received more attention than any other nuclear reaction, with regard to neutron polarization measurements. Yet in spite of this, considerable disagreements in published results occur, as may be seen from the comprehensive tabulations of Galloway[6].

The present work describes the design and construction of a polarimeter to study the polarization of the neutrons emitted in this reaction for incident deuteron energies within the operating range of the Cockcroft-Walton type accelerator of Edinburgh University, the object being to produce a set of thin target measurements, and while so doing to examine critically the experimental technique for sources or error which may have passed unnoticed in earlier work.

Figure 1 provides a compilation of the results of other authors published since 1957 for reaction angles around 45^{o} (Lab) and in the relevant deuteron energy range. Table 1 provides a key to figure 1, and in addition lists details of these measurements including the experimental technique employed, a subject to be discussed more fully in section 1.3. That these measurements show little evidence for a strong energy dependence provides some justification for the plotting of both

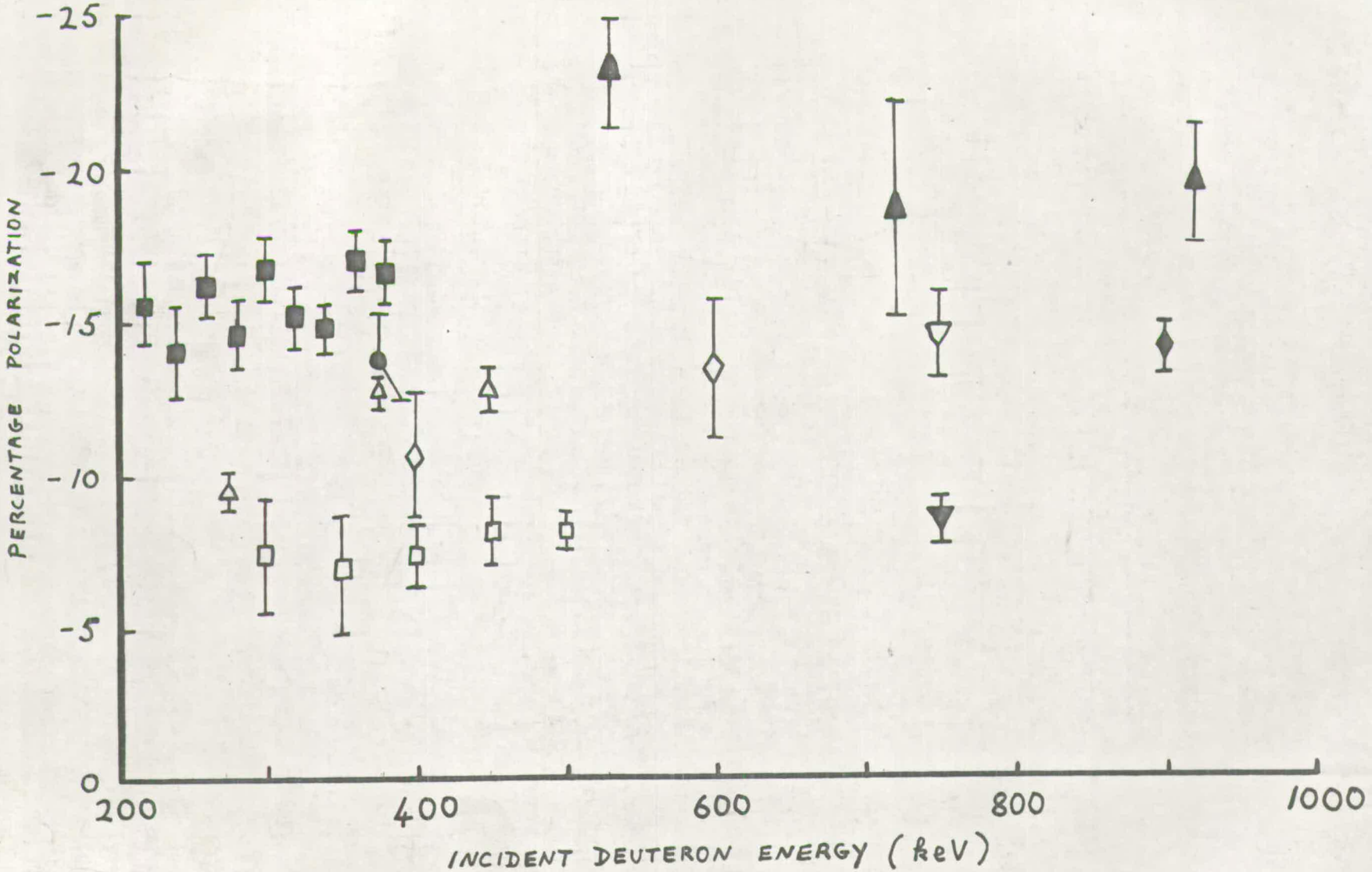

FIG. 1 POLARIZATION OF NEUTRONS EMITTED AT A LABORATORY ANGLE OF ABOUT 45° FROM THE $^{2}H(d,n)^{3}He$ REACTION. KEY IN TABLE 1

Table 1 - Key to Fig.1.

Polarization of neutrons emitted at a laboratory angle of about 45° from the $^{2}H(d,n)^{3}He$ reaction.

▲ - The results of Roding and Scholermann[7] (1969), recorded for neutrons emitted at a 40° (Lab.) reaction angle from a thin titanium-deuterium target ($\sim$50keV stopping power). A helium gas scintillator was employed as scatterer-analyser, and the phase shift angles for n-^{4}He scattering of Hoop and Barschall[15] were used.

■ - The results of Behof, May and McGarry[8] (1968), recorded for neutrons emitted at a 47° (Lab.) reaction angle from a thick heavy ice target. A helium gas scintillator was employed as scatterer-analyser, and the phase shift angles for n-^{4}He scattering of Dodder and Gammel as published by Seagrave[16] (DGS) were used.

● - The result of Mulder[9] (1966), recorded for neutrons emitted at a 46.5° (Lab.) reaction angle from a thin heavy ice target ($\sim$50keV stopping power). A helium filled cloud chamber was employed as an analyser, and the phase shift angles for n-^{4}He scattering of Austin et al.[17] were used.

△ - The results of Boersma, Jonker, Nijenhuis and Van Hall[10] (1963), recorded for neutrons emitted at a 53° (Lab.) reaction

angle (for a deuteron energy of 275keV), at a 46° (Lab.) reaction angle (for a deuteron energy of 375keV) and at a 51° (Lab.) reaction angle (for a deuteron energy of 450keV), from a thin titanium-deuterium target (~50keV stopping power). A helium gas scintillator was employed as scatterer-analyser, and the phase shift angles for n - ^{4}He scattering of Austin et al.[17] were used.

▽ - The result reported by Steuer, Bucher and Hereford[11] (1959) as including previously published data[12]. The reaction angle is given as 53° (C of M) and various thick targets were employed. Carbon was used as scatterer-analyser, the analysing power being calculated from the n - ^{12}C scattering phase shift angles of Wills et al.[18]

▼ - as ▽ , but with the analysing power calculated from the n - ^{12}C scattering phase shift angles of Meier et al.[19]

□ - The results of Pasma[13] (1958), recorded for neutrons emitted at a 47° (Lab.) reaction angle from a thin heavy ice target (~50keV stopping power). A helium gas scintillator was employed as scatterer-analyser, and the polarization values shown plotted were recomputed by Boersma et al.[10] using the phase shift angles for n - ^{4}He scattering of Austin et al.[17]

◇ - The results of Levintov, Miller, Tarumov and Shamshev[14]

(1957), recorded for neutrons emitted at a 49° (Lab.) reaction angle from a thick zirconium-deuterium target. Helium filled proportional counters were employed as analysers, and their own phase shift angles for n-^{4}He scattering were employed.[20]

◆ - as ◇ , but employing a zirconium-deuterium target with ~150keV stopping power.

thin and thick target measurements versus incident deuteron energy. Whilst making allowances for such variations in target thickness, it is yet obvious that there exists considerable disagreement as to the magnitude of the polarization. That this cannot be explained as being due to the small spread in the reaction angles at which these measurements were made may be seen from the polarization angular distributions of Boersma et al.[10], Behof et al.[8], and Roding and Scholermann [7], all of whose measurements, although differing substantially in magnitude, exhibit a broad maximum around the favoured angle of 45°. Further, such a broad maximum is supported by the polarization angular distribution P(v) theoretically proposed by Blin-Stoyle [21] for low deuteron energies, namely -

$$P(v) = \frac{B \sin 2v}{6(v)}$$

Where: v is the centre of mass reaction angle of the emitted neutron

: $6(v)$ is the differential cross section in the centre of mass frame for the $^{2}H(d,n)^{3}He$ reaction

: B is a deuteron energy dependent constant.

1.2 The Principles of Fast Neutron Polarization Measurement

Consider the system shown in figure 2; all directions being with reference to the laboratory frame. An unpolarized beam of particles travelling in the direction k_1, strikes unpolarized target nuclei, the reaction producing the neutrons of energy En to be studied along direction k_2. Then the reaction angle

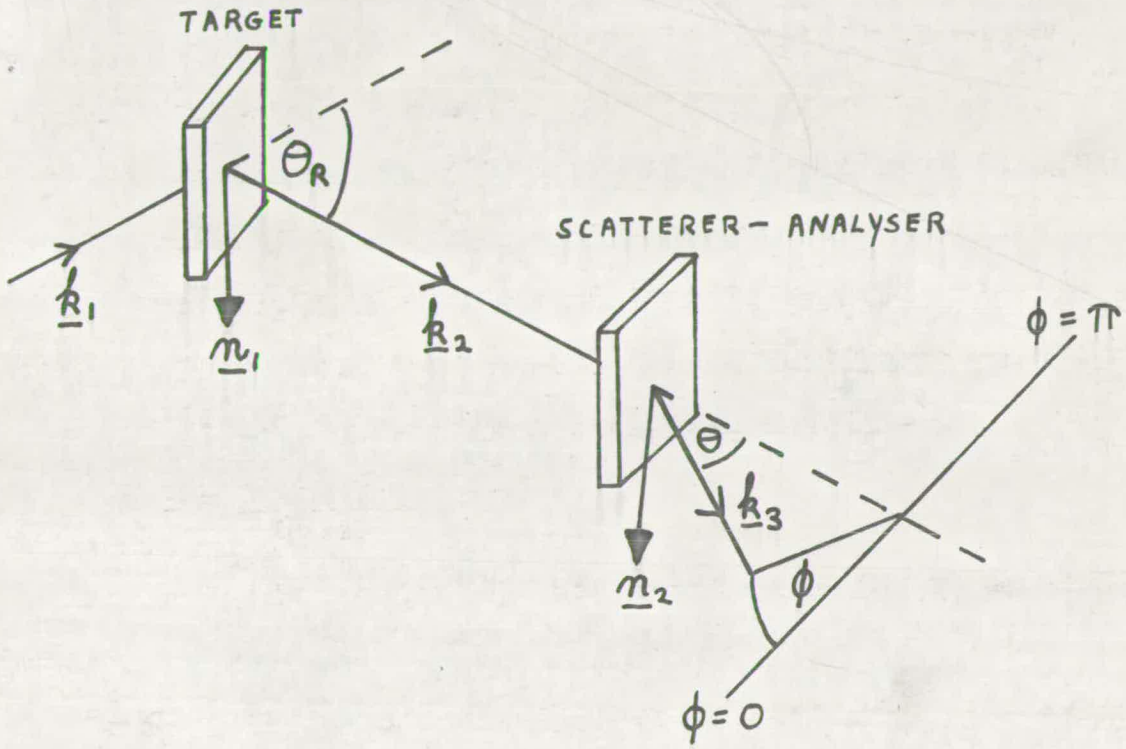

FIG. 2 GEOMETRY OF A POLARIZATION EXPERIMENT

θ_R is the angle between $\underline{k}_1$ and $\underline{k}_2$, and the polarization may be written as $\underline{P} = P\underline{n}_1$, where $\underline{n}_1$ is a unit vector in the direction $\underline{k}_1 \wedge \underline{k}_2$, and the magnitude of the polarization, P, is defined as $P = (N_+ - N_-) / (N_+ + N_-)$ where N_+ and N_- are the number of neutrons with spin parallel and antiparallel to $\underline{n}_1$ respectively.

Now utilising the predominantly favoured polarization measurement technique outlined by Schwinger[2], let these neutrons be elastically scattered along direction $\underline{k}_3$ from suitable analysing nuclei. Further, let a unit vector $\underline{n}_2$ be defined as lying in the direction of $\underline{k}_2 \wedge \underline{k}_3$, then the scattering angle θ is the angle between $\underline{k}_2$ and $\underline{k}_3$, and an azimuthal angle ϕ may be defined as being the angle between $\underline{n}_1$ and $\underline{n}_2$. The differential cross section for this scattering of the transversly polarized neutrons will depend not only on θ but also on ϕ according to the relation

$$\sigma(\theta,\phi) = \sigma(\theta) \left\{ 1 + P\, A(\theta) \cos(\phi) \right\}$$
$$= \sigma(\theta) \left\{ 1 + \underline{P} \cdot \underline{A}(\theta) \right\}$$

where $\sigma(\theta)$ is the differential cross section for the scattering of unpolarized neutrons of energy E_n, and $\underline{A}(\theta) = A(\theta)\, \underline{n}_2$, is the analysing power of the scatterer (and is equal to the polarization produced in its scattering of initially unpolarized neutrons of energy E_n at an angle (θ).

Thus by placing two identical point neutron detectors located at equal angles θ equidistantly from a point scatterer-analyser, but with $\phi = 0, \pi$ respectively, the measured asymmetry $\mathcal{E}$ in the count rate I for neutrons scattered by the analyser into the neutron detectors will be

$$= \frac{I_o - I_\pi}{I_o + I_\pi} = P\,A(\theta)$$

It follows that before estimating P, one must evaluate A (θ). The most prevalent choice of analyser is a light spin zero nucleus, almost exclusively ^{12}C or ^{4}He. For such nuclei the total and differential cross sections for unpolarized neutron scattering are reasonably well determined over a wide range of neutron energies, and A (θ, E_n) may be evaluated from phase shift analyses of such data. Mott - Schwinger [22] scattering has also been used for polarization analysis. This relies on the interaction between the magnetic moment of the neutron and the coulomb field of a (preferably large atomic number) nucleus acting as scatterer-analyser. Significant analysing powers are obtained for θ very small, but the technical difficulties of making scattering measurements at small angles have discouraged its use in the neutron energy range below 20 MeV.

As an alternative to elastic scattering for polarization analysis, Barschall [23] has indicated that under restricted conditions one could measure the asymmetry produced in the inverse reaction to that producing the neutrons, this asymmetry depending on the square of the polarization.

1.3 Practical Techniques for the Measurement of Fast Neutron Polarization

The following discussion will be restricted to the use of nuclear elastic scattering as a polarization analyser, the technique used in all of the measurements listed in Table 1.

Further it should be noted that in these observations ^4He and ^{12}C analysers have been used exclusively, the former being much preferred. Thus this discussion will be further restricted to these two analysers.

One may obtain a well defined analysing power close to unity over a wide range of neutron energies by scattering the neutrons from ^4He at an angle $\theta \sim 120^\circ$. A fuller discussion of this will occur in section 2.1, figures 4a,b,c,d illustrating this observation. In addition, ^4He also has the advantage of conveniently acting as a scintillator in both its gaseous and liquid states. Thus a coincidence requirement between a ^4He scintillator acting as an analyser and a neutron detector measuring the azimuthal asymmetry may be utilised to reject background events occurring in the neutron detector due to neutrons arriving by other than the desired scattering process.

In contrast to this the analysing power of ^{12}C is strongly energy dependent and is much less well determined, the latter being evidenced from the result of Steuer et al[11] in figure 1, shown computed using the analysing power of carbon obtained from the n - ^{12}C scattering phase shift angles of Wills et al.[18] and also from those due to Meier et al.[19]. In the neutron energy range around 3 MeV which is directly relevant to the present experiment, attempts have been made to evaluate the analysing power of carbon by measuring the asymmetry resulting from the scattering of neutrons whose polarization is assumed known from previous measurements using helium as an analyser.

Thus Wenzel and Steuer[24] used neutrons from the $^{2}H(d,n)^{3}He$ reaction assuming the fit to previously published results of Pasma,[13] while Miller and Biggerstaff [25] used neutrons from the $^{12}C(d,n)^{13}N$ reaction, and took the values of polarization given by Morgan et al.[26] Although both of these sets of results tend to favour the analysing power calculated using the phase shifts of Wills et al [18] to that calculated using the phase shifts of Meier et al,[19], their support is by no means conclusive, these results being particularly contradictory for neutron energies around 4 MeV. Further Hansgen and Nitzsche[27] have very recently reported measurements of the analysing power of ^{12}C using neutrons from the $^{2}H(d,n)^{3}He$ reaction and taking the polarization to be that measured by Behof et al.[8] These results purport to show previously unknown resonances in the analysing power for neutrons of $\sim 2{\cdot}8$ MeV energy, although these observations seem somewhat suspect since they indicate a factor of $\sim$ two variation in the measured asymmetry for a change in mean neutron energy of 7 keV despite a ~ 300 keV spread in the energy of the neutrons employed.

A scintillator using carbon in the form of a diamond has been reported[28], as has a technique for separating the scintillations due to carbon recoils from those due to hydrogen recoils in an organic scintillator, by using a pulse shape identification procedure [29]. Finlay [30] has reported the use of an associated particle time of flight technique in order to reduce unwanted background when employing a solid non-

scintillating carbon analyser. Part of the data for the result of Steuer et al.[10] shown in figure 1 was obtained using an organic scintillator as analyser, pulse amplitude selection being employed to separate carbon recoils from hydrogen recoils.

Thus in conventional polarimeters one scatters the (possibly collimated) neutrons from the chosen analyser and detects the scattered neutrons in a pair of side neutron detectors shielded from the direct neutron flux originating at the target. These neutron detectors are located symmetrically with respect to the analyser, the centre of each corresponding to the same scattering angle θ, but to different azimuthal angles, namely $\phi = 0$ (to the 'right') and $\phi = \pi$ (to the 'left'). If these detectors are then interchanged periodically, and their detection efficiencies remain unchanged by this process, then no normalisation by a beam monitor is required, since the duration of the measurements, the fluctuation in the neutron flux, and the differences in the two counter efficiences cancel entirely if one defines a 'right-left ratio' r as

$$r = \sqrt{\frac{I_{ox}\, I_{oy}}{I_{\pi x}\, I_{\pi y}}}$$

where I_{ox} is the number of counts observed in detector X located at $\phi = 0$, during which period $I_{\pi y}$ is the number of counts observed in detector Y located at $\phi = \pi$ etc. Hence the asymmetry ε is

$$\varepsilon = \frac{r - 1}{r + 1} = \langle A \rangle P$$

where $\langle A \rangle$ is a 'mean' analysing power evaluated over the spread in scattering and azimuthal angles produced by having an analyser and detectors of a finite size. Its computation will be considered further in chapter 5.

To avoid introducing instrumental asymmetries, on moving a detector from $\phi = 0$ to $\phi = \pi$ and vice versa the analyser to detector distance must not alter. A convenient technique to ensure this is to rotate the rigid assembly of scatterer and detectors about an axis joining the neutron producing target to the centre of the analyser. Further if one is able to rotate the assembly such that the side detectors might be positioned at a scattering angle θ and azimuthal angles $\pi/2$ and $3\pi/2$, then a measurement of the asymmetry (which should be zero) in this plane will be a valuable check on the presence or lack of instrumental asymmetries.

As an alternative to mechanically interchanging the roles of the side detectors, the polarization vector of the incident neutron beam may be rotated using a magnetic field. This was first proposed and used by Hillman et al.[31] who employed an air-cored solenoid through which the neutrons passed, a current through the windings capable of rotating $\underline{P}$ by $\pi/2$, and when reversed by $-\pi/2$, being utilised. Thus the asymmetry was measured in a plane perpendicular to the reaction plane. The use of a transverse magnetic field rotating the polarization vector by π has also been reported. Considerable care must be taken when using these powerful magnetic fields to ensure

that the fringeing fields do not affect the operation of the customarily employed photomultiplier - scintillator side neutron detectors. Further Atkinson and Sherwood [32] have discussed depolarization effects in such fields.

Neutron polarization measurements have also been made by a few workers who studied the asymmetry of the recoiling helium analysing nuclei instead of the scattered neutrons. The measurements of Levintov et al.[14] and Mulder [9] plotted in figure 1 both employed such a technique, the former utilising amplitude selection of pulses from a long ^{4}He filled proportional counter angled to the neutron beam, the latter observing tracks in a ^{4}He filled cloud chamber.

For the present study it was determined to use a conventional polarimeter as shown in figure 3, and described in more detail in chapter 2. Helium was preferred to carbon as an analyser on the basis of its reasonably well defined analysing power, its convenience in use as a scintillator to reduce background, and because of its use by most other workers in this energy range, thus allowing an intercomparison of the results obtained by these workers and by the present author without having the added complication of uncertainties arising due to the use of a different analyser. Further the use of a high pressure ^{4}He gas scintillator as an analyser was preferred to that of a (more dense) liquid ^{4}He scintillator on the grounds of technical ease. Miller[33] has reported the difficulties of using a liquid helium scintillator for measurements taking longer than

one hour. Similarly reasons of convenience led to the favouring of a mechanically rotating assembly rather than the use of magnetic spin rotation.

CHAPTER 2.

THE CONSTRUCTION OF A FAST NEUTRON POLARIMETER.

The polarimeter constructed for the present experiment is shown diagramatically in figure 3. Briefly, the neutrons emitted from the target after collimation are scattered through a mean angle θ from a high pressure gas scintillator into two liquid scintillator neutron detectors symmetrically placed to the 'right' and 'left' of the gas scintillator. These three detectors are mounted on a cradle which may be rotated accurately through angles up to 360° about an axis joining the neutron producing target to the centre of the gas scintillator.

The present chapter describes the construction of this polarimeter in some detail. A short description of the polarimeter and its initial operation has been published by the present author in conjunction with Galloway [34].

2.1 The Choice of Scattering Angle

In selecting the scattering angle θ to be employed in the present polarimeter, both the uncertainty in the analysing power and the rate of collection of data were considered as functions of θ. Although the angle chosen was that most appropriate to the analysis of polarization in neutrons of the energy to be studied, namely $\sim$ 3MeV, its suitability for use with neutrons of a higher energy will also be examined.

The n - ^{4}He scattering phase shift angles on which a computation of the helium analysing power relies, although

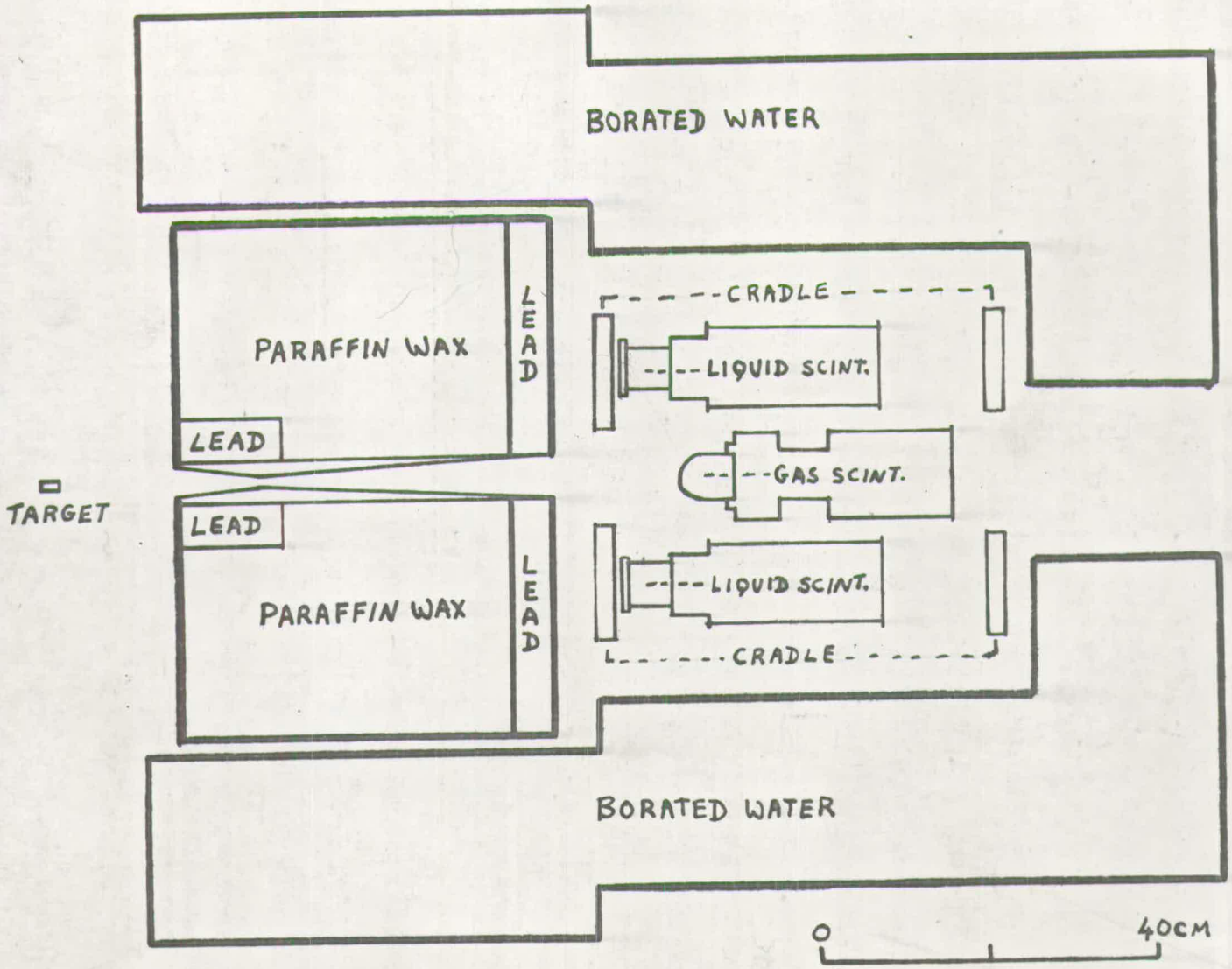

FIG. 3 THE FAST NEUTRON POLARIMETER

initially extracted from p - ^{4}He scattering data by Dodder and Gammel and published by Seagrave[16] (hereafter called the D.G.S. phase shifts), have been further investigated in later n - ^{4}He scattering experiments. Satchler et al[35] have recently reviewed this work and fitted the experimental data by an optical model calculation.

Because of the complex manner in which the phase shift angles are interrelated in their computation from an analysis of scattering data, it is difficult to determine the accuracy to which they, and in turn the analysing power are known. As an estimate of this uncertainty, the analysing power was calculated and compared using those sets of published phase shifts most commonly employed, including phase shifts of partial waves up to $\ell = 3$ where provided. Figures 4a and 4b show the ^{4}He analysing power for neutrons of energy 3 and 6 MeV respectively, calculated using the phase shifts of Austin et al[17] (dotted curve) and Morgan and Walter[36] (dashed curve). The D.G.S.[16] results (not plotted) match closely those of Austin et al[17] around the turning points. Figures 4c and 4d show the analysing power at 12 and 18 MeV respectively. The dotted curve is based on the data of Hoop and Barschall[15] which is an extension of the work of Austin et al[17] to higher neutron energies. Because of the lack of other comprehensive data in this energy region, the dashed curve was calculated using the phase shifts of Satchler et al[35] from their optical model fit which is primarily obtained from the lower energy data of

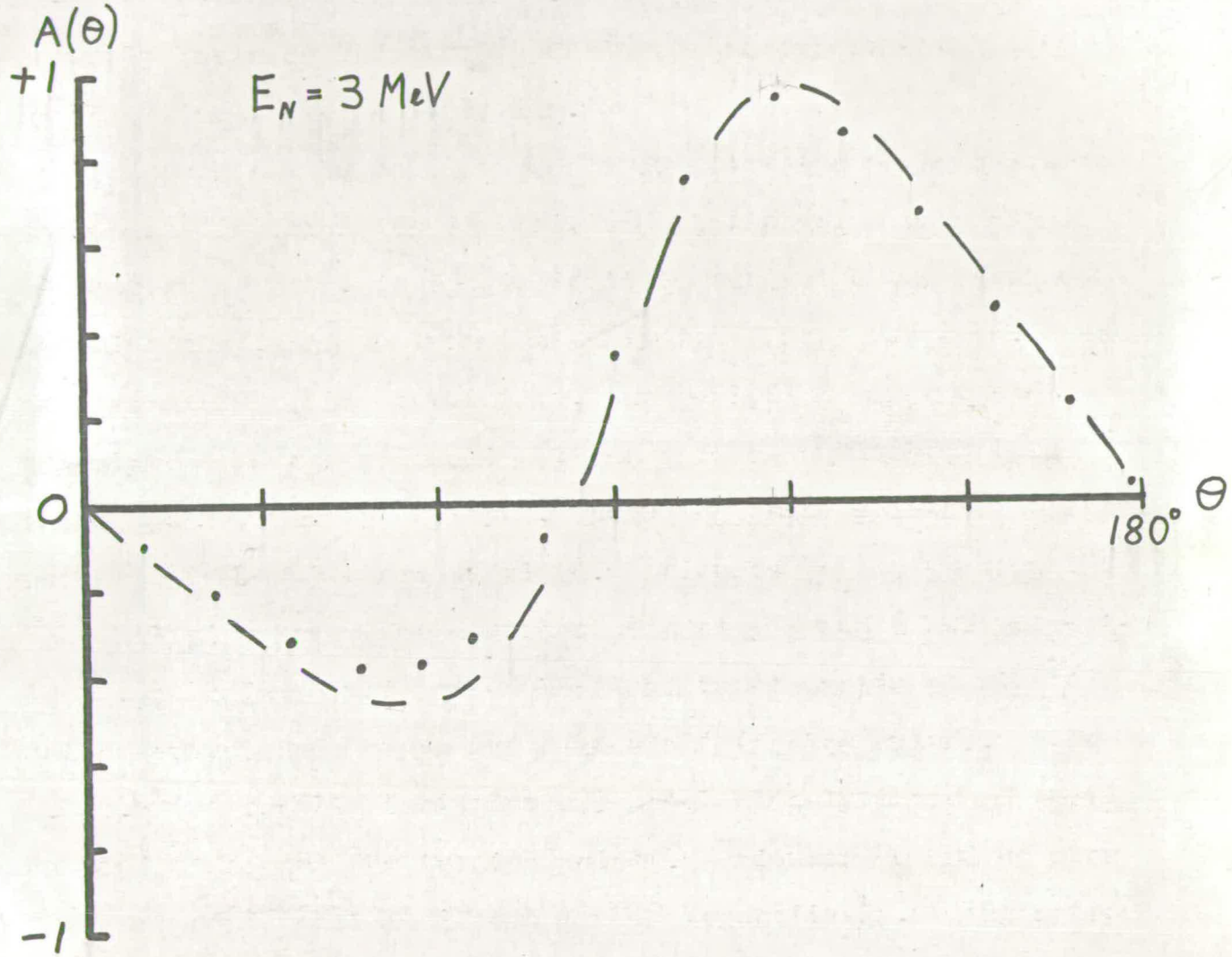

FIG. 4a ANALYSING POWER [A(θ)] OF ^{4}He FOR 3MeV NEUTRONS AS A FUNCTION OF LABORATORY ANGLE [θ]. DOTTED CURVE CALCULATED USING THE PHASE SHIFTS OF AUSTIN ET AL., DASHED CURVE USING THE PHASE SHIFTS OF MORGAN AND WALTER.

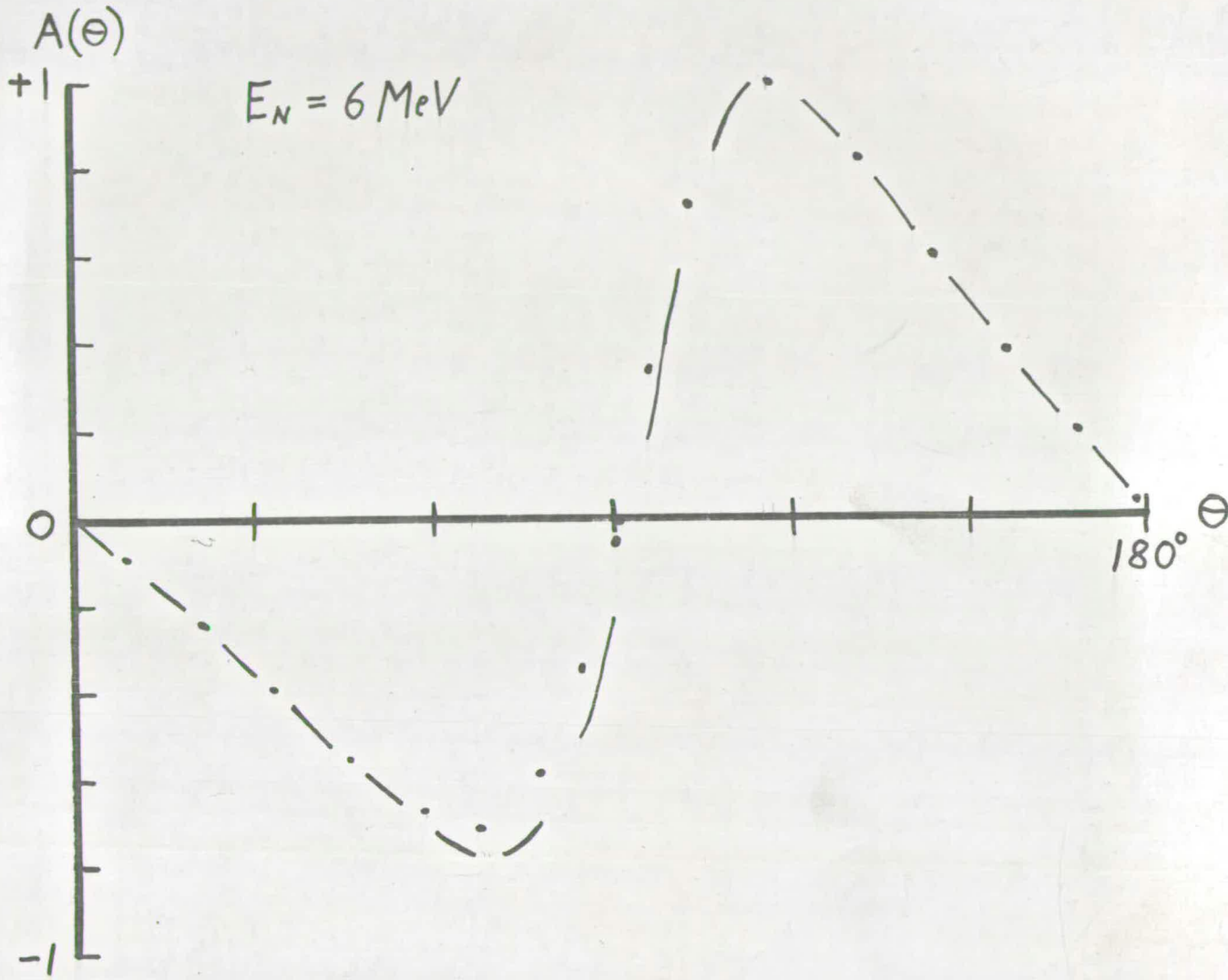

FIG. 4b ANALYSING POWER [A(θ)] OF ^{4}He FOR 6 MeV NEUTRONS AS A FUNCTION OF LABORATORY ANGLE [θ]. DOTTED CURVE CALCULATED USING THE PHASE SHIFTS OF AUSTIN ET AL., DASHED CURVE USING THE PHASE SHIFTS O MORGAN AND WALTER.

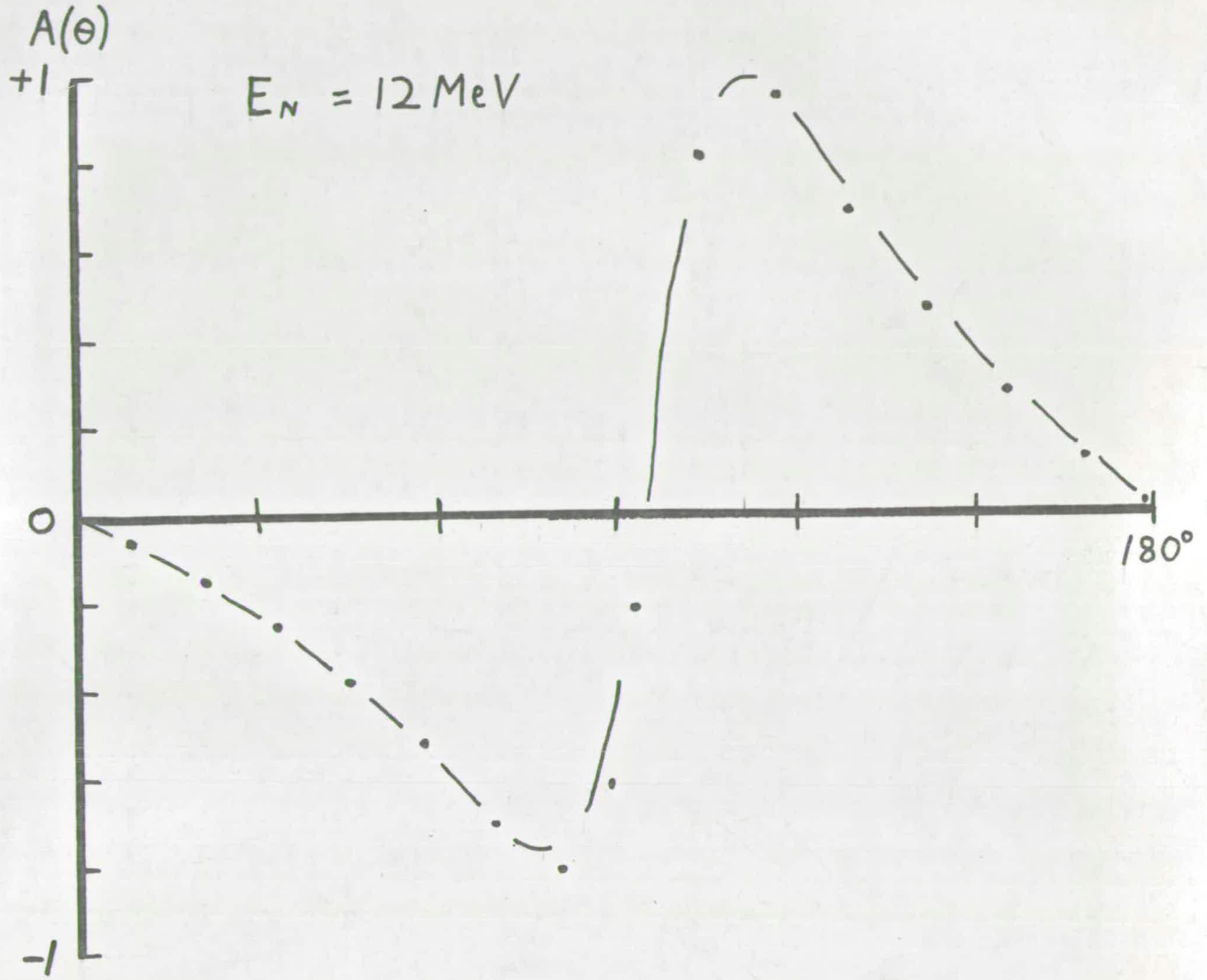

FIG. 4C ANALYSING POWER [A(θ)] OF ^{4}He FOR 12 MeV NEUTRONS AS A FUNCTION OF LABORATORY ANGLE [θ]. DOTTED CURVE CALCULATED USING THE PHASE SHIFTS OF HOOP AND BARSCHALL, DASHED CURVE USING THE PHASE SHIFTS OF SATCHLER ET AL.

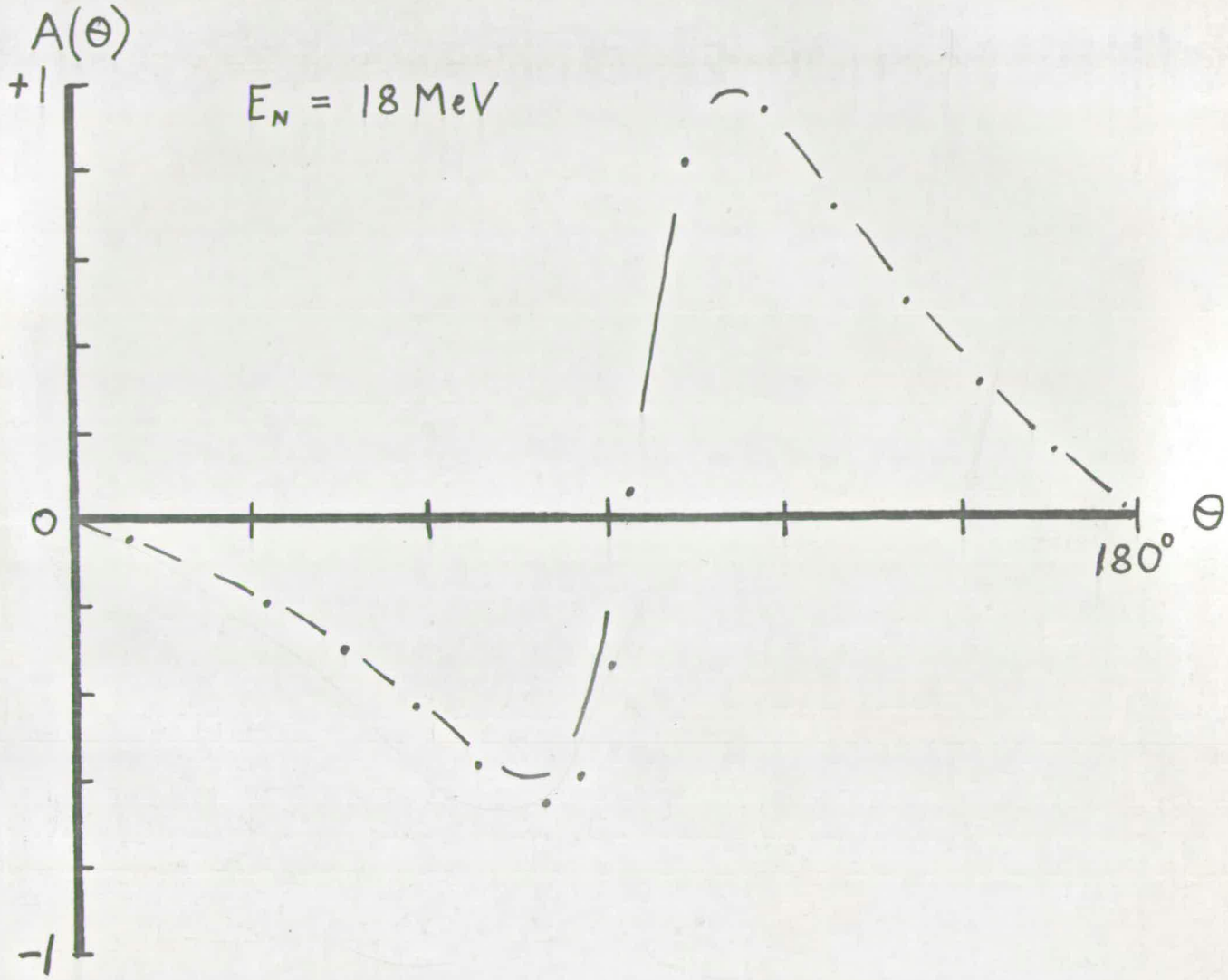

FIG. 4d ANALYSING POWER [A(θ)] OF ^{4}He FOR 18 MeV NEUTRONS AS A FUNCTION OF LABORATORY ANGLE [θ]. DOTTED CURVE CALCULATED USING THE PHASE SHIFTS OF HOOP AND BARSCHALL, DASHED CURVE USING THE PHASE SHIFTS OF SATCHLER ET AL.

Morgan and Walter[36].

At all four energies, the agreement between the curves is much better at the backward scattering maximum than at the forward scattering minimum. Indeed for 3 MeV neutrons, the analysing power differs by $\sim 20\%$ at the forward scattering minimum for the two curves, while only a $\sim 3\%$ difference exists at the backward scattering maximum.

Another factor to be considered in the selection of the scattering angle is the rate at which information may be collected. In an idealised polarimeter consisting of a point scatterer and point side detectors, for a given incident neutron flux of polarization P, ignoring background and counting for equal times to 'left' and 'right' with each side detector, the time to reach a given statistical accuracy ΔP in the measurement of P is proportional to

$$\frac{1 - P^2 A(\theta)^2}{A(\theta)^2 \sigma(\theta) (\Delta P)^2}$$

in the notation of section 1.2 but with the addition that $\sigma(\theta)$ here refers specifically to the differential cross section in the laboratory frame. If the (infinitely small) solid angle subtended by the side detectors at the scatterer is kept constant, but θ, the laboratory scattering angle is varied, then the position of fastest data collection will occur for $\frac{1 - P^2 A(\theta)^2}{A(\theta)^2 \sigma(\theta)}$ a minimum. In comparing two angles for fast data collection the numerator of this expression will most commonly vary little. Thus the denominator provides a

convenient figure of merit, the maximisation of which will be a good guide to fast data collection. This figure of merit is plotted in figure 5, the computations having been performed using the phase shift angles of Hoop and Barschall[15].

It may be seen that in the case of 3 MeV neutrons, there is little to choose between the forward and back scattering peaks. However for energies of 6 and 12 MeV data accumulation will be substantially faster if scattering at a forward angle is employed. At 18 MeV the forward scattering peak still remains favoured, but not by so significant a factor as at 6 and 12 MeV. In considering the rate of data collection in a real polarimeter of the type presently described, account should be taken of the finite dimensions of the scatterer and side detectors, and the resulting spread in scattering angle (θ). However since both the forward and backward scattering peaks of $A(\theta)^2 \sigma(\theta)$ exhibit similar angular widths, the general observations for a point scatterer and detector should remain valid. Further, while the use of a different set of n-^{4}He scattering phase shifts changes the figure of merit significantly in some situations, it does not alter the above general conclusions.

Thus a mean laboratory scattering angle θ of $\sim 120^\circ$ was chosen for the present polarimeter, being both a position of well defined analysing power, and good data collection efficiency for 3 MeV neutrons. Although at higher energies a superior data collection efficiency could be obtained by

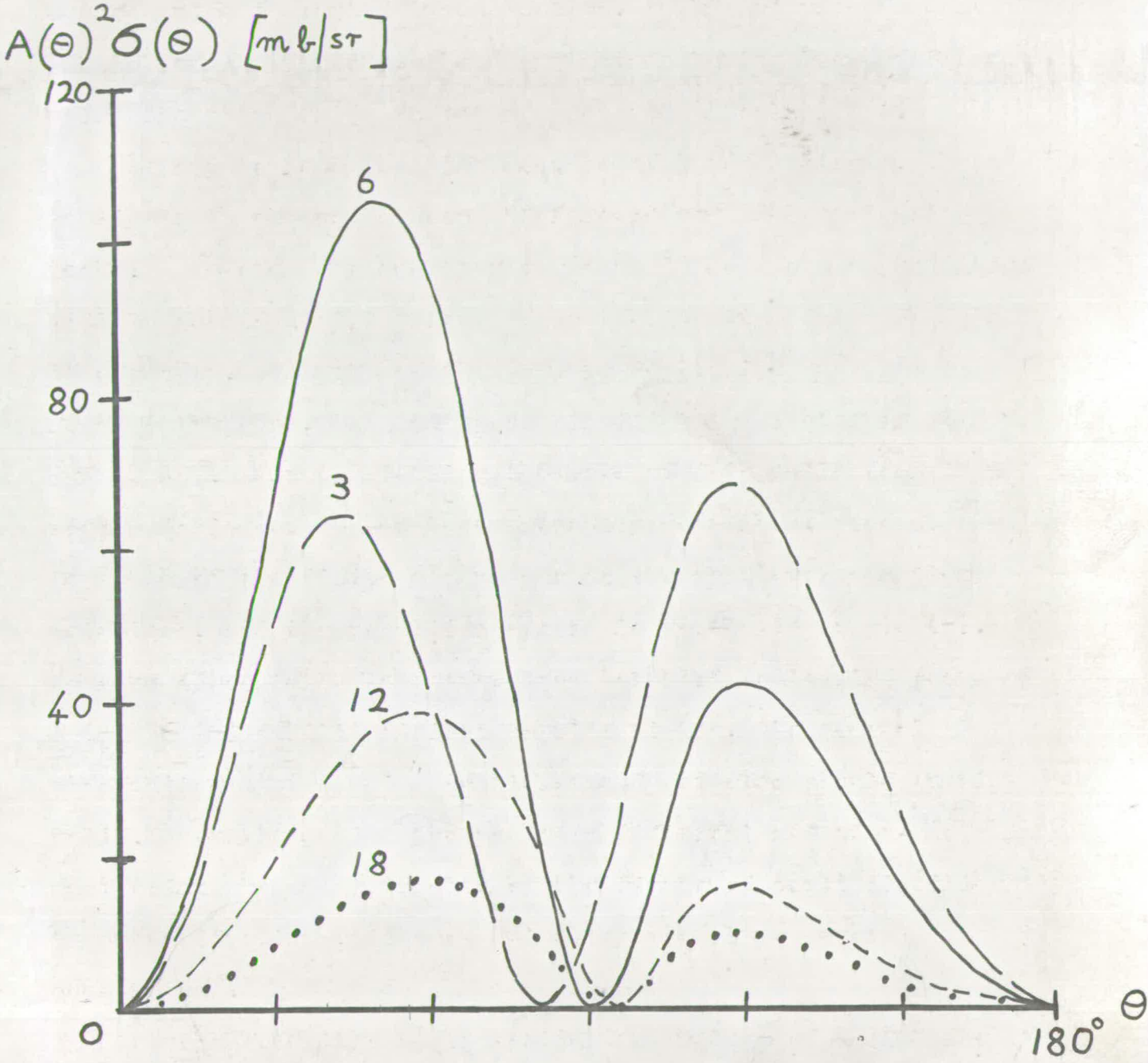

FIG. 5 FIGURE OF MERIT $[A(\theta)^2\sigma(\theta)]$ PLOTTED AS A FUNCTION OF LABORATORY ANGLE $[\theta]$ FOR NEUTRON ENERGIES OF 3, 6, 12 AND 18 MeV

selecting a forward scattering angle, it should be noted that this optimum angle and its associated analysing power varies considerably with energy, while for $\theta \sim 120^{\circ}$ one is located near the centre of the back scattering maximum of the figure of merit and has a near constant analysing power over the whole range of energies examined.

2.2 The High Pressure Helium Gas Scintillator

Since the pioneering use by Pasma[13] of a high pressure ^{4}He gas scintillator in a neutron polarization experiment, a number of reports on such scintillators have been published (e.g. references 10, 37, 38, 39, 40) not all agreeing on operational details. There is broad agreement that the addition of a quantity of xenon ($\sim 10\%$) to the helium is required to produce a good light output from the scintillator. It is also reported that the wavelengths of the scintillations emanating from such a helium-xenon mixture lie inconveniently in the near ultra-violet, and so the use of a quartz viewing window with a quartz window photomultiplier is advised. As an alternative, or an addition, to this use of quartz, much larger photomultiplier signals may be obtained by the deposition of a wavelength shifting material on the internal reflecting surfaces of the scintillating volume and on the viewing window. Early workers [10] reported a rapid loss of light output with time when using wavelength shifters so deposited, but later workers [36 - 40] have not experienced this difficulty, these using

most commonly diphenyl stilbene (D.P.S.) as a wavelength shifter, deposited in advised densities which vary, according to author, by orders of magnitude. There is also broad agreement that loss of light output may result from contamination by impurity gases, thus necessitating the careful evacuation of the scintillator prior to filling.

A section through the helium gas scintillator assembly constructed for the present scintillator is shown sketched in figure 6. The scintillating volume is contained in a stainless steel cylinder of 5cm. diameter, closed at the front by a hemisphere, the wall thickness being 2mm. The rear of this active volume of 6cm. axial length is closed with a 2·5cm. thick quartz window, seated on a P.T.F.E. 'O' ring seal, and held in position by a stainless steel surround clamped with 10 bolts. Into this surround screws the brass photomultiplier case which has a 'neck' whose axis of cylindrical symmetry is accurately co-linear with that of the active scintillating volume, this neck being used in the mounting and alignment procedure outlined in section 2.6.

The reflective coating of the inner walls of the scintillating volume followed the most commonly reported procedure, namely these surfaces, after polishing were coated with a vacuum evaporated layer of aluminium, then with a layer approximately 1mm. thick of electrostatically deposited [41] magnesium oxide, and finally with a vacuum deposited film of D.P.S. varying in thickness from $\sim 300 \mu g/cm^2$ on the walls close to the viewing

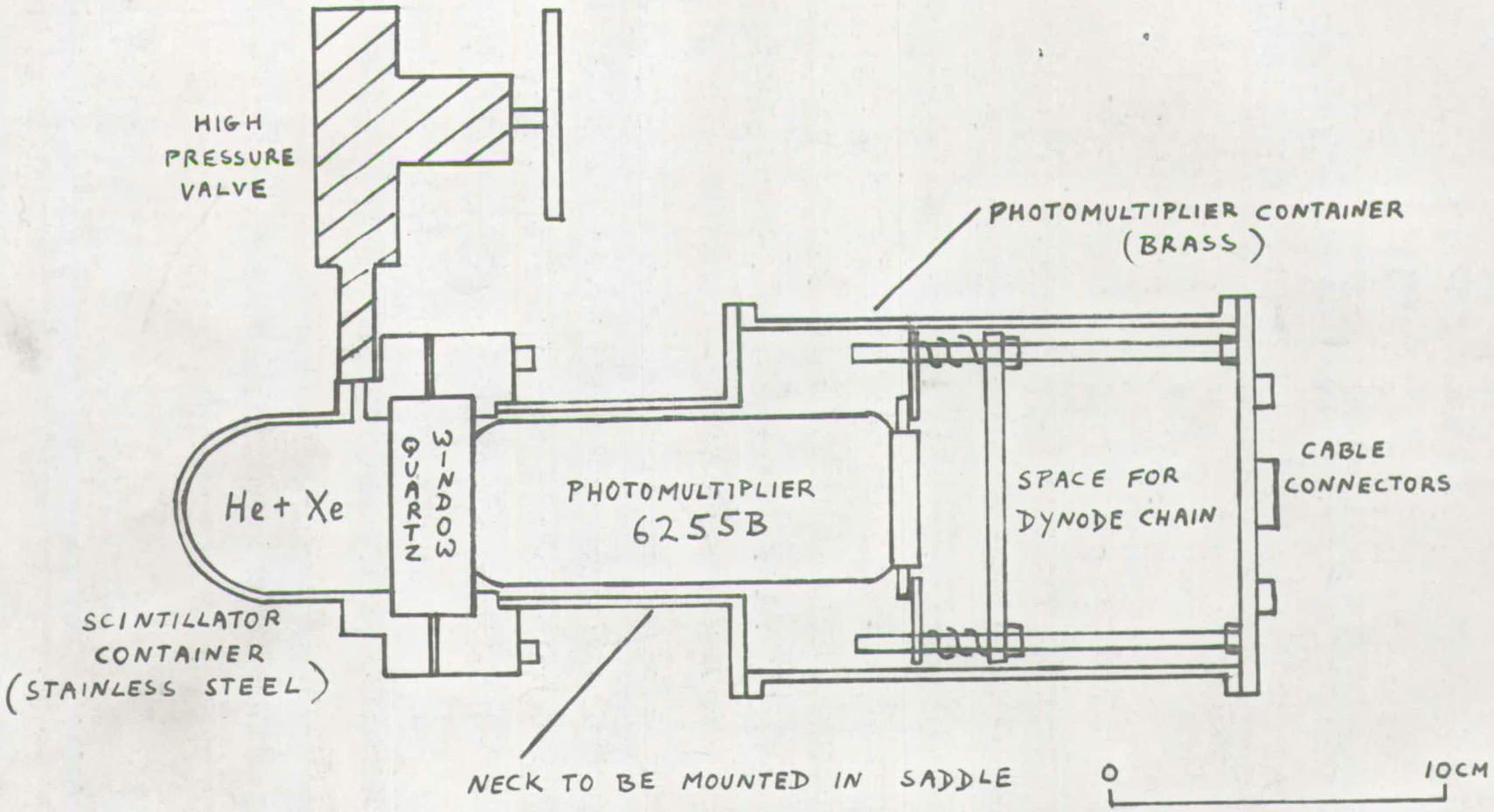

FIG. 6 SKETCH OF HELIUM GAS SCINTILLATOR

window to $\sim 100\,\mu g/cm^2$ on those of the hemispherical end, - the density and distribution as advised by Jenkin and Shamu[37]. The quartz window was also coated on the scintillating volume side with D.P.S. as advised by Jenkin and Shamu[37] ($\sim 25\,\mu g/cm^2$ thickness), and the scintillations were observed with a quartz window photomultiplier, namely an E.M.I. type 6255B.

The filling proceeded by first evacuating the scintillator volume and the filling line with a rotary and a diffusion pump and utilising a liquid nitrogen trap. Then the system was flushed with helium and pumped down with the rotary pump, this being repeated several times before filling with ~ 5 atmospheres of xenon and ~ 65 atmospheres of helium. A loss in gas pressure and an accompanying loss in light output in the scintillator necessitated refills after operational periods of a few months, although no re-coating proved necessary. On so refilling the gas scintillator, the light output regained or improved on its initial value provided the evacuation and filling procedure outlined above was adhered to.

The photomultiplier was operated with an E.H.T. across the dynode chain of 1500V, this producing a standing current therein of 0·5mA. The linear output to a pre-amplifier was taken from the 11th dynode.

2.3 The Liquid Scintillator Neutron Detectors

Organic scintillators offer a convenient and efficient means of detecting fast neutrons. They are however sensitive

also to γ-rays, the detection of which in the present polarimeter would not only increase the random background count rate, but would also introduce an error into a polarization measurement due to the observing of real coincidences produced by those γ-rays which are scattered (and detected) by both the helium gas scintillator and an organic scintillator. Thus to reject γ-ray events it was decided to use a pulse shape discrimination (P.S.D.) technique which relies on the observation that in certain organic scintillators the decay time of the scintillations due to proton recoils from incident neutrons is different from the decay time of the scintillations due to electron recoils from incident γ-rays.

The liquid Ne213[+] was chosen as the appropriate scintillator, there being no conveniently available solid of the desired size with good P.S.D. properties. Such a liquid scintillator is conventionally encapsulated with a bubble of nitrogen to allow for expansion of the liquid due to temperature fluctuations. To maintain on rotation of the cradle a constant efficiency for the detection of neutrons scattered by the gas scintillator, the liquid scintillator used in the present polarimeter was encapsulated in non standard[‡] 'bubble free' cylindrical cells of 5cm length and 5cm. diameter, the nitrogen expansion bubble being contained in a coiled capillary tube on the outside of an end face and thereby unable to enter the volume viewed by the photomultiplier through the window on the opposite end face.

‡ Footnote. Supplied by Nuclear Enterprises Limited.

A cross sectional sketch of such a cell is contained in the diagram of figure 7 which represents a complete liquid scintillator neutron detector assembly as used in the present polarimeter.

The photomultiplier used in each of these detectors was an E.M.I. type 6262B operated with an E.H.T. of 1200V across the dynode chain, so producing a standing current therein of $\sim \frac{1}{3}$ mA. The final dynode to anode potential was a few volts, the intention being to utilise the saturated pulses so produced from the last dynode with the Owen[42] technique of pulse shape discrimination. However a considerable variation in the amplitude of these saturated pulses occurred when the detector assembly was rotated, thus producing unacceptable changes in detector efficiency on rotation, since the Owen[42] technique of P.S.D. relies on amplitude selection of these pulses. This effect was observed with both of the presently described detectors and with a laboratory monitor, all containing a type 6262B photomultiplier. The output from the 11th dynode of each of the side neutron detectors which was taken to provide pulse heights proportional to the light output from the scintillator (a 'linear' output) appeared unaffected by the rotation. Thus it was decided to use these linear signals with external circuitry of the type proposed by Roush et al. to provide pulse shape discrimination.

The circuitry so designed for the present study will be treated in detail in section 3.5, however briefly the linear

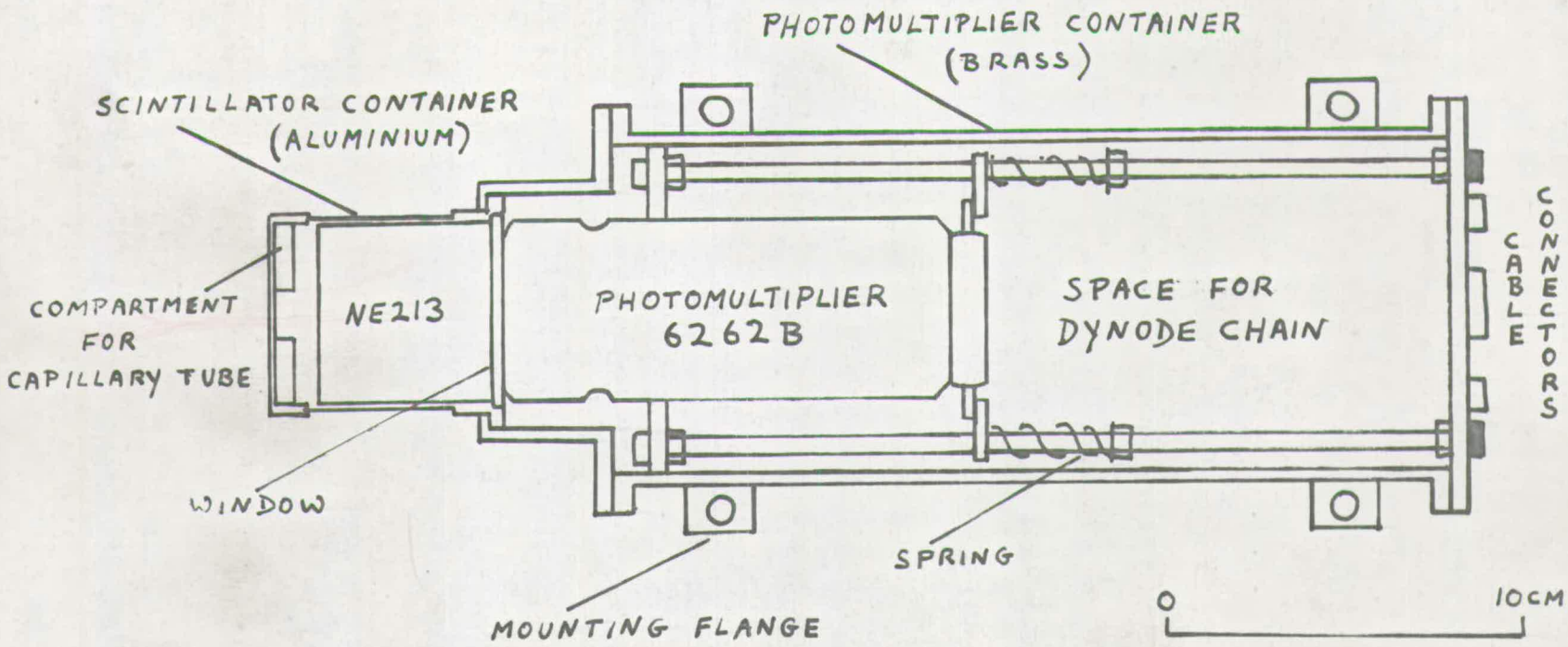

FIG. 7 SKETCH OF A LIQUID SCINTILLATION NEUTRON DETECTOR

current pulses from the photomultiplier were RC integrated in the preamplifier, and then this was followed by an RC differentiation. Now the time from the start of such a processed pulse to its crossing the zero amplitude baseline will be longer for neutron associated events than for those due to γ-rays. Hence the circuitry used in the present investigation converts this time interval into a proportional pulse height, a pulse height spectrum of the output being shown in figure 8. This was obtained with a neutron detector as presently described, and using a polonium-beryllium source, the pulse height analyser being gated to accept events with a light output greater than that produced by a 500keV electron recoil in the scintillator. It is obvious from this spectrum that amplitude selection by an integral discriminator of the output pulses from the P.S.D. circuitry will provide one with the desired rejection of γ-ray events.

2.4 The Target Assembly

The vertical deuteron beam from the Cockcroft-Walton type accelerator used in the present investigation was analysed by a 30° bending magnet and hence directed on to the neutron producing target. The presently reported results were all taken for neutrons produced at a mean laboratory reaction angle of 46° and with a vertical reaction plane. Small displacements of the deuteron beam spot normal to this reaction plane could be corrected by a subsidiary steering magnet.

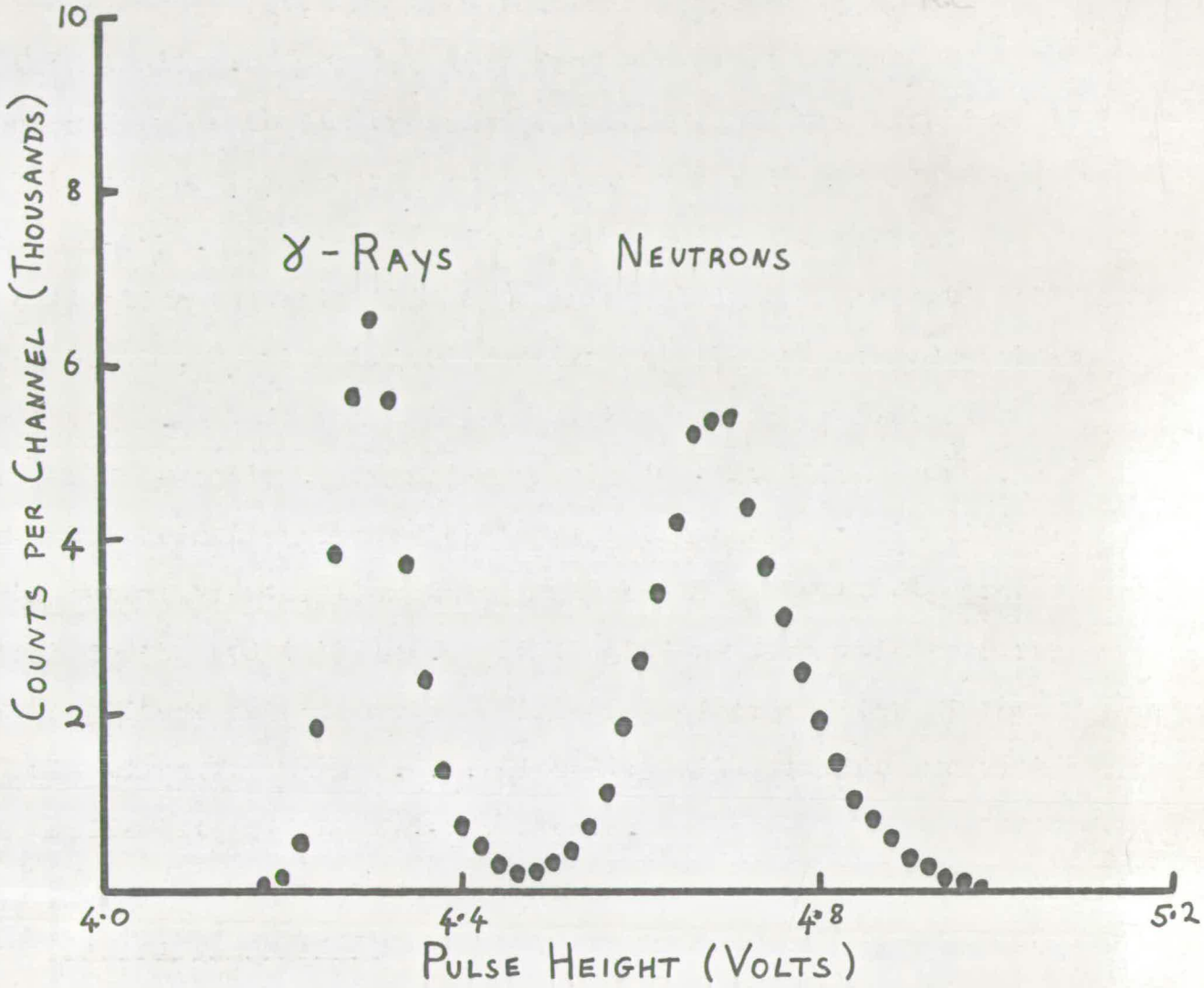

FIG. 8 PULSE HEIGHT SPECTRUM OF THE OUTPUT FROM THE PULSE SHAPE DISCRIMINATION UNIT, ONLY EVENTS WITH A LIGHT OUTPUT GREATER THAN 500keV RECOIL ELECTRONS BEING RECORDED. Po-Be SOURCE.

The target holder used was of a design adopted for use with a Mott-Schwinger scattering experiment[44] with the same accelerator. It is shown in the photograph of figure 9 and consists of a brass stalk vacuum sealed into the quartz beam tube at its base with an 'O' ring. Water entering and exiting this base outside the vacuum system circulates within the interior of the stalk thus cooling the target material soldered to and covering its upper surface. This target strip is of 3mm width normal to the reaction plane and 2cm long in the reaction plane, the top surface of the target stalk being so angled such that this longitudinal axis is inclined to the horizontal only slightly more steeply than the collimator axis. Thus beam spot movement due to small accelerator voltage fluctuations effectively takes place along the collimator axis, consequently maintaining the neutron irradiation of the gas scintillator.

The target material used in the present investigation was supplied by the Radiochemical Centre, Amersham, and consisted of a copper backing coated with a titanium layer containing absorbed deuterium gas in a near one to one Ti to D atomic ratio.

2.5 Collimation and Shielding

Primary shielding of the side detectors from the neutrons produced at the target was provided by a collimator shown diagramatically in figure 3 and also in the photographs of

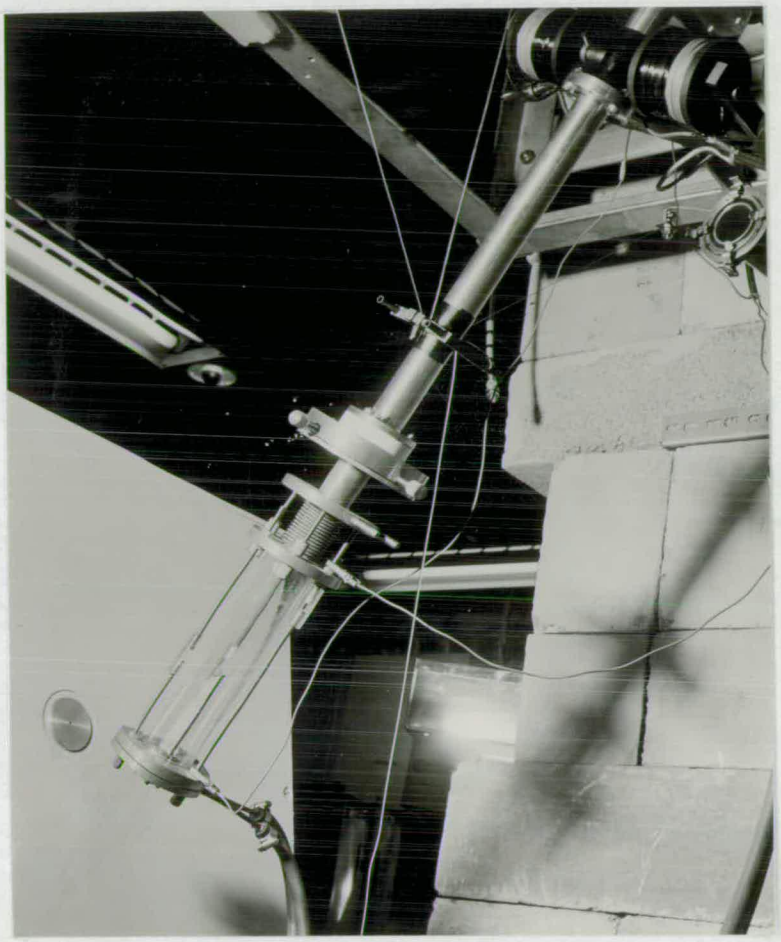

FIG. 9 PHOTOGRAPH OF TARGET ASSEMBLY

figures 9, 10. The end faces of this shield perpendicular to the collimated neutron beam are 60cm. square, the length being 45cm. The shielding material contained in this collimator consists of a cylinder of lead as shown close to the target to provide attenuation of the neutron flux by inelastic scattering, this lead further serving to attenuate the annihilation γ-ray flux from the target, due to positron decay of ^{13}N produced by a (d,n) reaction on ^{12}C target contamination. The bulk of the collimator volume is filled with paraffin wax to further degrade the incident neutron energies, and finally a 5cm. thick wall of lead is used to shield the polarimeter from the γ-rays produced by neutron capture in this wax. The neutron beam tube consists of a cylinder of $\sim$5cm. diameter into which inserts are placed to provide a throat and a taper. Brass is used for the inserts around the throat, and polythene otherwise. The throat was chosen such that all of the gas scintillator active volume was illuminated by the target, and the taper from the throat to the end remote from the target was chosen such that the inserts in this region just failed to be directly illuminated by the target, this being done to reduce contamination of the direct neutron beam with contributions from collimator wall scattered neutrons.

Secondary shielding at least 25cm. thick, consisting mainly of borated water contained in polythene bags inside metal boxes was built round the polarimeter, an exit being left to the rear for the neutron beam and for signal and E.H.T. cables.

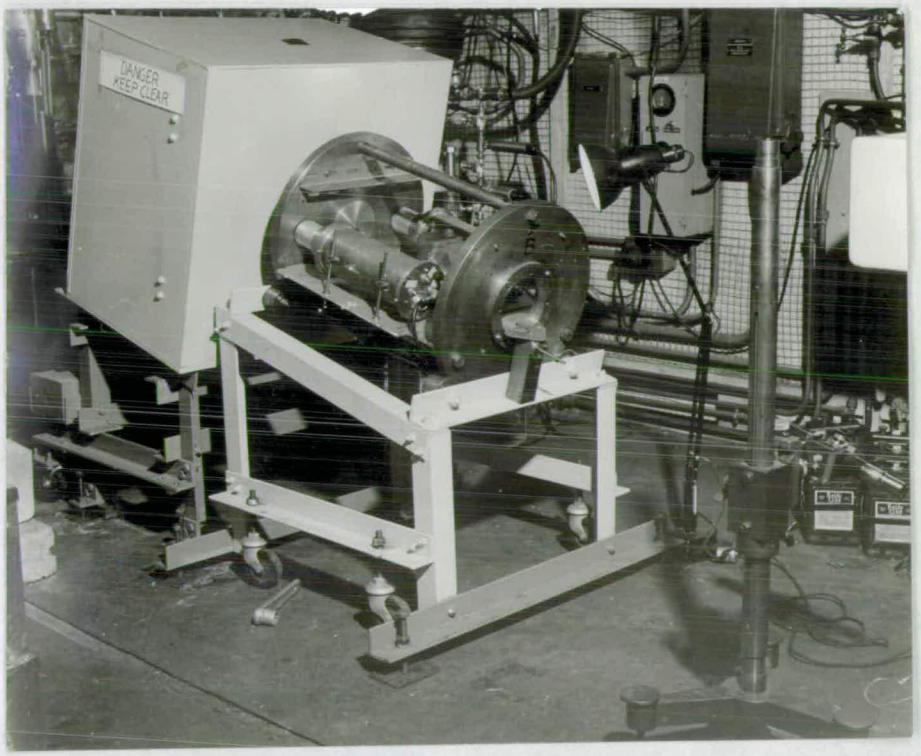

FIG. 10 PHOTOGRAPH OF COLLIMATOR AND CRADLE

2.6 The Rotating Cradle and the Alignment Procedure.

The cradle consists of two accurately turned cylindrical steel plates, of 2.5cm thickness with central holes to allow the passage of neutrons and cables, these plates being held accurately parallel and 50cm apart by three steel pins of 2.5cm diameter. This cradle is mounted in a steel frame, its end plates resting on four rotating bearings. Thus the cradle is free to rotate, the axis of rotation being the line joining the centres of the two end plates. A pin and socket arrangement at the rear (i.e. remote from the target) plate allows the cradle to be held in the four desired orientations - corresponding to $\phi = 0, \pi/2, \pi, 3\pi/2$ for a neutron detector.

Upon this cradle is located an aluminium plate, perpendicular to the end faces, to which the liquid scintillators are attached via steel rods through their mounting lugs. The gas scintillator lies along the axis of rotation, its 'neck' being held in a brass saddle which is also attached to the aluminium plate.

The checking of the axial alignment of the polarimeter was performed with the gas scintillator removed. A telescope, located to the rear of the polarimeter was used to view the target through a series of cylindrical alignment inserts with 2mm diameter axial holes, these inserts fitting accurately into each end of the collimator beam tube, into the centre holes on the end faces of the cradle, and into the brass saddle mounted on the cradle. Alignment accuracy of these holes to

within ~ 0.5mm was achieved, and checks made after several months of operation showed no need of further adjustment. Further, to allow speedy replacement of target material, more than one target holder was employed, these proving sufficiently identical to eschew the need for alignment adjustments. That the gas scintillator located truly axially on the cradle was also checked, by using an alignment jig mounted through the central hole of the cradle front plate.

2.7 The Fast Neutron Polarimeter

The photographs of figures 9,10,11,12,13, show the polarimeter at several stages of construction. Figure 9 shows the target and the collimator with an alignment insert located in the beam tube. Figure 10 shows the collimator and the cradle also with alignment inserts in place and with the telescope in position to its rear. In figure 11 are shown the walls of tin boxes partially constructed around the cradle on which the neutron detectors and the gas scintillator are mounted. Figure 12 is as figure 11, but in addition the pre-amplifiers are mounted on the cradle. Figure 13 shows the walls of shielding surrounding the polarimeter, the cables exiting at the rear carrying power to photomultipliers and pre-amplifiers, and signals from these pre-amplifiers to be further processed.

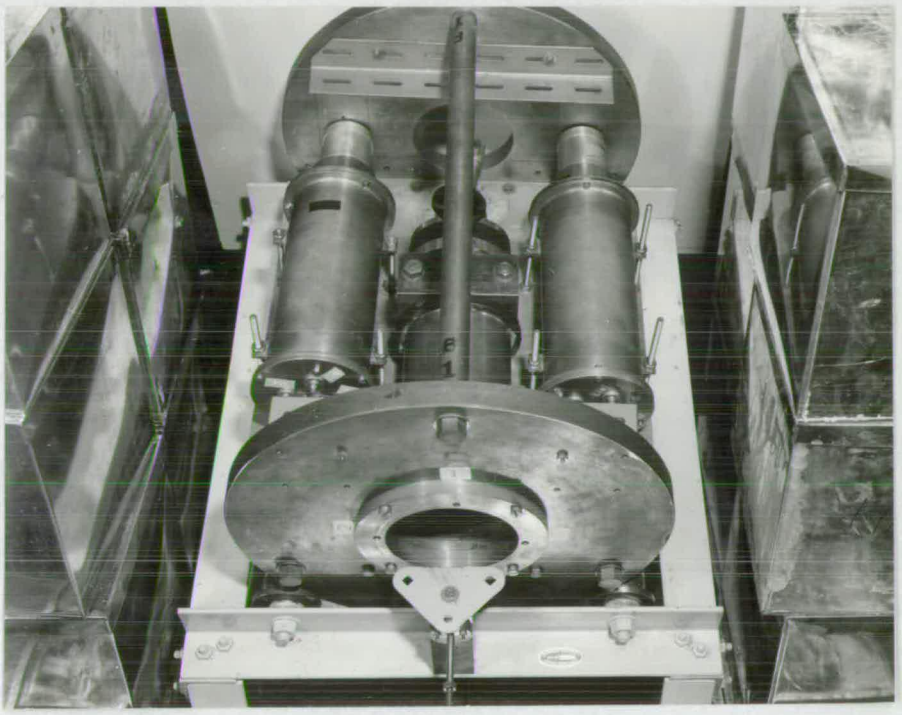

FIG. 11 PHOTOGRAPH OF CRADLE WITH SCINTILLATORS MOUNTED

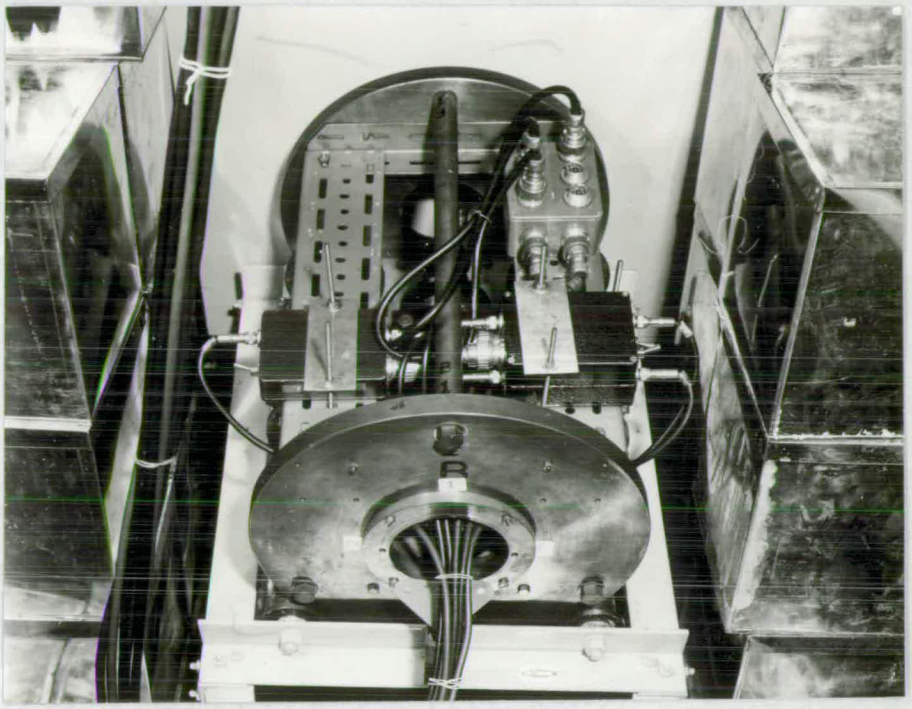

FIG. 12 PHOTOGRAPH OF CRADLE WITH SCINTILLATORS AND PRE-AMPLIFIERS MOUNTED

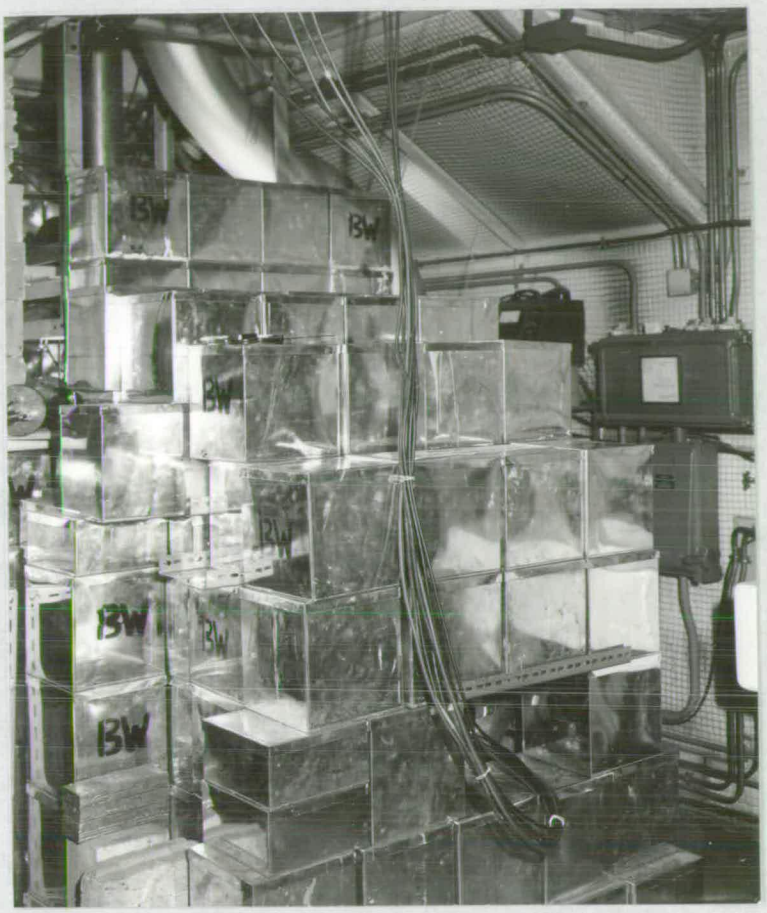

FIG. 13 PHOTOGRAPH OF POLARIMETER WITH SHIELDING WALLS IN POSITION

CHAPTER 3.

The Design and Construction of the Electronic Circuitry Employed with the Fast Neutron Polarimeter

Due to the lack of other than aged electronic units containing valves (mainly A.E.R.E. 1000 series) whose reliability proved inadequate to the present task, the design and construction of a series of electronic units using transistors and integrated circuits proved necessary. A block diagram of the circuitry used with the present polarimeter is shown in figure 14 with an accompanying key. With the exception of the power supplies, all the units here represented were designed as part of the present work. Thus in the present chapter after a consideration of the collective functioning of the polarimeter electronic circuitry, the construction and operation of the individual electronic units designed for and used with the polarimeter will be examined.

3.1 Functional Description of the Polarimeter Electronic Circuitry

Referring to the block diagram of figure 14, it may be seen that both prompt (i.e. real and random) and delayed (i.e. random) coincidences between each side detector and the gas scintillator are recorded, and the four corresponding outputs a, b, c, d shown in the figure are used to 'gate' the multichannel analyser (not shown) employed to pulse height analyse the output marked 'He Linear' from the gas scintillator amplifier. Hence four

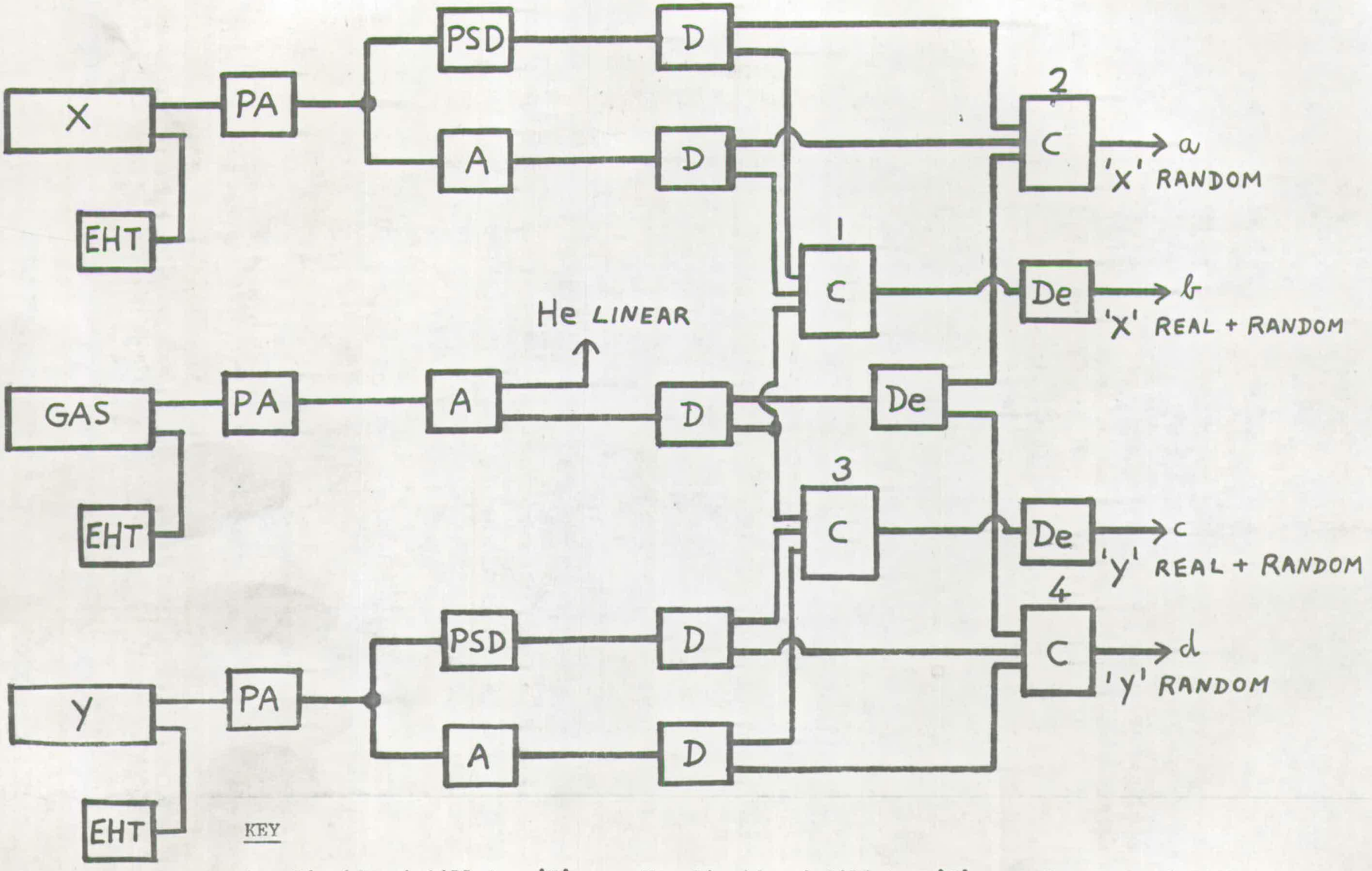

KEY

X - Liquid scintillator 'X'
Y - Liquid scintillator 'Y'
G - Gas scintillator
EHT - EHT power supply
PA - Pre-Amplifier
A - Amplifier
PSD - Pulse shape discriminator
D - Integral discriminator
C - Triple coincidence unit
De - Delay

FIG. 14 BLOCK DIAGRAM OF ELECTRONIC CIRCUITRY USED WITH POLARIMETER

pulse height spectra of the 'He Linear' signals are obtained, each one containing only events recorded in association with one of the four 'gating' outputs (a,b,c,d).

The production of these four 'gating' outputs is as follows: Triple coincidence unit 1 receives from the 'X' liquid scintillator an input corresponding to linear signals above a selected energy (usually set at 100keV electron recoil energy) and a neutron identifying input, which are required to be in coincidence with an input from the gas scintillator. A resolving time of ~ 1 /us is used. Triple coincidence unit 2 receives identical signals to unit 1 from the 'X' liquid scintillator, but the input from the gas scintillator is delayed by ~ 3/us to give outputs due only to random coincidences. Triple coincidence units 3 and 4 operate as units 1 and 2 respectively, but for the 'Y' liquid scintillator. The 3 /us delays after coincidence units 1 and 3 serve to bring all four coincidence outputs into the same time relation with respect to the 'He linear' output, in order to produce the desired gated spectra.

3.2 Standards of Construction

Due to the comprehensive nature of the design task, it became clear that the circuits could serve in other than the present experimental study. Thus in order to allow a flexibility of use, it was decided to construct these units using a modular racking system‡, to operate them from a standard set of

‡ Footnote: The Standard Telephones and Cables Ltd. 'ISEP' range.

stabilised power supply voltages, and to maintain a uniformity of output levels.

The plug-in module initially favoured is shown in figure 15, this being used for the amplifiers, the pulse shape discrimination units and the interface units (not shown in figure 14) which drive the gating inputs of the multi-channel analyser. Three such modules plus one module containing the ± 12 Volt stabilised power supplies from which these units operate, fit into a 19 inch rack mounting frame as shown in figure 16.

The multiplicity of the interconnections between the discriminators and coincidence units suggested that a closer packing density than that allowed by the above module would be more convenient for such units. Further since these units handle mainly digital ('logic') signals, inter unit pick up is not a severe problem. Thus the plug in module as shown in figure 17 was used, 9 of these fitting into a 19 inch rack mounting frame as shown in figure 18, and the stabilised + 12 and - 6 Volt supplies to power these units are mounted to the rear of the frame.

The pre-amplifiers, which were mounted on the rotating cradle close to their respective scintillation counters were constructed in die-cast boxes as shown in figure 19, and these were supplied with ± 12V from their associated amplifier power supply via a 6 core cable.

In the following sections the design and operation of these electronic units are described, commencing with the

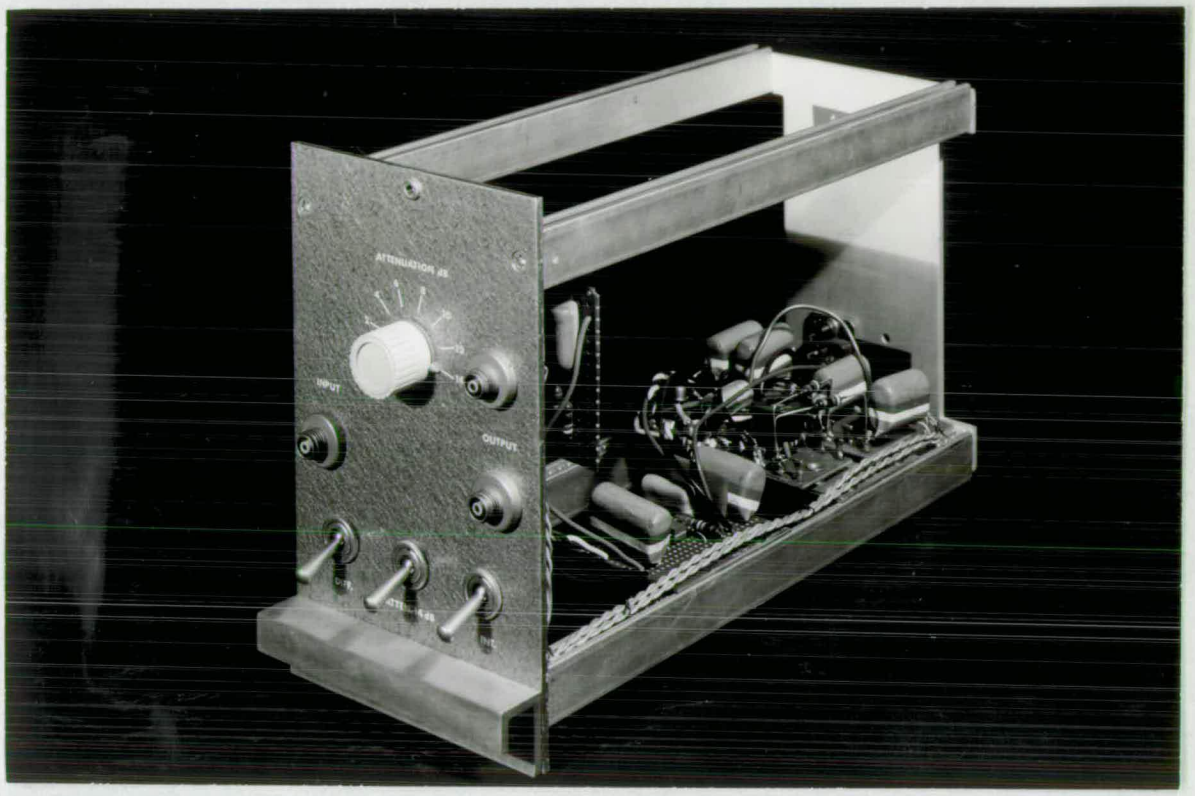

FIG. 15 PHOTOGRAPH SHOWING THE MODULAR CONSTRUCTION OF THE LINEAR PULSE AMPLIFIER

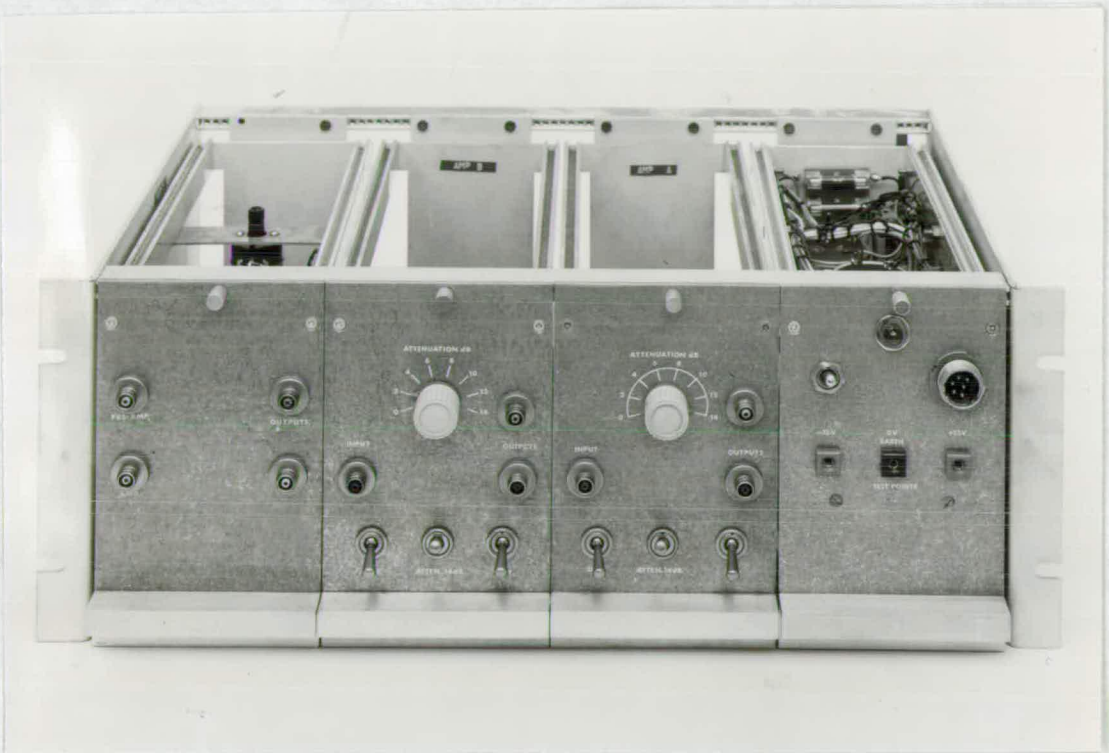

FIG. 16 PHOTOGRAPH SHOWING THE MOUNTING OF MODULES IN A FRAME

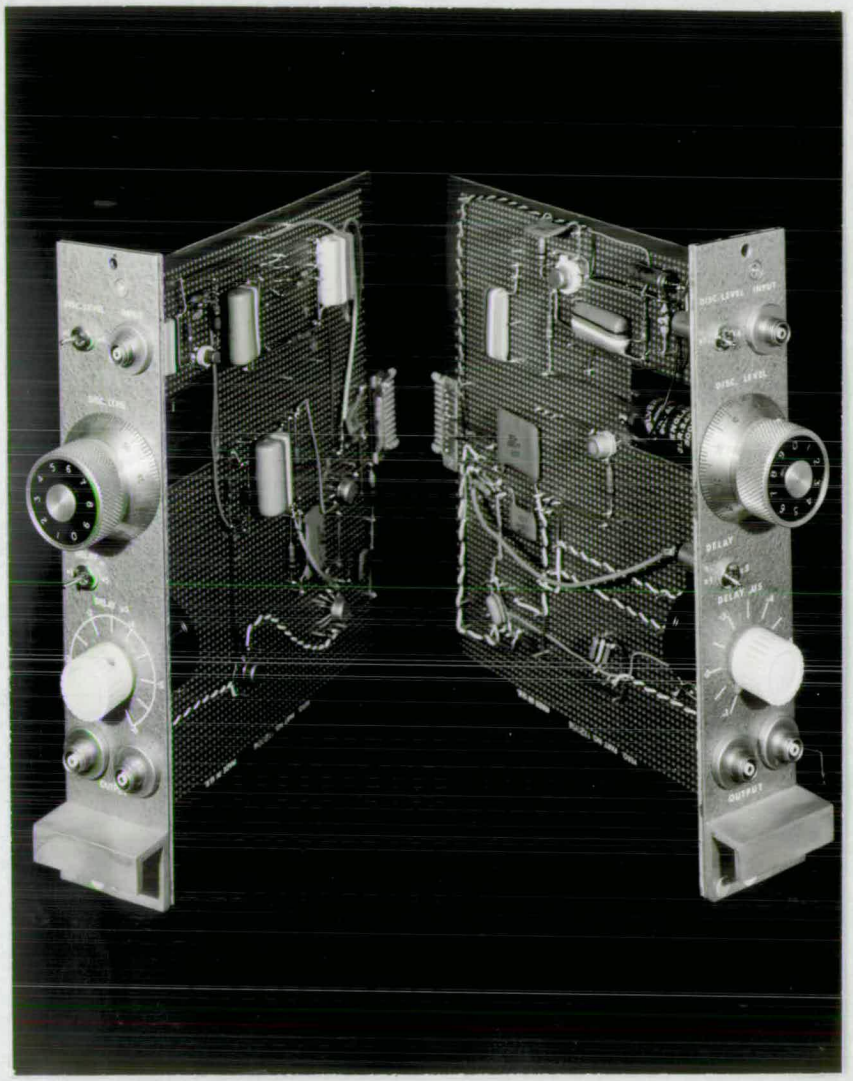

FIG. 17 PHOTOGRAPH SHOWING THE MODULAR CONSTRUCTION OF THE INTEGRAL DISCRIMINATOR

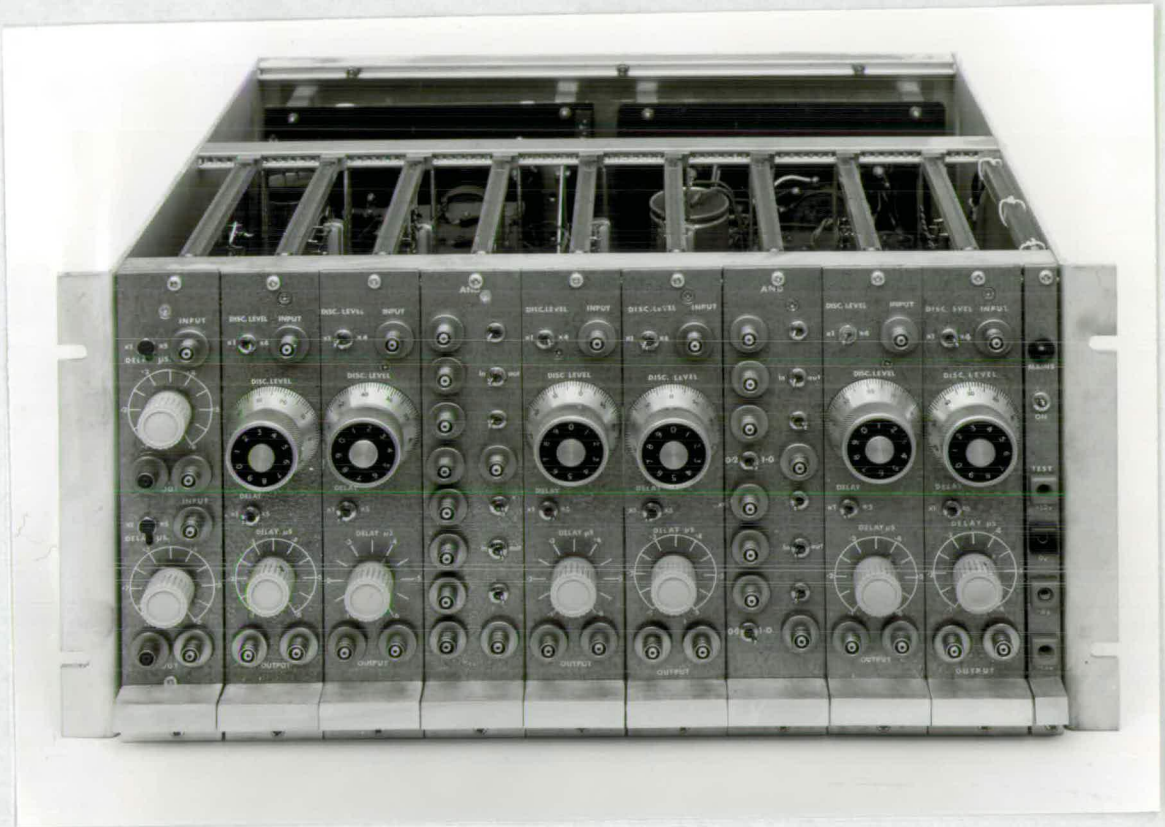

FIG. 18 PHOTOGRAPH SHOWING THE MOUNTING OF MODULES IN A FRAME

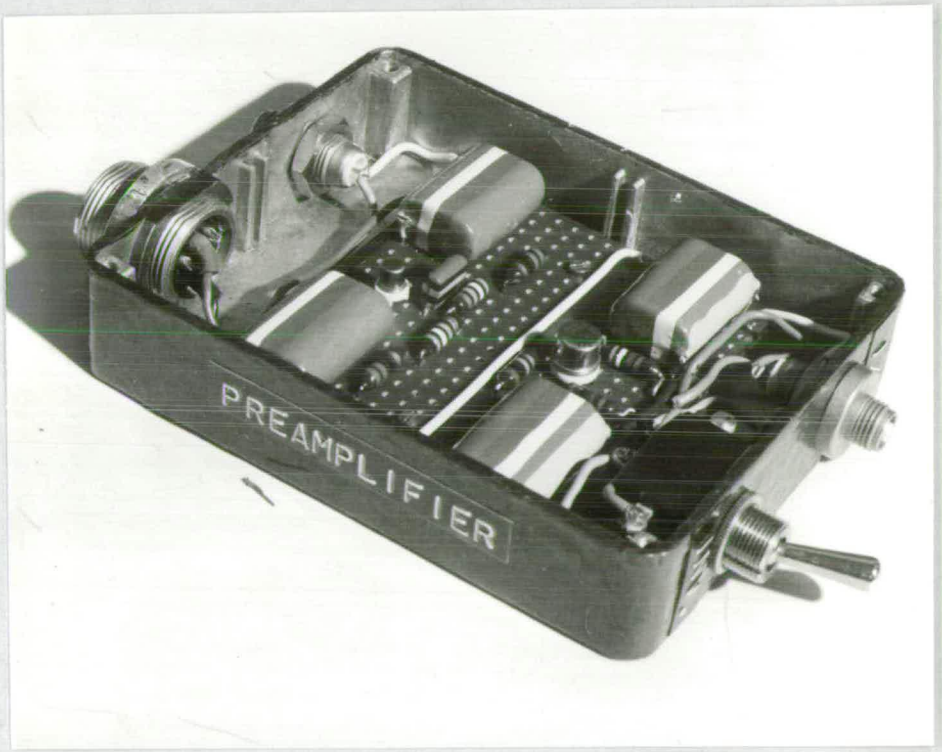

FIG. 19 PHOTOGRAPH OF A PRE-AMPLIFIER WITH TOP COVER REMOVED

pre-amplifier at the detector end of the signal processing line and concluding with the interface units designed to route the analysed pulses into appropriate sections of the pulse height analyser's memory.

3.3 The Pre-Amplifier

The pre-amplifier, used in conjunction with the amplifier to be described in the following section, was designed so that in preliminary studies it could also be used with A.E.R.E. type 1008 and 1430 valve amplifiers. Thus it possesses an inversion facility and a capability of driving a 100Ω terminated cable. The circuit diagram of this pre-amplifier is shown in figure 20.

With switch S1 in the 'b' position, transistors T1, T2 act as a non inverting unity gain compound emitter follower, R9 providing a nominal 100Ω output impedance. With switch S1 in the 'a' position, transistor T1 acts as an emitter follower driving the unity gain inverting stage T2, resistor R5 giving the circuit a 100Ω output impedance in this configuration. Now the pre-amplifier is operated with the output connected to a cable terminated at the receiving end by 100Ω , and so with the switch in either position the magnitude of the signal voltage appearing across this termination will be one half of the magnitude of the signal voltage applied to the pre-amplifier input.

No 'bootstrapping' of the resistors R1, R2 supplying bias to the transistors is employed, thus an input signal to

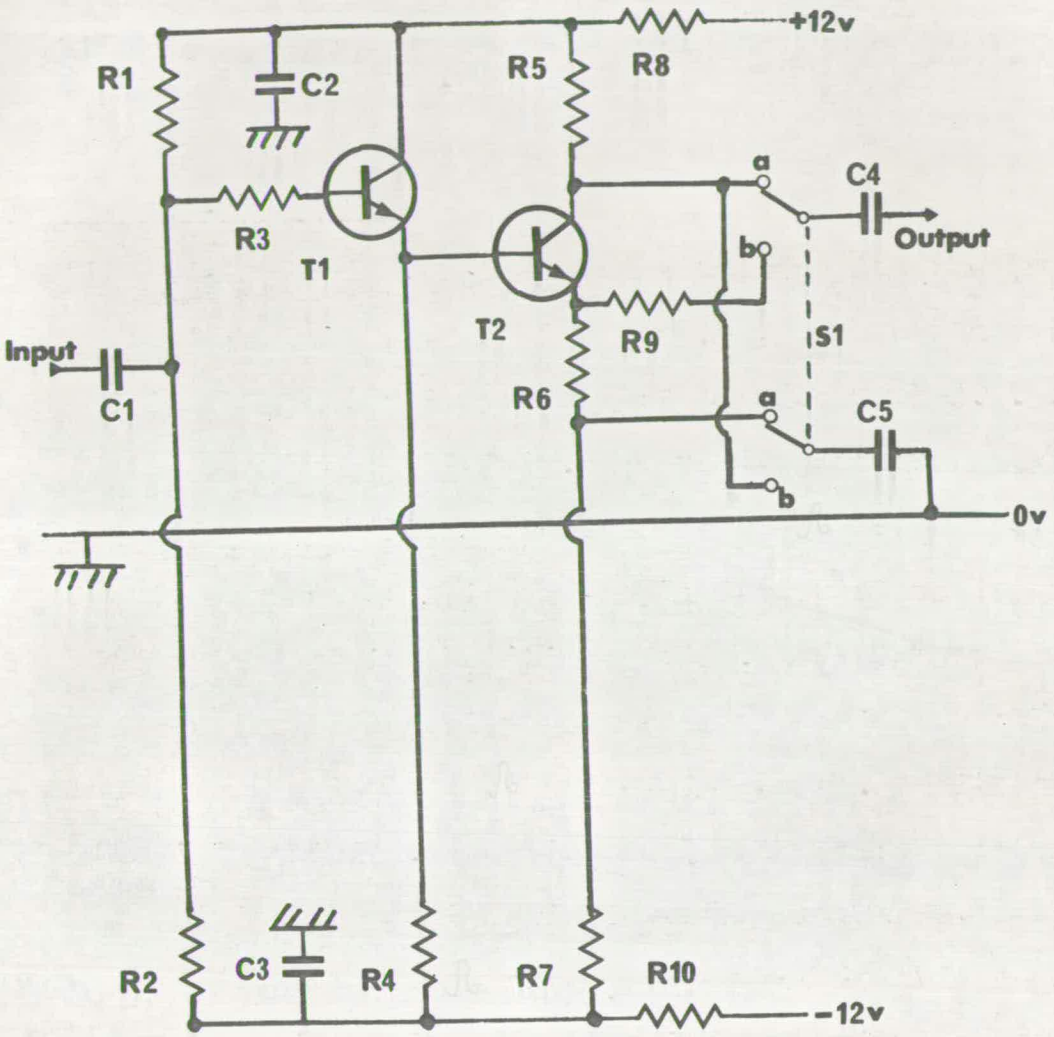

R1	= 39kΩ	R6	= 100Ω	C1	= 0.1μF	T1	= BFY75
R2	= 39kΩ	R7	= 100Ω	C2	= 2.2μF	T2	= 2N1711
R3	= 1.5kΩ	R8	= 68Ω	C3	= 2.2μF		
R4	= 8.2kΩ	R9	= 100Ω	C4	= 2.2μF		
R5	= 100Ω	R10	= 68Ω	C5	= 2.2μF		

FIG. 20 THE PRE-AMPLIFIER

the pre-amplifier sees an input load of R1, R2, both in parallel with the input impedance (Z) of the transistor pair. Now the resistive component of Z is approximately given by the product of the emitter signal load of T2 (100 Ω), the current gain of T1 ($\sim$100) and the current gain of T2 ($\sim$100), and hence is clearly much greater than R1, R2. Thus the resistive component of the input impedance (R') seen by the input signal is 19k Ω , this being defined by resistor R1 in parallel with R2, and is largely independent of transistor characteristics. Now the input signal will see a capacitance (C') in parallel with R', this containing contributions from the photomultiplier, the dynode chain, the interconnecting cable, and the pre-amplifier itself.

The RC integration time constant thereby produced at the input was typically $\sim$ 1 μs, this being adequately long to collect the current pulse from the photomultiplier-scintillator assemblies, and it also provides a convenient pulse shape for further processing in the amplifier. Since it was initially intended to use the Owen [42] technique of pulse shape discrimination, the RC differentiation time constants of the coupling networks in both the pre-amplifier and amplifier were kept as large as were conveniently possible, an overall figure of $\sim$ 250 μs being obtained.

Transistor T2 is operated with 40mA of standing current, allowing adequate signal drive into a 100 Ω load for both negative going and positive going input signals, and ensuring

that the (internal) incremental emitter resistance of T2 is much less than the external emitter signal load, thus preventing non linearity and temperature dependence of gain arising from this source. Resistor R3 serves to inhibit parasitic oscillations, resistor R4 improves the slew rate for negative going input signals, and resistors R8 and R10 in conjunction with C2 and C3 provide power supply line decoupling.

3.4 The Linear Pulse Amplifier

The circuit diagram of the amplifier designed for the present experiment is shown in figure 21, and its construction is shown in figure 15. This operates as a non-inverting linear amplifier for positive input pulses, and provides switch selectable amplification and shaping.

Thus an input signal (from a pre-amplifier) sees a nominal 100 Ω input impedance defined by R1 in series with R2, switch S1 allowing the signal amplitude to be attenuated by a factor of 5 (14 dB) at this stage if desired. With switch S2 closed, the pulse passes on to the base of T1, but with switch S2 open an RC differentiation with a time constant of ~0.8 μs first occurs, this being defined by C2 and the bias resistors R3, R4 which are effectively (as in the pre-amplifier) the signal loads at the base of T1. Transistor T1 inverts the signal, its voltage gain being inversly proportional to the signal load between the emitter of T1 and earth. This we may adjust using switch S3, the pole of which is effectively a signal earth.

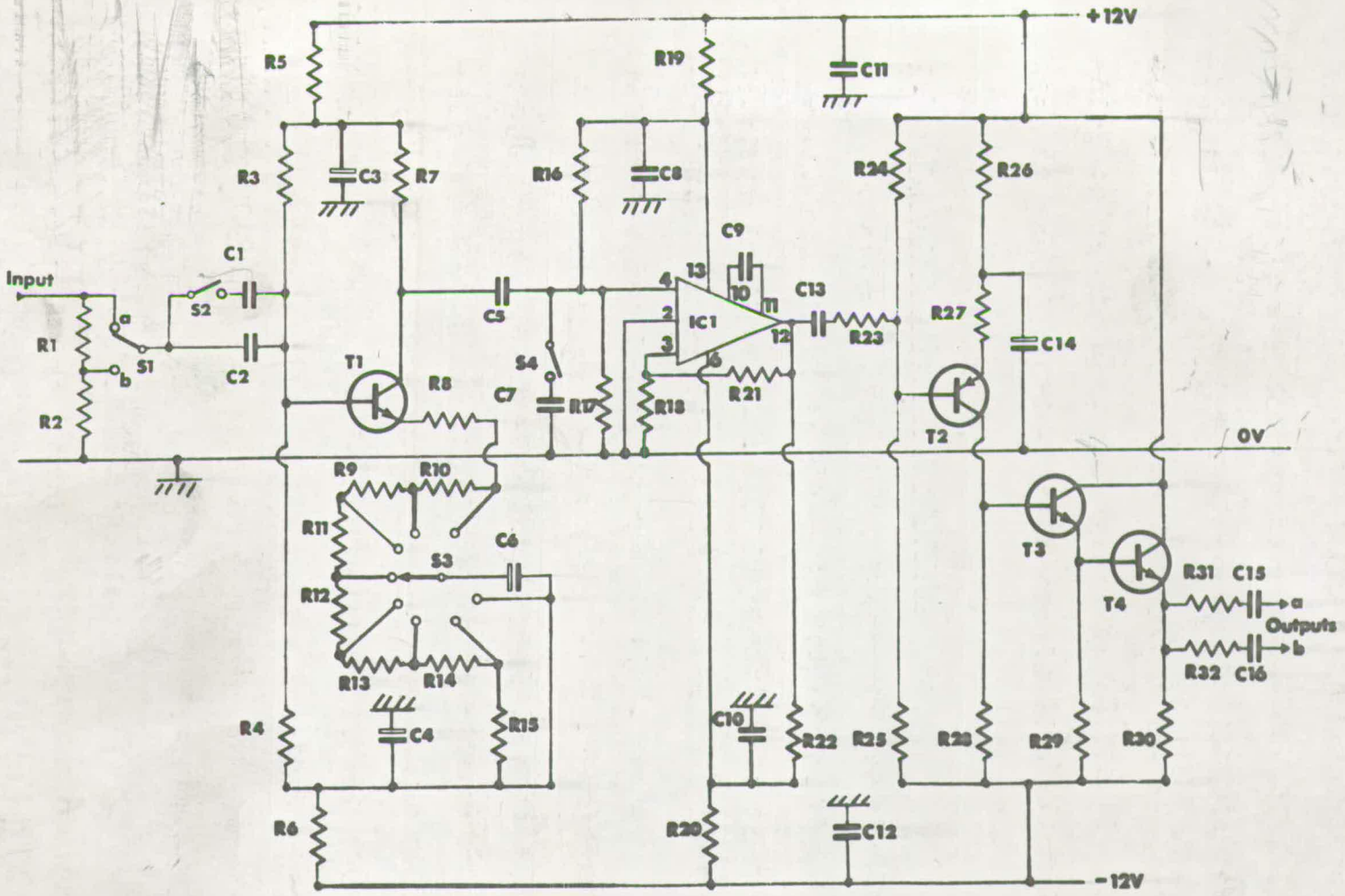

R1	= 82Ω	R9	= 33Ω	R17	= 100Ω	R25	= 39kΩ	C1	= 1μF	C9	= 470pF	T1	= BFY75
R2	= 22Ω	R10	= 27Ω	R18	= 100Ω	R26	= 180Ω	C2	= 0.001μF	C10	= 2.2μF	T2	= BFX48
R3	= 4.3kΩ	R11	= 39Ω	R19	= 47Ω	R27	= 150Ω	C3	= 32μF	C11	= 2.2μF	T3	= BFY75
R4	= 1kΩ	R12	= 51Ω	R20	= 47Ω	R28	= 1kΩ	C4	= 32μF	C12	= 2.2μF	T4	= 2N1711
R5	= 47Ω	R13	= 68Ω	R21	= 6.8kΩ	R29	= 2.2kΩ	C5	= 0.68μF	C13	= 0.47μF	IC1	= CA3030
R6	= 47Ω	R14	= 82Ω	R22	= 1.5kΩ	R30	= 390Ω	C6	= 32μF	C14	= 32μF		
R7	= 1.5kΩ	R15	= 100Ω	R23	= 470Ω	R31	= 100Ω	C7	= 8200pF	C15	= 2.2μF		
R8	= 100Ω	R16	= 68kΩ	R24	= 4.7kΩ	R32	= 100Ω	C8	= 2.2μF				

FIG. 21 THE LINEAR PULSE AMPLIFIER

Resistors R8 to R15 have been chosen to allow the voltage gain to be thus varied in seven 2dB (nominal) steps. The emitter standing current (Ie) in T1 is 8m A, thus the incremental emitter resistance which in a transistor at room temperature is $\frac{25}{Ie}\,\Omega$ (where Ie is expressed in milliamps) is therefore much less than R8, and hence has been ignored in the above analysis as may also any non linearity introduced by its variation with signal size. The load seen by signals at the collector of T1 is effectively R17 and with switch S4 closed C7 is placed in parallel with this load thus shaping the signal with an RC integration of time constant ~0.8 /us. The maximum gain of this input stage, being the collector load of T1 divided by R8 is approximately (minus) unity.

The main gain element of this linear pulse amplifier is the integrated circuit operational amplifier IC1‡ to which the signal now passes. This operational amplifier has a differential input, the signal being applied to the non inverting input (pin 4 in figure 21), the feedback being applied to the inverting input (pin 3). Now since the output impedance of the operational amplifier is small w.r.t. R21 and the input impedance is large w.r.t. R18, then the gain of this stage G is given by

$$G = A \Big/ \left(1 + \frac{A.\,R18}{R18 + R21}\right)$$

where A is the open loop gain of the operational amplifier.

‡ Footnote: A type CA3030 produced by the Radio Corporation of America.

Now for

$$\frac{A \cdot R18}{R18 + R21} \gg 1$$

this reduces to

$$G = \frac{R18 + R21}{R18}$$

showing the notable independence of the gain on the operational amplifier characteristics, this independence being a function of the amount of feedback applied. However, as the signal frequency increases, the open loop gain of the operational amplifier falls off, and further a phase difference appears between the input and output signals. To ensure the stability of the operational amplifier connected in the feedback mode, one must ensure that the product of the feedback fraction $\left(\frac{R18}{R18+R21}\right)$ and the open loop gain at which this phase difference is 180° (say Af) is less than unity. This places a theoretical limit on the fraction of the signal fed back to be less than 1/Af, and in practice one must keep well within this limit to ensure that the closed loop gain does not peak severely at high frequencies. To obtain an adequate margin of stability with the present feedback network, it is necessary to modify the open loop frequency response of the operational amplifier. Thus capacitor C9 is employed, its action being to increase the frequency at which the phase difference of 180° occurs, and consequently reducing Af. This technique is known as phase lead compensation, the alternative being phase lag compensation which, however, much reduces the band width of the operational amplifier.

Thus this stage provides approximately 70 times gain, however to provide linear output signals of up to + 10 Volts in size with adequate current drive, further amplification and inversion is required.

The signal from the operational amplifier is fed via resistor R23 to the base of transistor T2, this resistor being included to prevent excessive current being drawn from the operational amplifier should T2 saturate on receiving an overloading pulse. Now since the input impedance of transistor T2 (ignoring its bias resistors R24, R25) is approximately R27 multiplied by the current gain of T2, which is therefore much greater than R23, then R23 will not introduce a dependence on transistor characteristics of the signal size at the base of T2. A consideration of the bias resistors R24, R25 will show however that their load will introduce a small attenuation of the signal size on passing through R23. Now the load seen by the signal between the emitter of T2 and earth is R27, which is much greater than the incremental emitter resistance, thus the voltage amplification of this stage is $\sim -$ R28/R27 $\sim -$ 6.5. The signal at the collector of T2 is fed through transistors T3 and T4 which act as a unity gain compound emitter follower, the output impedance at the emitter of T4 being very small and so the output impedance at 'a' and 'b' is defined by the resistors R31, R32, each being 100 Ω .

Thus an amplifier so constructed and with switch S2 in the closed position and S4 open will, when fed with an input

step function, provide an output pulse with a rise time of less than 100ns, and a decay time constant of ~400 /us. The fast rise time was desired to allow the amplifiers to be used with coincidence units employing resolving times as short as 100ns should this have proved necessary. As previously mentioned the long fall time was also desired to allow the amplifiers to be used with the Owen[42] technique of pulse shape discrimination. However most commonly the amplifiers were operated with S2 open and S4 closed, the 0.8 /us differentiation time constant so employed reducing the low frequency noise and giving a negative undershoot to the pre-amplifier pulses thus improving base line stability at high count rates and for large overloads. The 0.8 /us integration time constant also so employed provided high frequency noise attenuation and produced a suitably shaped pulse for pulse height analysis and for operation with coincidence units employing the (ultimately) chosen resolving time of ~1/us.

The maximum overall voltage gain of the amplifier (with S2 closed and S4 open) is ~ x 350. Using S1, S3 the gain may be adjusted in 14 2dB attenuating steps to 1/25 of this value. The maximum output voltage before limiting is +14V. The linearity of the output up to +10V was checked for one of the amplifiers at maximum gain but with the 0.8/us differentiation and integration switched in, this being done by feeding a constant size pulse from a pulse generator via a precision variable attenuator to the input of the amplifier. The output signal size from the amplifier was measured in a 512 channel analyser,

while the attenuation was adjusted in calibrated (to a 1% accuracy) steps. Within the accuracy of the technique the amplifier was found to be linear. Further to check the resolution of the present design of amplifier, one was connected via a pre-amplifier to a photomultiplier with a sodium iodide scintillator, the output of the amplifier being displayed in a multi-channel analyser. By employing a ^{60}Co source which emits γ-rays of 1.33 and 1.17 MeV energy, one may obtain a sensitive measure of the resolution of the system from the ratio of the height of the 1.33MeV photopeak to the height of the valley between it and the 1.17MeV photopeak. In this test the amplifier of the present design was found to compare more than favourably with a commercial transistorised pulse amplifier available on loan. Finally it should be noted that since the output impedance at the emitter of T4 is near zero, there should be little coupling between the outputs 'a' and 'b'. This was checked by placing a 100Ω load on one putput and thereby reducing the associated pulse height by one half, while the pulse height from the other output was found to remain constant within $\sim$1%.

3.5 The Pulse Shape Discrimination Unit

The technique employed to provide pulse shape discrimination between γ-rays and neutrons in the present study has been outlined in section 2.3 and is similar to that investigated by Roush et al.[43]. The circuitry designed to exploit this

technique in the present experiment is described below, reference being made to the circuit diagram of figure 22, and to the pulse shapes in the unit as sketched in figure 23.

The positive current pulses from the photomultiplier's 11th dynode are integrated in the pre-amplifier then fed along a cable with a characteristic impedance of 100 Ω to the matching resistor network R1, R2, R3 (of figure 22) which feeds the signal (of shape 'a' in figure 23) to the base of transistor T2 and also to the input of the amplifier. Transistors T1 and T2 act as an inverting cascade type amplifier, this configuration being chosen to allow a high gain without introducing a large capacitance across the input due to Miller effect. Resistor R7 in series with capacitor C2 is effectively the signal load between the emitter of T2 and earth, thus providing the desired differentiation with a time constant given by the product of R7 and C2, and hence causing the pulse to cross-over the zero amplitude axis. The load resistor R6 seen by the signal at the collector of T1 is effectively shunted by the pair of fast silicon clipping diodes D1 and D2, limiting the signal size to $\pm$ 0.6 Volt at this stage, and further preventing transistor T1 from being driven into saturation by large signals which might thereby have their zero cross-over time altered due to charge storage effects. The shape of a signal at the collector of T1 so clipped is shown in 'b' of figure 23.

Transistor T3 now further amplifies and inverts the pulses,

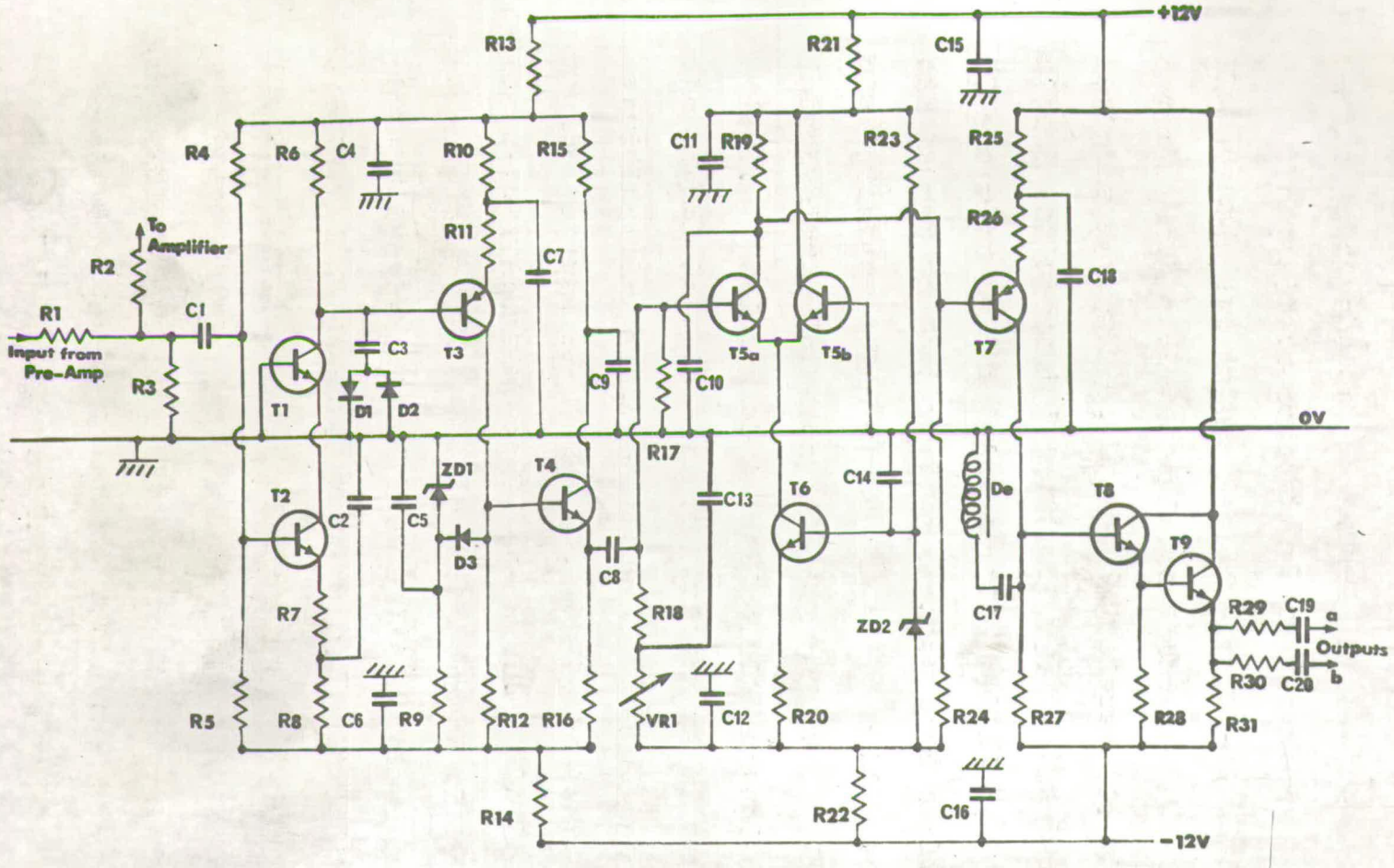

R1 = 33Ω	R12 = 1.5kΩ	R23 = 4.7kΩ	C1 = 0.22μF	C12 = 2.2μF	T1 = BFY75	D1 = 1N251
R2 = 33Ω	R13 = 68Ω	R24 = 18kΩ	C2 = 6000pF	C13 = 2.2μF	T2 = BFY75	D2 = 1N251
R3 = 150Ω	R14 = 68Ω	R25 = 680Ω	C3 = 0.22μF	C14 = 0.22μF	T3 = BFX48	D3 = 1N251
R4 = 15kΩ	R15 = 680Ω	R26 = 270Ω	C4 = 2.2μF	C15 = 2.2μF	T4 = BFY75	ZD1 = BZY88-C4V3
R5 = 3.9kΩ	R16 = 680Ω	R27 = 4.2kΩ	C5 = 0.22μF	C16 = 2.2μF	T5 = 2C444	ZD2 = BZY88-C4V3
R6 = 1.8kΩ	R17 = 10kΩ	R28 = 3.3kΩ	C6 = 2.2μF	C17 = 0.22μF	T6 = BFY74	
R7 = 68Ω	R18 = 33kΩ	R29 = 82Ω	C7 = 2.2μF	C18 = 0.01μF	T7 = BFX48	
R8 = 1.5kΩ	R19 = 2.2kΩ	R30 = 82Ω	C8 = 0.22μF	C19 = 0.22μF	T8 = BFY75	
R9 = 4.7kΩ	R20 = 1.2kΩ	R31 = 1.2kΩ	C9 = 0.22μF	C20 = 0.22μF	T9 = 2N1711	
R10 = 1.2kΩ	R21 = 100Ω		C10 = 1500pF			
R11 = 100Ω	R22 = 100Ω	VR1 = 1M	C11 = 2.2μF			

FIG. 22 THE PULSE SHAPE DISCRIMINATION UNIT

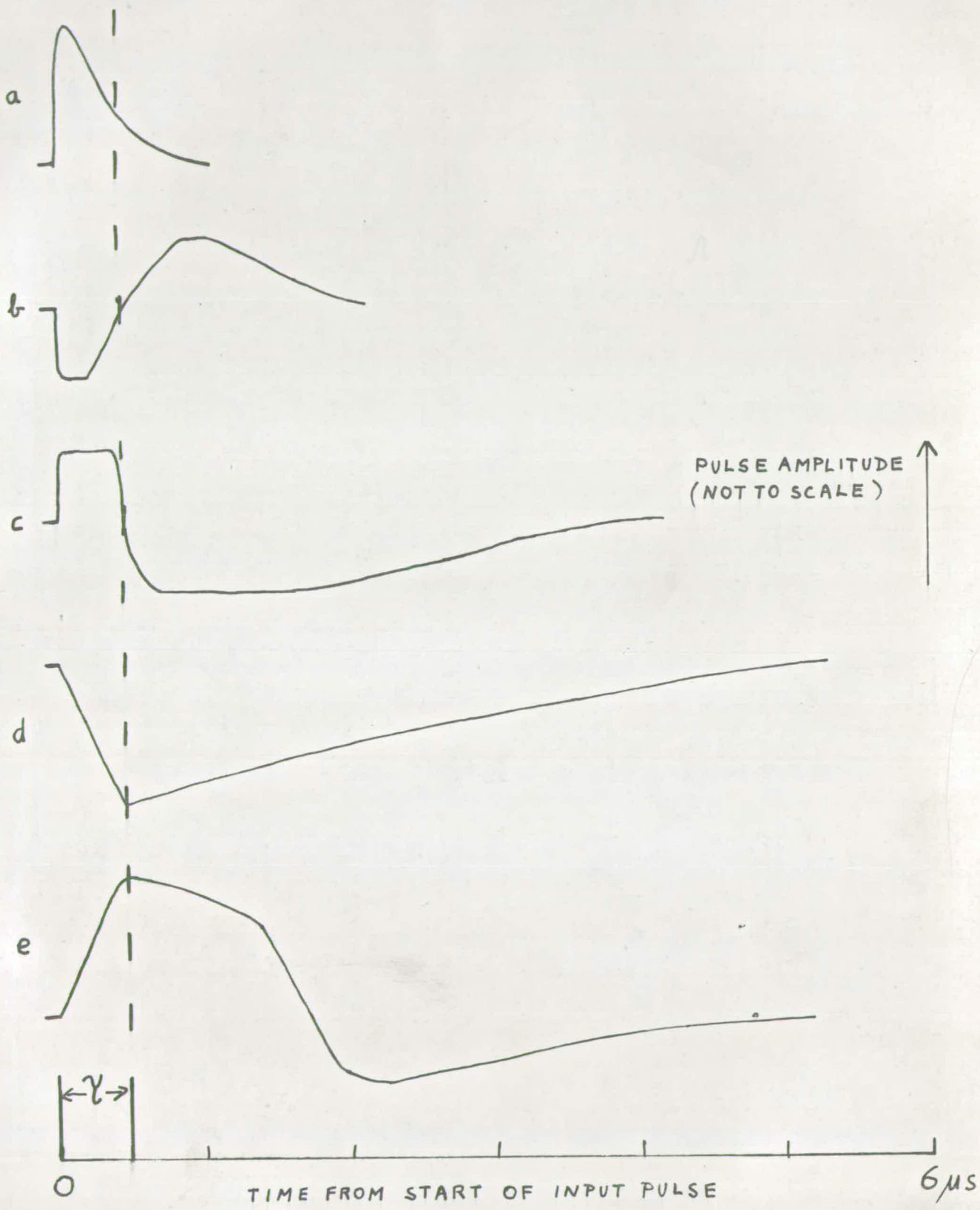

FIG. 23 SKETCH OF PULSE SHAPES IN P.S.D. UNIT

the output being limited in its positive swing by diodes D3 and ZD1 (a voltage reference diode) and in its negative swing by the switching off of T3. Thus a signal so limited is of shape 'c' in figure 23, and this is passed via the emitter follower T4 to the base of T5a.

Transistors T5a, T5b and T6 now serve as a time to amplitude converter (T.A.C.), producing an output pulse whose amplitude is proportional to the zero crossover time γ shown in figure 23. Thus T6 acts as a constant current source feeding the dual transistor T5a,b, and since resistors R17, R18, VR1 serve to keep the base of T5a slightly more negative than that of T5b, then all of the current from T6 passes through T5b. However, the arrival of a positive pulse at the base of T5a switches all of this current through T5a, thus charging up capacitor C10 during the time which the input pulse remains (ideally) greater than zero. The discharge time constant of this capacitor is given approximately by the product of C10 and R19, since the input impedance of the following stage is R19. Thus at the collector of T5a we have signals of shape 'd' in figure 23. Now throughout the input amplifying stages of the P.S.D. unit the coupling time constants have been kept deliberately long to avoid introducing sizeable positive overshoots on the tail of the pulses applied to the T.A.C. stage. However with large input pulses, small overshoots occur, and so resistor VR1 is set to require a small positive voltage step ($\sim$ 0.1V) before the T.A.C. will switch, in order

to inhibit triggering due to such overshoots and/or noise. Thus in practice the time measured is not quite the zero crossover time.

The output from the T.A.C. stage at the collector of T5a is fed to transistor T7 which inverts and amplifies it. Its collector load is a 0.5 μs delay (De) with a matching resistor at its input and a short at its far end. This serves to clip the length of the pulses from the T.A.C., thus reducing the chance of a γ-ray event sitting on the tail of a previous pulse and thereby producing an output signal as large as that due to a neutron. As in the amplifier output, a pair of transistors (T8, T9) are now employed as a compound emitter follower giving two outputs 'a', 'b' with nominal 100 Ω output impedances. The shape of the signal at these outputs is of type 'e' in figure 23.

The selection of suitable time constants for the RC integration in the input circuit of the pre-amplifier and for the RC differentiation in the first stage of the P.S.D. unit will obviously depend on their ability to provide good time separation of the zero crossovers due to neutrons and γ-rays. A second important criterion to be considered is the slope of the shaped pulses at the zero crossover, since a steep gradient will minimise time 'jitter' caused by the finite (non-zero) level at which a practicable zero crossover detector operates (e.g. the present T.A.C.). Roush et al.[43] have defined a figure of merit for the selection of these shaping

networks to be the product of the time separation at zero crossover between a neutron and a γ-ray event, and the slope of the shaped pulse at zero crossover (for a standard unshaped size). Using the data of Peuckert[45] relating to the decays of the scintillations due to neutrons and γ-rays in Ne213, Roush et al.[43] have computed such figures of merit with the differentiation and integration time constants as independent variables, the results being plotted in a contour diagram. This diagram shows that using RC shaping as described above, the figure of merit is a maximum for an integration time constant $\sim$ the differentiation time constant $\sim 0.4/\mu s$. Thus the differentiation time constant of the P.S.D. unit was selected to be $\sim 0.4/\mu s$, and a 15kΩ resistor was placed across the input of the pre-amplifiers used, thus reducing their input impedance to provide a similar $\sim 0.4/\mu s$ integration time constant.

A pulse height spectrum of the output from the P.S.D. unit is displayed in figure 8, the source and gating level allowing a convenient comparison with other published spectra (e.g. Nadav and Kaufman[46], and Schweimer[47]). The pulse height spectrum shown in figure 24 was taken also with a Po-Be source, however the multichannel analyser was gated to accept events in the scintillator with a light output greater than that due to $\sim$100 keV recoil electrons, this being the linear bias level used in the present experiment. This shows the satisfactory performance of the circuit with such a lower level, and with a count rate of $\sim 3 \times 10^3$/S (the maximum obtainable with the source

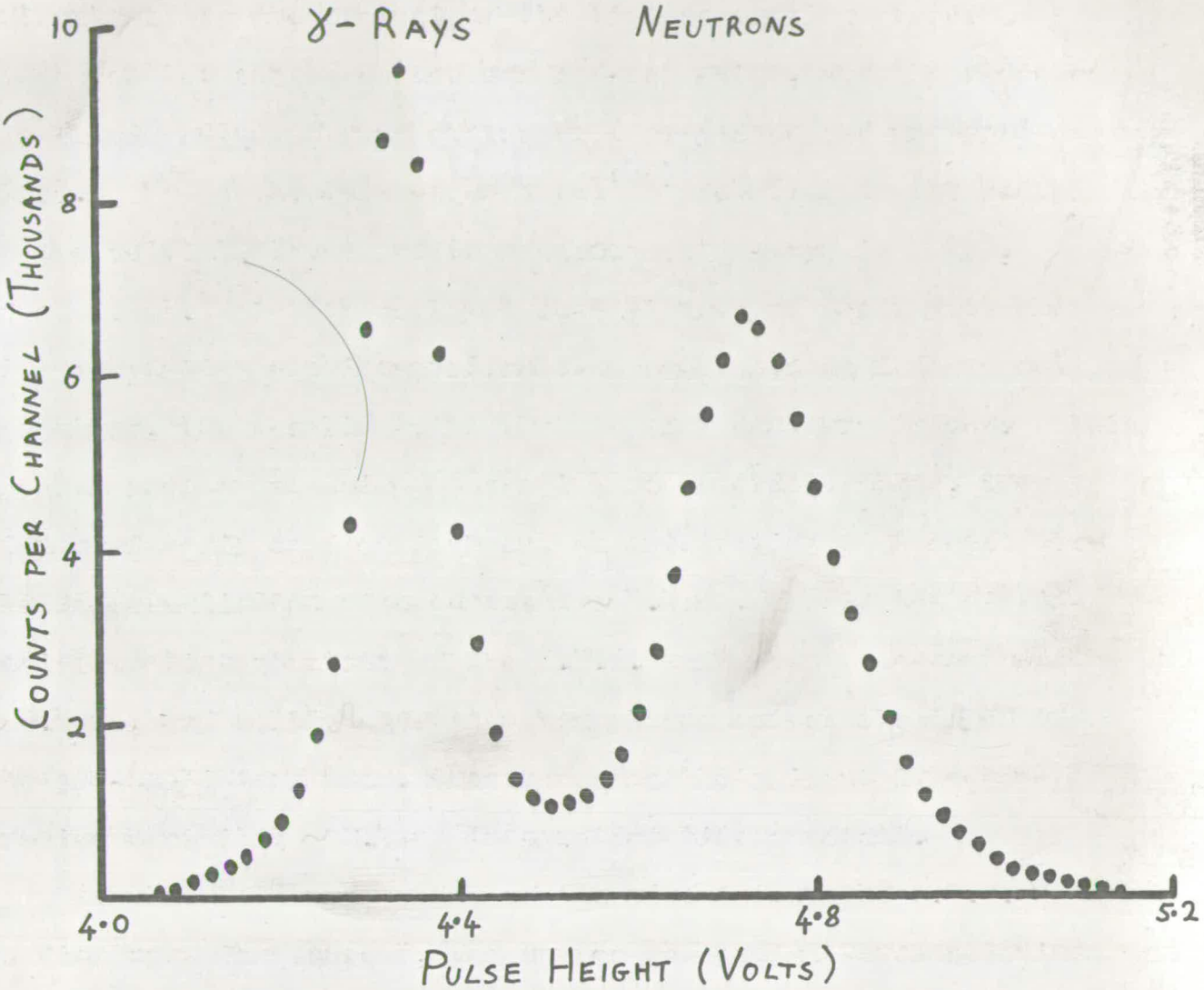

FIG. 24 PULSE HEIGHT SPECTRUM OF THE OUTPUT FROM THE PULSE SHAPE DISCRIMINATION UNIT, ONLY EVENTS WITH A LIGHT OUTPUT GREATER THAN 100 keV RECOIL ELECTRONS BEING RECORDED. Po-Be SOURCE.

used), greater than that normally encountered in the present series of measurements.

3.6 The Integral Discriminator

The construction of an integral discriminator (with its associated delay and shaping circuitry) is shown in figure 17, and a circuit diagram is displayed in figure 25, an explanation of the logic symbols utilised in this and in following circuit diagrams being provided by figures 26 and 27.

This unit provides for the conversion of an input pulse, when it exceeds a selected level, into a standard size ('logic') pulse. This pulse is passed through a variable delay to allow flexibility of use in coincidence experiments, the output being of a standard height and duration, thus allowing it to be fed into an 'And' gate which will act as a coincidence unit.

A μA710C type integrated circuit comparator‡ was chosen to convert the analogue signal into a logic pulse. This integrated circuit is basically a high gain operational amplifier with a differential input, thus only a few millivolts of difference across these inputs is required before the output voltage limits. The μA710C has been so designed as to have an output voltage swing in going from one such limiting state to the other (induced by an input signal of opposite polarity) compatible with most commonly used integrated circuit logic families. Further it will change its output state (for a few

‡ Footnote: Originally manufactured and marketed by the Fairchild Camera and Instrument Corporation (U.S.A.)

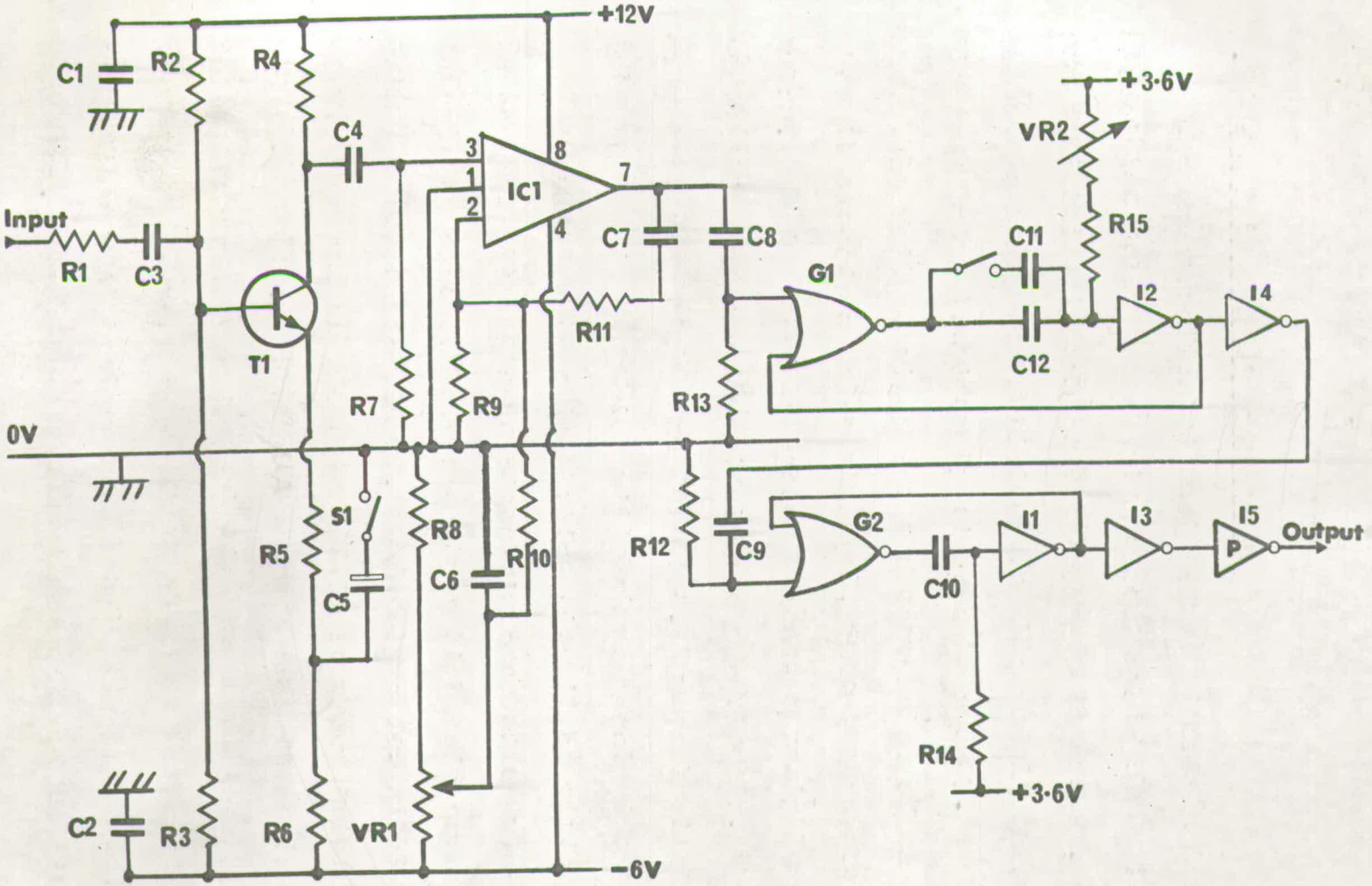

R1 = 3kΩ	R7 = 330Ω	R13 = 1kΩ	C1 = 2.2μF	C7 = 100pF	T1 = BFY75
R2 = 2.7kΩ	R8 = 120Ω	R14 = 1kΩ	C2 = 2.2μF	C8 = 50pF	IC1 = μA710C
R3 = 1.1kΩ	R9 = 330Ω	R15 = 1kΩ	C3 = 0.47μF	C9 = 25pF	
R4 = 1.5kΩ	R10 = 3.3kΩ		C4 = 1μF	C10 = 1000pF	
R5 = 270Ω	R11 = 1kΩ	VR1 = 500Ω	C5 = 4μF	C11 = 500pF	
R6 = 820Ω	R12 = 1kΩ	VR2 = 5kΩ	C6 = 1μF	C12 = 125pF	

FIG. 25 THE INTEGRAL DISCRIMINATOR

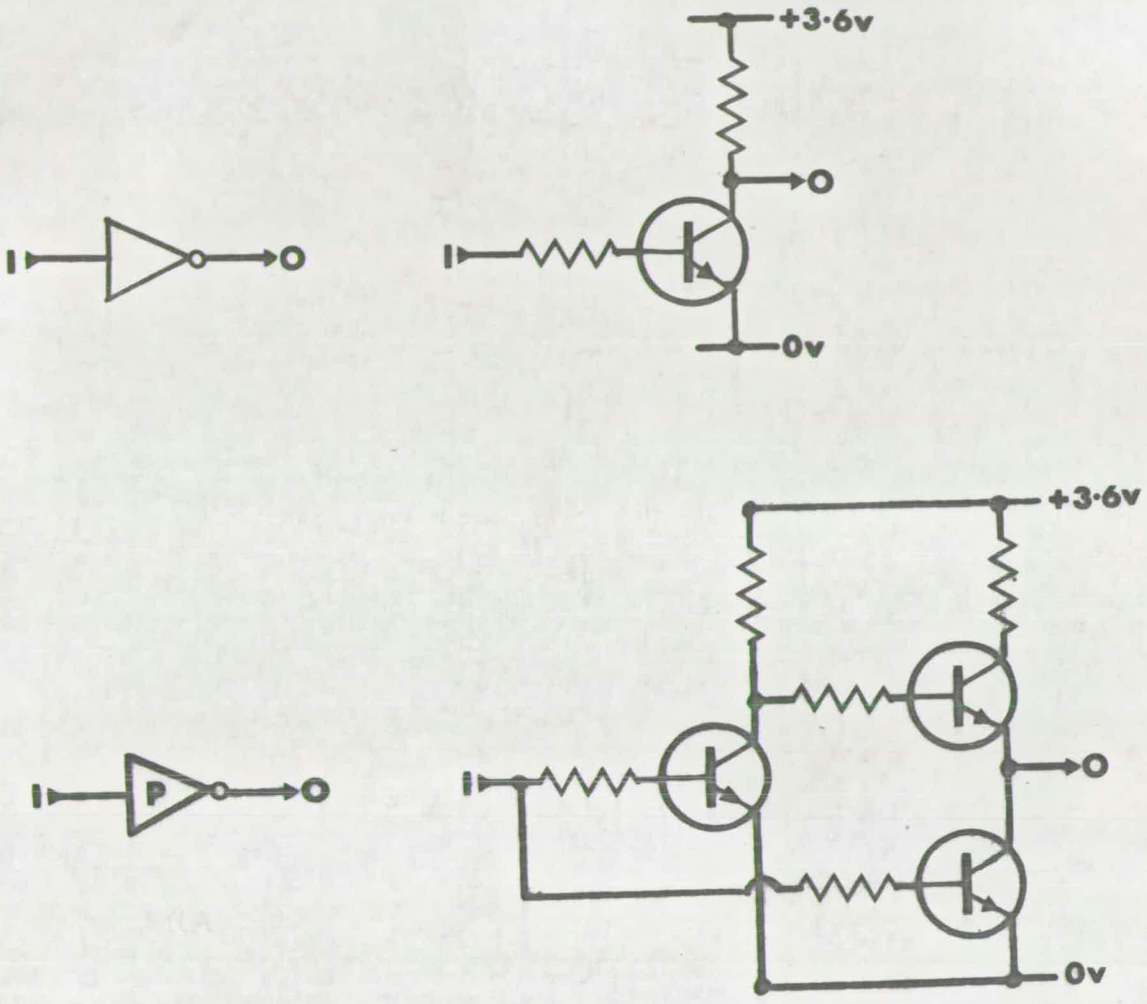

FIG. 26 RESISTOR-TRANSISTOR-LOGIC INVERTERS
UPPER DIAGRAM = ONE QUARTER OF A µUL927
LOWER DIAGRAM = µUL900

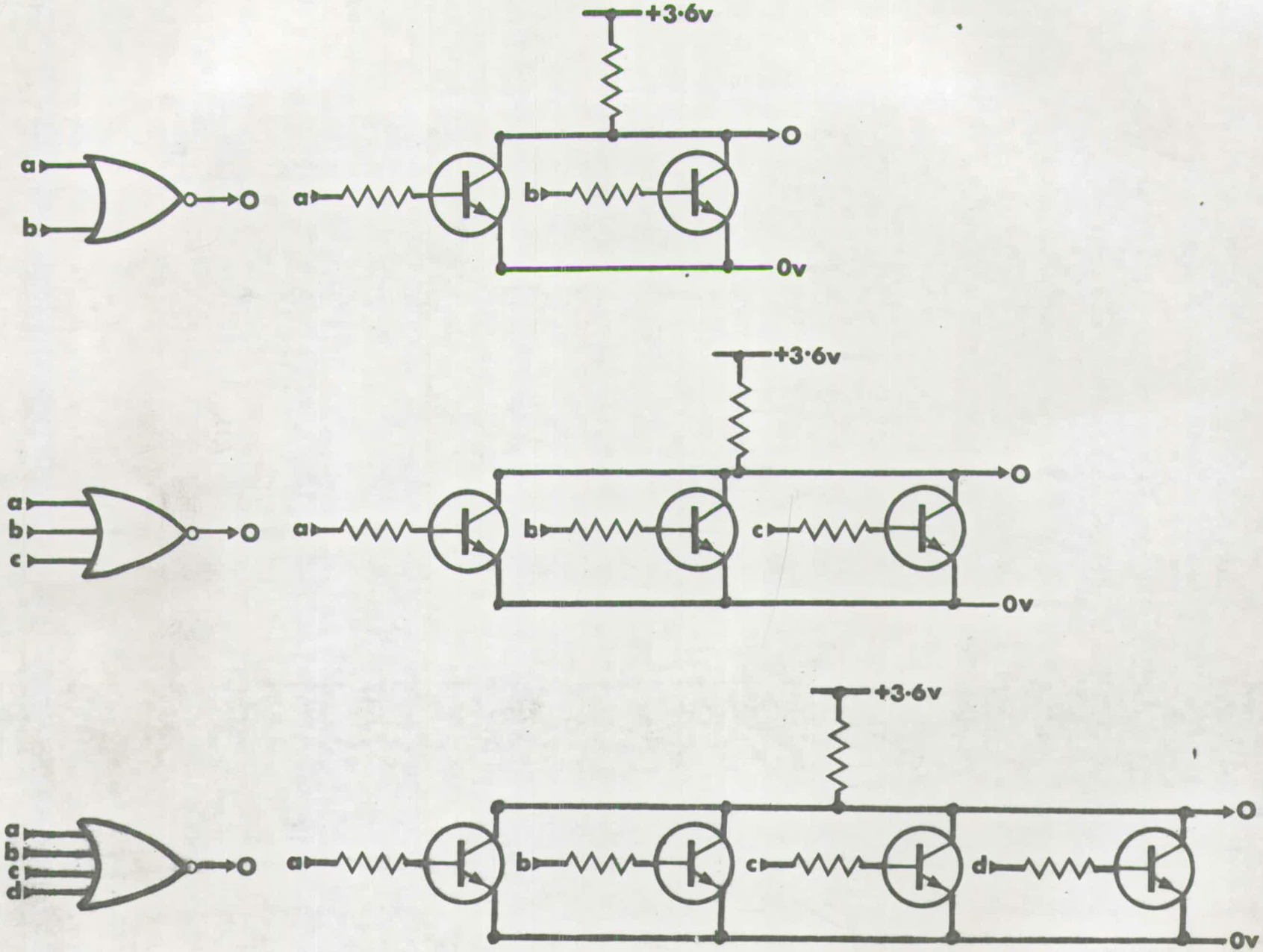

FIG. 27 RESISTOR-TRANSISTOR-LOGIC GATES
UPPER DIAGRAM = ONE HALF OF A µL914 : CENTRE DIAGRAM = µL903 : LOWER DIAGRAM = µL907

millivolts differential input) in ~40ns, a performance which may be much improved by the use of positive feedback.

The logic circuitry into which this comparator drives, and indeed the logic circuitry used throughout the electronic units described in this chapter, employs medium power elements from the Resistor-Transistor Logic (R.T.L.) family‡ of integrated circuits as shown in figures 26 and 27. R.T.L. was chosen in preference to other logic families available at the time of design inception on the grounds of its convenience in the construction of monostable circuits. However all the R.T.L. outputs from the presently described series of units come from buffer stages of the type shown in the lower half of figure 26, thus providing adequate drive to other R.T.L. circuits or to operate the now more popular Transistor-Transistor Logic (T.T.L.) family. To obtain a power supply of +3.6V to supply the R.T.L. elements, each module containing these circuits also possesses a circuit of the type shown in figure 28, which provides a stabilised + 3.6V supply from the +12V rail.

Thus the circuit of figure 25 operates as follows, reference being made to the pulse shapes labelled 'a', 'b' etc. shown in figure 29. The input pulses of shape 'a' say (from an amplifier or pulse shape discrimination unit) are fed to the base of T1 which inverts them and allows switch (S1) selectable attenuation. A negative potential selected using the ten turn helical potentiometer VR1 is applied to the non inverting input

‡ Footnote: Originally manufactured and marketed by the Fairchild Camera and Instrument Corporation (U.S.A.)

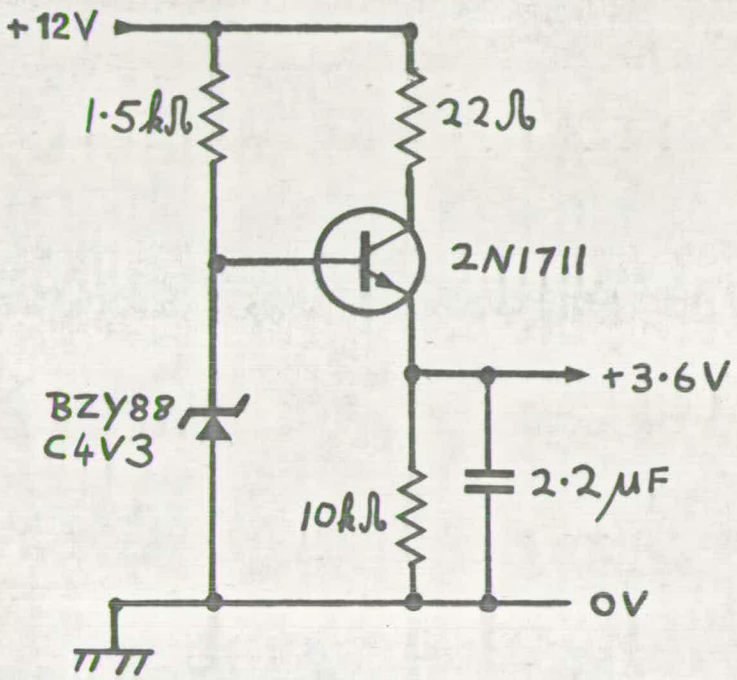

FIG. 28 CIRCUIT TO PRODUCE A +3.6V SUPPLY FROM A +12V SUPPLY

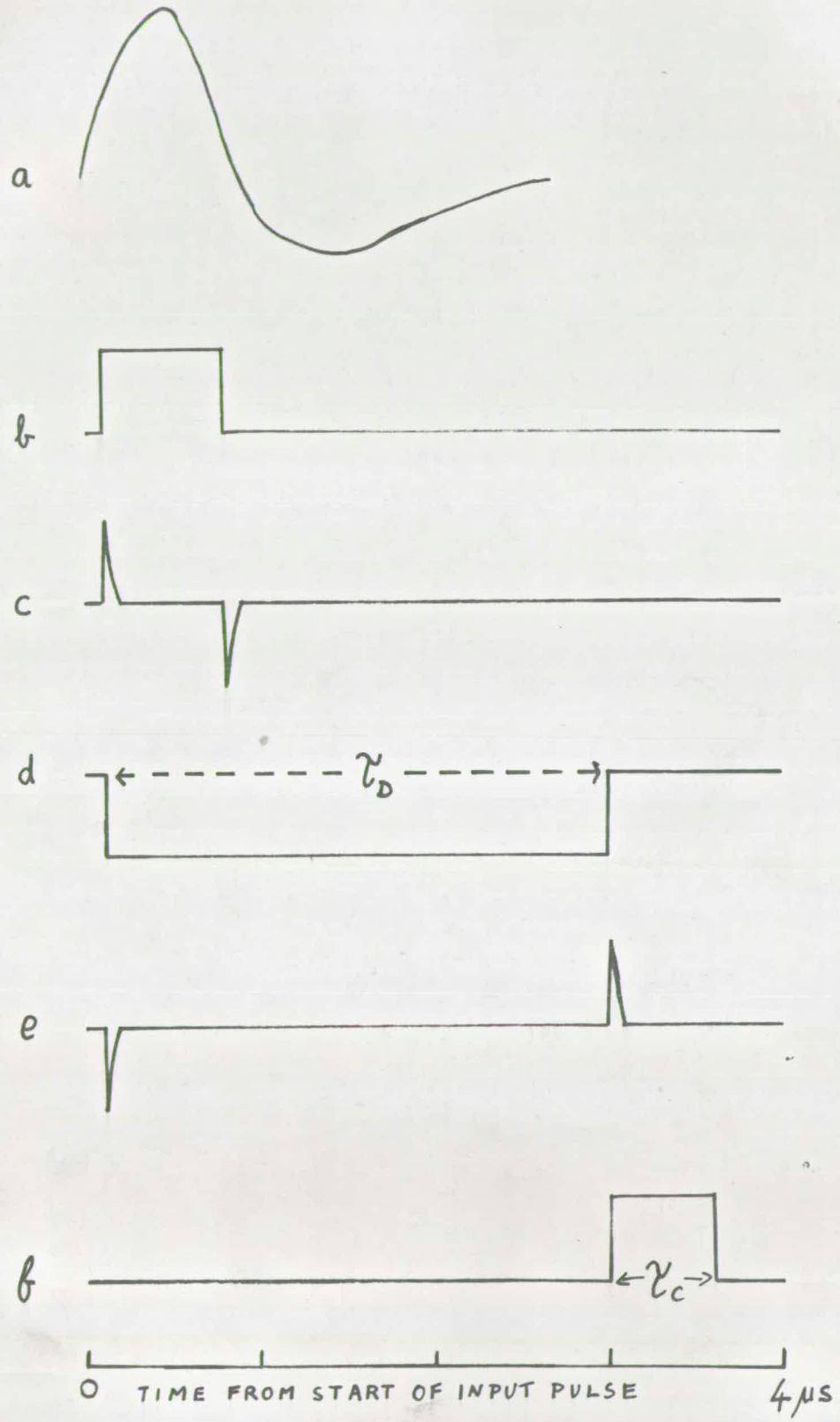

FIG. 29 SKETCH OF PULSE SHAPES IN DISCRIMINATOR

of IC1 (/uA710C), and thus when a pulse from T1 applied to the inverting input of IC1, becomes more negative than this selected potential, then the output of the comparator (IC1) will commence to change state, this change being speeded by the positive feedback provided by R11 and C7. Thus we obtain an output from IC1 (pin 7) of shape 'b' in figure 29, this occurring when the input pulse to the unit exceeds a level set (by VR1) in the range of from 0.5V to 2.75V (approx.) with S1 closed, or from 2V to 11V (approx.) with S1 open.

These pulses of type 'b' are RC differentiated and applied (as shown in 'c' of figure 29) to the input of G1, the positive spikes so produced triggering the monostable formed by G1 and I2 whose period (γ_D) is defined by C11, C12, R15, VR2. I4 inverts the output from I2 thus providing negative pulses of length γ_D as shown in 'd'. These pulses are further RC differentiated as shown in 'e', and applied to the input of G2 which together with I1 forms a monostable of period γ_C defined by C10 and R14. This monostable is only triggered by a positive spike which arises from the rear edge of the pulse from the previous monostable, thus producing the desired delay γ_D which may be varied from 0.1/us to 0.6/us using VR2, these values being multiplied by a factor of ~5 on placing C11 in parallel with C12 by closing the associated switch.

Now the output from I1 is followed by two stages of inversion I3, I5, the latter stage being a buffer element, thus a fast rise and fall time (~10ns) positive output pulse, as in 'f'

of figure 29, is obtained with adequate current drive. Now these output pulses are often fed into a coincidence unit (as described below) which operates by providing an output when signals from the desired sources overlap in time. Thus clearly our resolving time will depend on the width (τ_c) of the discriminator output pulses. In practice a τ_c of $\sim$0.6/us was found convenient.

The pulse height resolution of the integral discriminator may be checked by feeding both a multichannel analyser and an integral discriminator from an amplifier connected (say) via a pre-amplifier to a scintillation detector. Then using the output from the integral discriminator to 'gate' the multi-channel analyser, one may examine the 'sharpness' of the cut off so produced in the multi-channel analyser spectrum. Typically with the present discriminator it was found that such a cut off could be set to occur within one channel (10 millivolts) for discriminator levels of around 5 Volts. The stability of the discriminator level depends on the -6 Volt stabilised power supply rail which it uses as a reference. Typically such commercially available power supplies quote stabilities of 0.001% against a 10% fluctuation in mains voltage. Further to reduce the possibility of fluctuations in this level due to large load variations, this -6V supply was reserved solely to supply these integral discriminators.

3.7 The Triple Coincidence Unit.

Two triple coincidence units were constructed in each module as shown in figure 30. The operation of a single unit is described below, reference being made to the circuit diagram of figure 31.

With all three inputs (1,2,3) connected to discriminators (of the type described in the previous section) and with all switches S1,2,3 in the 'a' position, then with no positive pulses arriving from the discriminators, the output of the three input gate G1 will be at near zero potential. A positive pulse will be required from all three discriminators in order to provide a near zero potential at all three inputs of G1 and so raise its output state to a positive level. Alternatively, by suitably changing the switch positions we may produce an output for positive input pulses arriving from any one or any pair of discriminators. In the coincidence mode (dual or triple) the length of the output pulse from G1 is equal to the overlap time of the pulses from the discriminators. In order to produce a standard output pulse shape from the coincidence unit, the positive leading edge (after RC differentiation) of the output from G1 is used to trigger the monostable formed by G2 and I4, thus giving a positive output pulse of $\sim 1\,\mu s$ length.

Throughout this discussion the finite rise time of the input pulses has been ignored as has the time to change state of the logic elements. This however is reasonable since both of these times is $\sim$ 10ns compared to the $0.6\,\mu s$ length of the

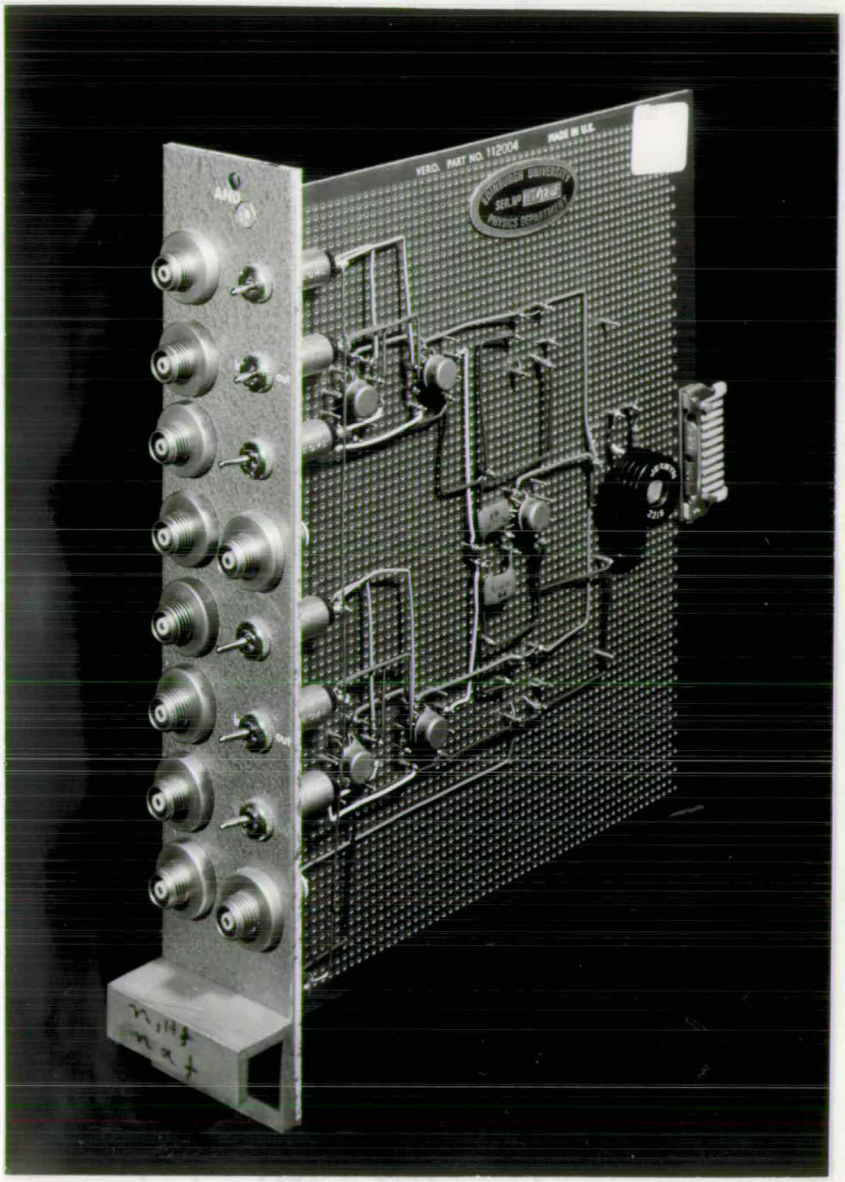

FIG. 30 PHOTOGRAPH OF A MODULE CONTAINING TWO TRIPLE COINCIDENCE UNITS

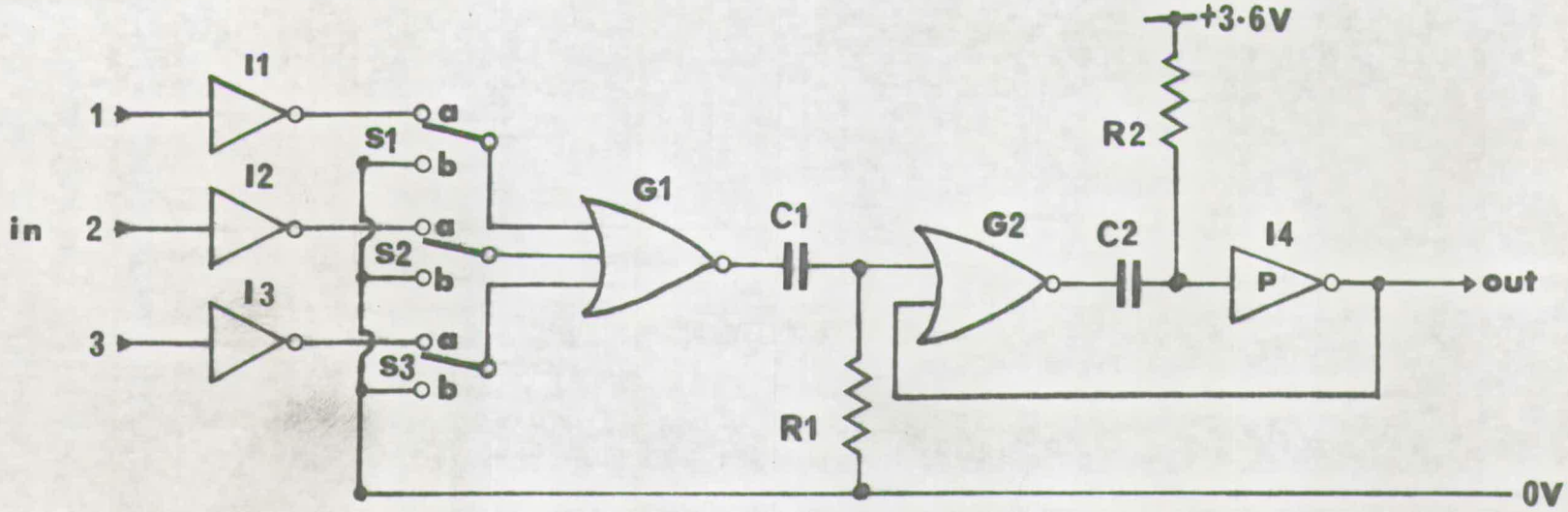

R1 = 1kΩ C1 = 50pF
R2 = 1kΩ C2 = 1000pF

FIG. 31 THE TRIPLE COINCIDENCE UNIT

input pulses.

3.8 The Delay Unit

To give a variable delay to the output pulses from a coincidence unit or discriminator as described above, a further discriminator unit may be employed with its level set to accept these logic pulses. This procedure was used to produce the additional delay in the gas scintillator channel shown in figure 14 for the purpose of determining the random rates. However in order to save space the two delay units after the coincidence units in this diagram were constructed in a single module, their circuits being similar to the logic circuitry employed in the discriminator after the comparator stage with minor additions.

3.9 The Multi-channel Analyser Coding Unit.

In many modern multi-channel pulse height analysers, a facility is provided whereby one may route the input analysed pulses into various sections of its channel storage or indeed inhibit it from carrying out the pulse height analysis at all, depending on the gating signals associated with the input pulse to be analysed. To achieve the desired routing, the gating pulses must be of the correct size and shape, and must be applied in a certain coded pattern to the routing inputs on the multichannel analyser. The unit described in this present section accepts the four gating outputs as shown

in figure 14 and described in section 3.1 and performs the coding in a flexible manner which allowed the splitting up of the channel storage of both the 512 channel Laben analyser initially used into sections of 64 or 128 channels, and the 400 channel Laben analyser finally employed into sections of 100 channels.

A circuit diagram of the coding unit is shown in figure 32, and an examination of this circuit will show that:
A positive input pulse at '1' will produce a similar pulse at both 'A' and 'B'.
A positive input pulse at '2' will produce a similar pulse at both 'A' and 'C'.
A positive input pulse at '3' will produce a similar pulse at both 'A' and 'D'.
A positive input pulse at '4' will produce a similar pulse at 'A', 'B' and 'D'.

The suitably coded signals at A, B, C, D are fed to a multi way connector at the rear of their module and hence to a module containing circuits to be described in the following section which change these R.T.L. pulses to a size and shape suitable for driving the routing inputs of the multi-channel analyser. Further the outputs 01, 02, 03, 04 from the coding unit which reproduce their respective inputs 1, 2, 3, 4 are fed to the front panel of the unit through a set of relay controlled switches (not shown). These outputs were fed to scalers and so allowed a monitoring of the progress of a measurement to be made

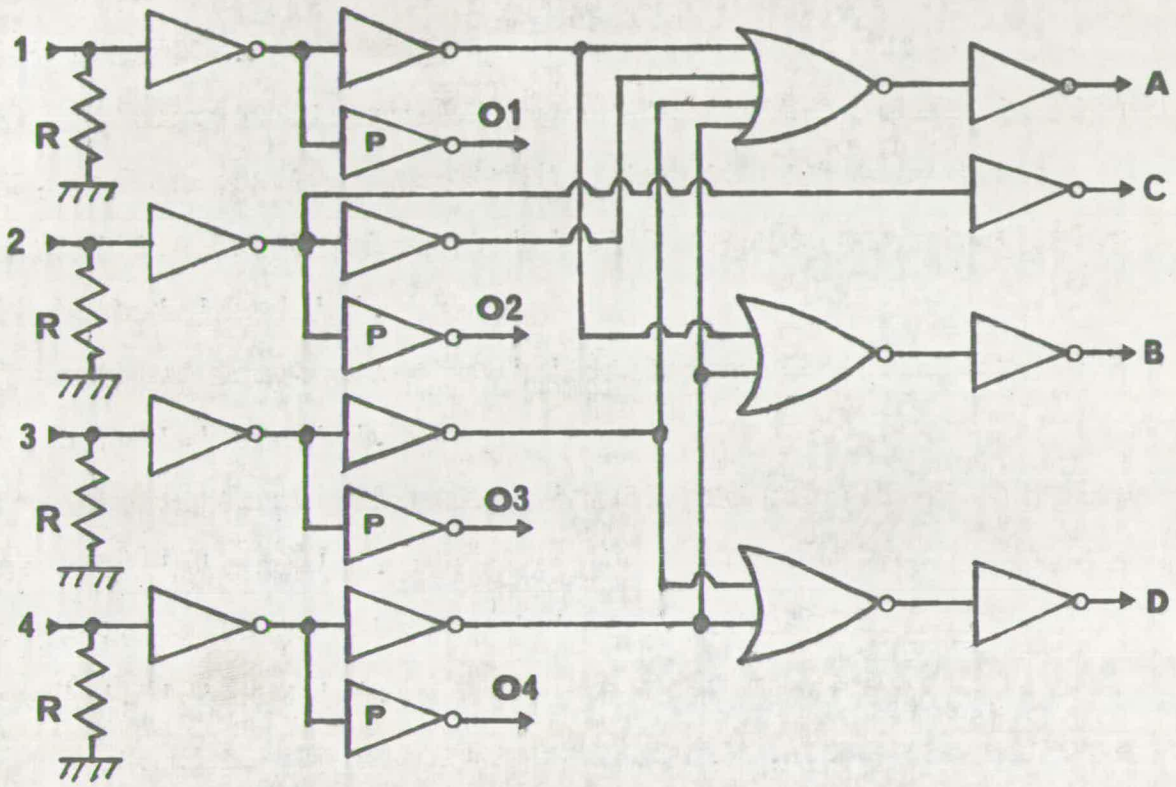

R = 120 Ω

FIG. 32 THE MULTICHANNEL ANALYSER CODING UNIT

and a check to be performed on the gating of the multichannel analyser. As a further convenience the relay connecting these outputs to the scalers was driven by circuitry (not shown) controlled from the pulse height analyser, and thus when the analyser count ceased (e.g. in order to print out the data stored) so also did the counting in the scalers.

3.10 The Multi-channel Analyser Shaping Unit.

The circuit described in this section was designed to accept pulses from discriminators, delays, coincidence units or the coding unit (all as described in the present chapter) and to produce from these, suitably shaped pulses to apply to various routing and coincidence inputs in both the Laben 400 and 512 channel analysers used in the present investigation. The circuit of one such shaping unit is shown in figure 33, four of these units being contained in the module shown in figure 34.

The input '1' of figure 33 is taken to a socket on the front panel of its module, while input '2' goes to a multi way connector at the rear of the module and so is connected to one of the four signal streams A, B, C, D from the coding unit. Thus one may drive the shaping unit directly from a socket on its front panel (when e.g. a simple coincidence spectrum is desired), or one may drive it through the coding unit to provide full routing facilities.

Thus an input positive pulse at either '1' or '2' will

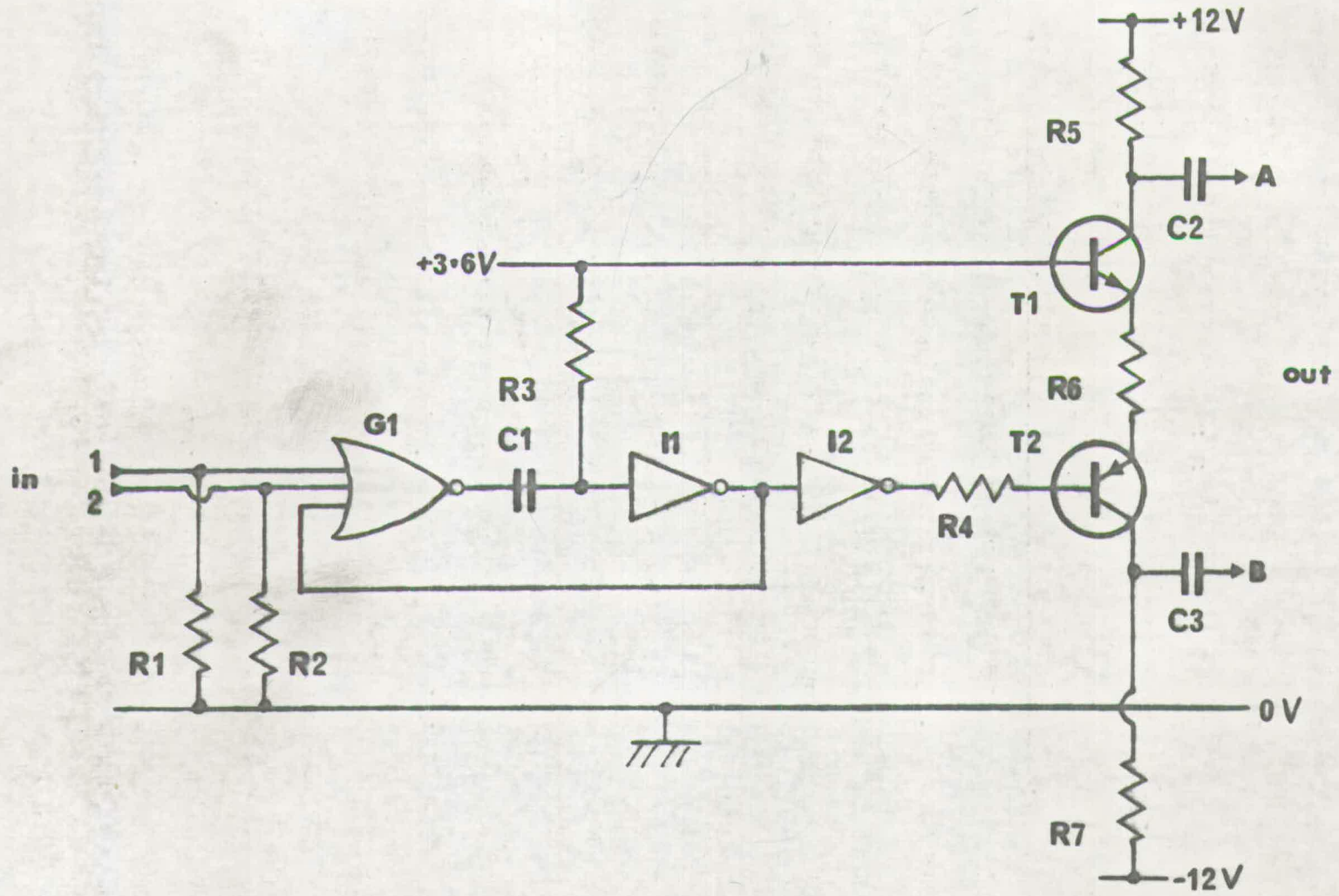

R1	= 120 Ω	R5	= 100 Ω	C1	= 1000pF	T1	= 2N1711
R2	= 1k Ω	R6	= 33 Ω	C2	= 0.1μF	T2	= 2N1132
R3	= 4.7k Ω	R7	= 100 Ω	C3	= 0.1μF		
R4	= 100 Ω						

FIG. 33 THE MULTICHANNEL ANALYSER SHAPING UNIT

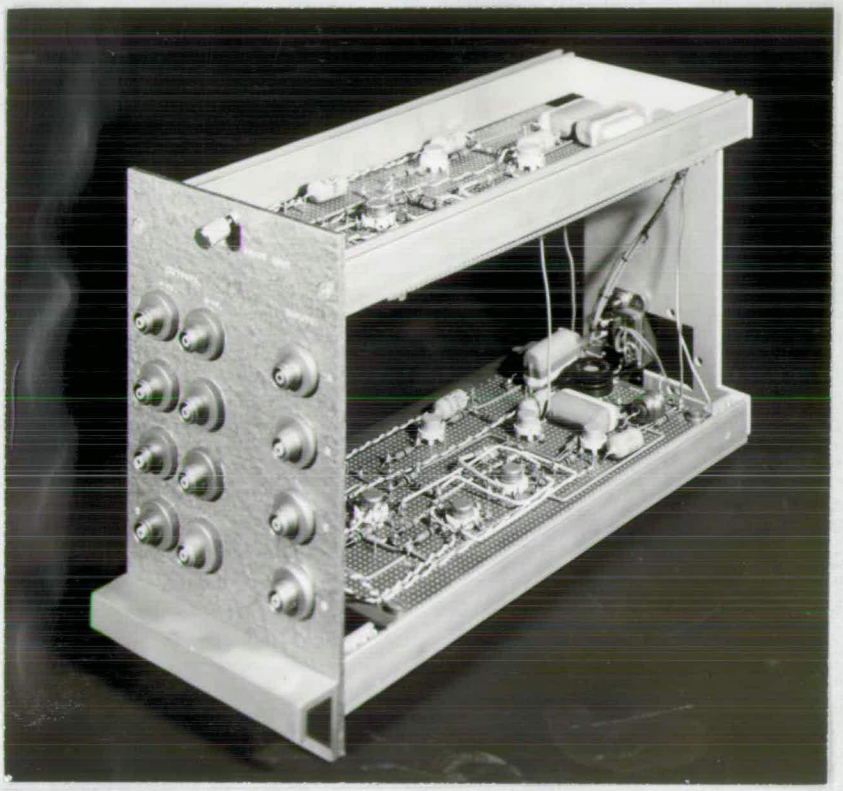

FIG. 34 PHOTOGRAPH OF A MODULE CONTAINING FOUR SHAPING CIRCUITS

trigger the monostable formed by G1 and I1, its period of ~3/us being defined by R3 and C1. I2 acts as an inverting stage, its output level switching from +3.6V to near zero and remaining so for the duration of the monostable period. Transistors T1 and T2 which are initially off are switched on by this pulse, and act as a pulse amplifying stage with complimentary outputs. Thus a negative 7Volt pulse of 3/us duration appears at 'A' and a similar but positive pulse at 'B', the former being the desired shape to operate most routing inputs on the analysers, the latter being required when it is desired to use the four input mixer in a coincidence mode on the 512 channel analyser. Since neither of the output transistors T1, T2 are driven into saturation, the output impedance at both 'A' and 'B' is merely their respective transistor's collector load, namely 100Ω. Thus they may be used to drive the pulse height analysers along long lengths of 100Ω cable without loss of pulse fidelity at the receiving end.

CHAPTER 4

The Operation of the Fast Neutron Polarimeter

The previous chapters have described the construction of the polarimeter with its associated electronic circuitry used to obtain the final results in the present investigation. The current chapter will relate the investigations made with or associated with the present polarimeter and will consider the data handling techniques evolved and the reliability of the system.

4.1 Count Rates and the Selection of Resolving Times

Although in the previous chapter it was indicated that a $\sim 1/\mu s$ resolving time was used in the coincidence circuitry associated with the polarimeter, this circuitry was designed to allow a flexible choice of resolving time depending on the experimentally observed count rates. The RF ion source supplying the Cockcroft-Walton was theoretically capable of providing ion beams of up to 1mA, however experimentally a $50/\mu A$ beam on target was found to be a more realistically obtainable maximum. Thus such a beam accelerated through a 600kV potential and incident upon a thick titanium - deuterium target produces what is representative of the highest neutron yields at which measurements were performed. Yet under such conditions, the typical count rate in a liquid scintillator mounted within the polarimeter and shielded as described in chapter 2 was $\sim 10^3/S$ for events with a light output in the

scintillator greater than that due to 100keV recoil electrons, and this reduced to $\sim 10^2$/S on the rejection of γ-rays by the pulse shape discrimination circuit (usually set to reject ~98% of the γ-rays from a test source of ^{60}Co). Thus at such modest count rates the dead times of a few microseconds in the associated electronic circuitry are of no consequence and gain variations in the neutron detectors and their associated electronics due to count rate fluctuations should be of no importance.

The count rate for neutrons detected in coincidence between a side neutron detector and the gas scintillator was for the above set of accelerator conditions ~5/S, the 'random' rate with the resolving times as described in chapter 3 being ~20% of the 'real' rate. Further the pulse height spectrum from the gas scintillator associated with this random rate fell off sharply with increasing pulse height (as did the ungated spectrum from the gas scintillator) and so if one considers only those 'random' events falling under the peak in the 'real' gated spectrum, then the real to random ratio is further increased by a factor of ~3 . Thus clearly with the circuitry of figure 14, no significant increase in data collection rates would have been gained by reducing the coincidence resolving times in order to further increase the real to random ratio.

The selected ~1/us resolving times also allowed convenient pulse shaping to be employed in the pulse amplifiers. Thus the pulses from a neutron detector pre-amplifier are sharply rising (< 50ns), corresponding to the fast decay time of the

EX BIBL. UNIV. EDINBURGEN

liquid scintillator, and they then decay exponentially with the integration time constant of the input circuit of the pre-amplifier (selected to be ~0.4/us for the pulse shape discrimination circuitry). These pulses were customarily RC integrated and differentiated with time constants of 0.8/us in the amplifier, which thereby produced output pulses with rise times of ~0.5/us with suitably flattened peaks to allow their pulse height analysis during the setting up procedures. In the case of the gas scintillator, its scintillation decay time was found to be ~1/us thus to produce similarly shaped amplifier output pulses to those due to the liquid scintillators, the integration in the amplifier was unnecessary.

Now the discriminators designed as described in chapter 3 trigger whenever an input pulse exceeds the selected level. Hence with a wide spectrum of input pulse heights, the time from the start of an input pulse to the production of an output pulse from the discriminator will have a 'jitter' of a similar magnitude to the rise time of the input pulses. Since a coincidence is determined by an overlap of these rectangular (constant length and amplitude) discriminator output pulses in the coincidence unit, then clearly in order to avoid losing significant numbers of real coincidences due to this time jitter one must ensure that the length of the discriminator output pulses is not significantly less than the rise time of the input pulses to the discriminator. This requirement is fulfilled, and a margin for timing error left, by using the

above described pulse shaping with the selected ~0.6 μs discriminator output pulse length.

Further it allowed a random coincidence rate to be observed on delaying one input to a coincidence unit by ~3 μs, and thus the delay between the four gating signals and the 'He linear' output (as described in section 3.1) was of this magnitude. Now the 400 channel analyser used to collect most of the polarization measurements here reported could be adjusted (internally by the service engineers) to 'gate' successfully with all the routing signals delayed w.r.t. the signals to be analysed, provided this delay was not much greater than ~5 μs, these conditions being satisfied in the present case. The use of significantly longer resolving times and the consequent use of longer delays to provide the random rates might necessitate a compensating delay of the signals to be analysed.

4.2 Preliminary Observations

With the electronic set up as described in chapter 3, one might expect that a 'gated' pulse height spectrum of the output from the helium scintillator so recorded and associated with 'real' neutron coincidences between the gas scintillator and a liquid scintillator would exhibit a single peak corresponding to the energy lost by neutrons from the target being scattered by helium nuclei through a mean angle of 120°, the width of the peak being a function of the spread in incident neutron energy, the spread in the scattering angle and the

resolution of the helium gas scintillator. Such a peak was observed in the 'real and random' spectra, but even after the 'random' events were subtracted, a 'tail' was also observed to be present, such a 'real' spectrum being shown in figure 35.

Now the gas scintillator is sensitive to γ-rays, albeit that the light output from most γ- ray events is considerably less than the light output associated with the desired scattered neutrons. Boersma et al.[10] have pointed out the desirability of employing some γ-ray rejection circuitry and have suggested that the lack of such might be a source of error in Pasma's[13] measurements. Thus to check whether this tail could be due to γ-rays 'breaking through' the presently employed P.S.D. circuitry, the count rate of the pulses from the discriminator ('A' say) attached to a liquid scintillator amplifier was noted during the recording of such a spectrum. Then with no neutron beam, γ-ray sources (^{60}Co, ^{22}Na, pitchbende, thorium) were placed beside the gas scintillator and a spectrum recorded, the count rate from the discriminator 'A' once more being noted. Then these two spectra, normalised to the same total number of counts from discriminator 'A' were compared. Such γ-ray breakthrough as was found was confined to the first few channels of the spectrum where it possibly amounted to a few per cent of the counts there recorded in the run with the neutron beam. Further it should be noted that in operation with a neutron beam, much of the γ-ray flux will originate in the shielding all round the polarimeter. However, in the presently described

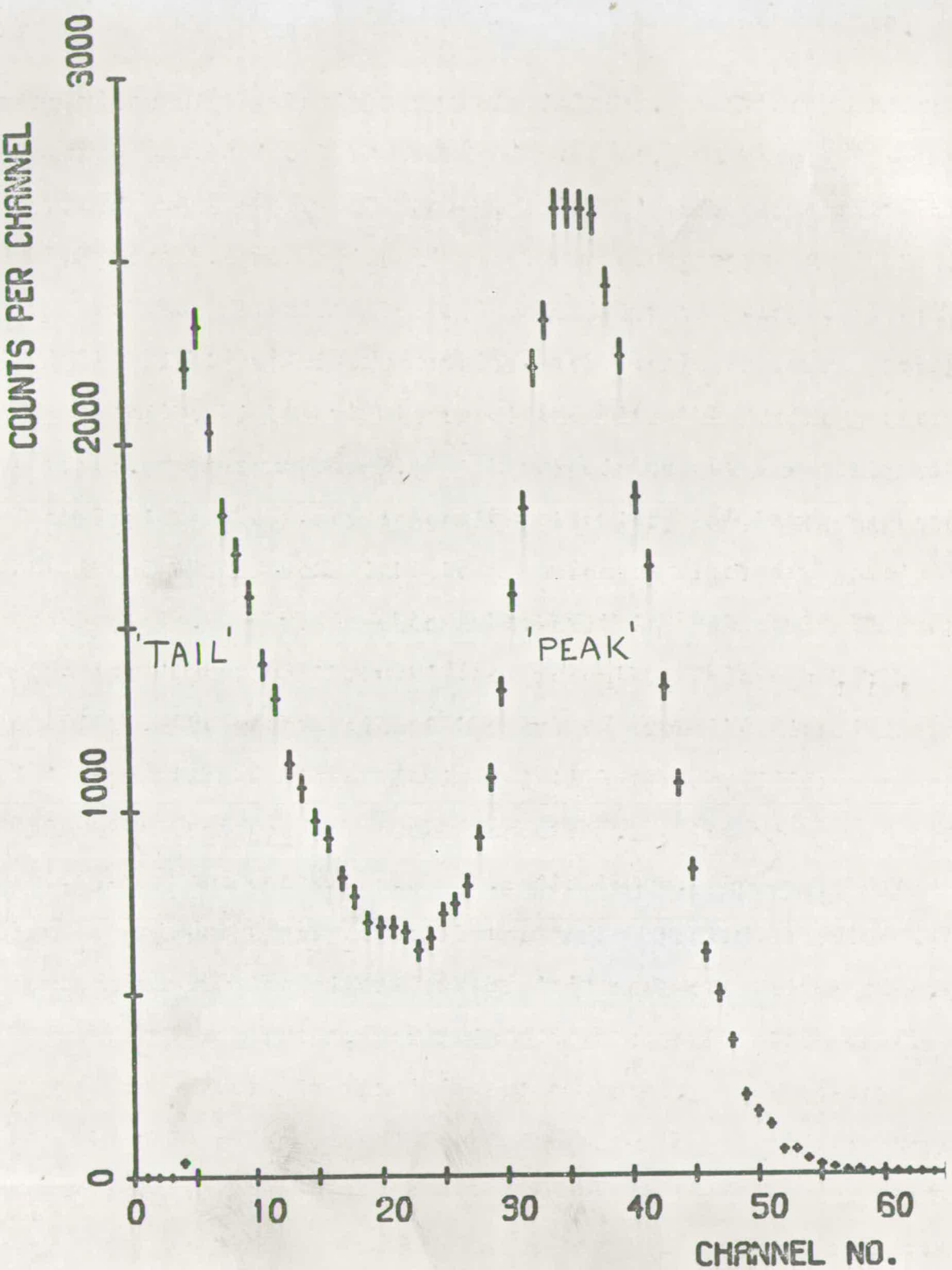

FIG. 35 A GATED HELIUM RECOIL SPECTRUM

test the source of the γ-ray flux was located at the gas scintillator, and normalisation was made with the count rate at the liquid scintillator, thus ensuring an overestimate of the effect. Therefore clearly the tail is not produced by γ-ray breakthrough.

To check whether this tail could be due to neutrons reaching the polarimeter after penetrating the shielding walls, a (gated) spectrum was recorded with solid inserts placed in the collimator beam tube, a boron loaded ZnS scintillator embedded in a moderator of paraffin wax being used to monitor the neutron yield from the target and so allow normalisation before comparison of this spectrum with one taken with the normal inserts. Once more a negligible number of counts were observed, so eliminating a further possible source of the tail.

A consideration of the dynamics of n - ^{4}He scattering shows that for a scattering angle of 120°(Lab) the neutron will lose approximately half of its energy to the recoiling ^{4}He nucleus, thus the events under the peak of the distribution shown in figure 35 will correspond to neutrons and helium nuclei each recoiling with $\sim$1.5 MeV of energy. Now the tail of this gated recoil spectrum rises steeply in the low energy region, indicating the detection of a considerable number of helium recoils with less than 0.3MeV of energy. However, the detection efficiency of the liquid scintillators falls off rapidly for neutron energies below 1MeV, the detection theshold energy for proton recoils being $\sim$0.4MeV (this corresponding to $\sim$0.1MeV for

electron recoils), so suggesting that these 0.3MeV ^{4}He recoils are not associated with recoiling neutrons of a similar energy scattered through 120°. Hence it seems unlikely that the main source of the tail is due to 120° scattering by the helium gas of low energy neutrons present in the collimated neutron beam, a conclusion further strengthened on considering from where such a flux of low energy neutrons might arise. Some carbon contamination of the target was observed, but the Q value for the ^{12}C (d,n) ^{13}N reaction is minus 0.26MeV, yet the tail was present at energies close to this threshold. Possibly the $^{2}H(d,n)^{3}He$ neutrons could be degraded by scattering in the collimator, but the discussion on neutron collimation and shielding by Langsdorf (48) indicates that such contamination should be at most only a few per cent of the direct beam.

Thus from the above observations it would appear that the tail arises from neutrons of ~3MeV which pass through the collimator aperture and yet are scattered by the helium through angles much less than 120° into the liquid scintillator, thus producing the low energy helium recoils observed in the tail. This process is possible if one considers double scattering of the neutrons, once by the helium and once by its solid surrounds (in either order) before they are detected by the liquid scintillators. The large volumes of stainless steel, quartz and brass to the rear of the helium scintillating volume all have dimensions comparable to a fast neutron mean free path

for scattering in them, and further the n - ^{4}He scattering cross-section peaks sharply at small angles. Thus one might expect a sizeable contribution to the tail from neutrons scattered by such a route, other scattering routes including scatters from the walls of the gas scintillator, the aluminium mounting plate, the liquid scintillator photomultiplier cases, the cradle end plates etc., also possibly contributing. In chapter 5 the results of some theoretical computations in support of this hypothesis will be considered.

Experimental support was obtained by temporarily re-orientating the gas scintillator such that its axis lay transverse to the neutron beam and most of the large volume of solid material to the rear of the active volume was removed from direct irradiation, whereupon a substantial reduction ($\sim$ a factor of two) and flattening of the tail was observed. Further on placing in contact with this re-orientated gas scintillator, on its side remote from the target, a slab of quartz of similar dimensions to the gas scintillator viewing window, then the (re-orientated) tail was found to substantially increase (by $\sim$50%) and the tendency of the tail to rise towards low helium recoil energies was found to re-appear.

Of the workers listed in table 1, Pasma[13], Boersma et al.[10], Behof et al.[8], and Roding and Scholermann[7] all employed gas scintillators. Pasma[13] and Boersma et al.[10] mounted their gas scintillators with their axis lying along the neutron beam, as in the present polarimeter (shown in figure 3), however, both

measured their asymmetry using counters attached to their coincidence units, and did not record the helium recoil spectra associated with these coincidences. Behof et al.[8] employed a gas scintillator lying transverse to the neutron beam, and their paper indicates that they did record the recoil spectra, however, no mention is made of its shape or of a possible tail. All three of these sets of results were taken with neutron scattering angles of 120°, while Roding and Scholermann[7] employed a forward scattering angle the value of which is not quoted in their paper. Further they employed a transverse mounting of the gas scintillator, but did not record the helium recoil pulse height spectrum.

Now in a polarization measurement with the present polarimeter, the 'expected' neutron scattering asymmetry ($\mathcal{E}$ of chapter 1) will be associated with ^{4}He recoils recorded within the peaks of the gated recoil spectra, while the many and varied scattering routes of the neutrons associated with the tails might suggest that these will exhibit little or no asymmetry. Thus clearly in order to accurately measure the 'expected' asymmetry it would seem advisable to record (as in the present experiment) the helium recoil spectra associated with neutron coincidences between a side neutron detector and the gas scintillator during a measurement, and in the following data analysis to make due allowance for the tail. This subject will be further examined in later chapters.

4.3 Preliminary Measurements

The preliminary measurements described in the present section were performed with the polarimeter mechanically constructed and aligned as described in chapter 2. Thus the polarization of the neutrons was studied at a mean laboratory reaction angle of 46°. The target material employed consisted of a layer of titanium approximately $1 mgm/cm^2$ thick containing absorbed deuterium and deposited on a copper backing, and was the thickest Ti-D target available in the laboratory, being thick for deuteron energies up to $\sim 400 keV$ when account is taken of the $\sim 40^{\circ}$ angle which the target strip makes with the deuteron beam. The measurements were made using a 512 channel Laben analyser to pulse height analyse the pulses from the helium scintillator, routing to produce the desired gated recoil spectra being performed into 64 or 128 channel sections of memory as desired.

As has been previously indicated the Owen[42] technique of pulse shape discrimination was initially employed, but the start of polarization measurements quickly showed up an asymmetry with the neutron detectors located in the horizontal plane (i.e. normal to the reaction plane) as well as an expected asymmetry in the vertical (reaction) plane. This instrumental asymmetry was traced to a variation in the size of the saturated Owen output pulses from the 6262B photomultipliers incorporated in the neutron detectors, and this measurement ceased until circuitry was devised and constructed as previously described

to allow a timing technique of P.S.D. to be employed with the linear signals from the 11th dynode of the photomultipliers.

The resumption of polarization measurements also proved a false start, since although the desired null asymmetry (within statistical uncertainties) was recorded in the horizontal plane, an early breakdown of a capacitor in the dynode chain of a neutron detector caused this detector to be stripped down in order to remedy the fault and it was found that in addition a bubble was occupying possibly a few per cent of the volume of the associated 'bubble free' scintillator. Since a bubble gravitates towards the highest point in the liquid scintillator volume, it may introduce instrumental asymmetries into the vertical (reaction) plane measurements, and further should the bubble be due to a leak in the scintillator container and so contain some oxygen, this will poison the P.S.D. properties of the Ne213 scintillator.

The faulty scintillator was returned to the manufacturer and while awaiting its return (6 weeks) some running of the polarimeter was performed with one bubble free (checked) scintillator, the ungated helium recoil spectrum also being recorded and used to normalise the coincidence count rate, only those events in the ungated spectrum above a pulse height threshold which rejected most γ-rays being used in the normalisation.

On the return of the second liquid scintillator, once more bubble free, the full electronic system as described in chapter 3

was employed, and two measurements were performed to a good statistical accuracy, one with a recorded accelerating voltage of 350kV, the other 800kV, these being near to each end of the useable range of the Cockcroft-Walton accelerator.

The technique used in these measurements (and in all subsequent ones) was to intersperse readings with the liquid scintillators in the horizontal plane with those taken in the vertical plane, thus allowing a continual check on the presence or lack of instrumental asymmetries. Thus spectra were recorded in one of the four selectable cradle positions for $\sim$15 minutes, then the data collected was typed out (automatically) on the typewriter coupled to the pulse height analyser, this taking $\sim$8 minutes. The cradle was then rotated to the next position, the procedure being repeated until all four positions were sampled. Thus such a measurement cycle lasted 90 minutes and these were repeated until the desired statistical accuracy was achieved. Since no data collection takes place during $\sim$30 minutes (i.e. $\frac{1}{3}$) of each cycle due to the print out from the multi-channel analyser, it would seem that longer measurement times before print out might produce a worthwhile increase in the data collection rate. However temperature fluctuations took place in the laboratory leading to gain fluctuations in the photomultipliers, and further deuteron beam conditions varied considerably, suggesting that a large number of short measurement cycles might be desirable to average out these variations. Thus the chosen measurement cycle time was a compromise between this

ideal and the requirement of a good data collection efficiency.

From the filling of the gas scintillator for these preliminary measurements to its use in taking the last results described above, a period of ~7 months elapsed. During this time, the light output of the gas scintillator decreased by a factor of ~3, with a consequent reduction in resolution. Further on summing the gated recoil spectra from many measurement cycles obtained over several days, the downward drift of the light output was noticeable and caused a further loss in resolution, a typical spectrum obtained over a two day period being as shown in figure 36.

An analysis of the data taken with the detectors in the vertical (reaction) plane showed that indeed the expected asymmetry was associated with the peaks in the gated recoil spectra there being little or no asymmetry associated with the tail, so clearly to obtain an accurate polarization measurement, one must estimate the contribution of the tail beneath the peak. On calculating the asymmetry occurring above a selected pulse height in the gated recoil spectra, then it was found that the asymmetry increased as the selected level increased, corresponding to less of the tail being included in the result. However as the level approached and passed through the summit of the peak, the asymmetry remained reasonably constant. Thus these preliminary results were analysed on the basis that the tail continued its initial downward fall beneath the peak, and provided little or no contribution to events (in the gated

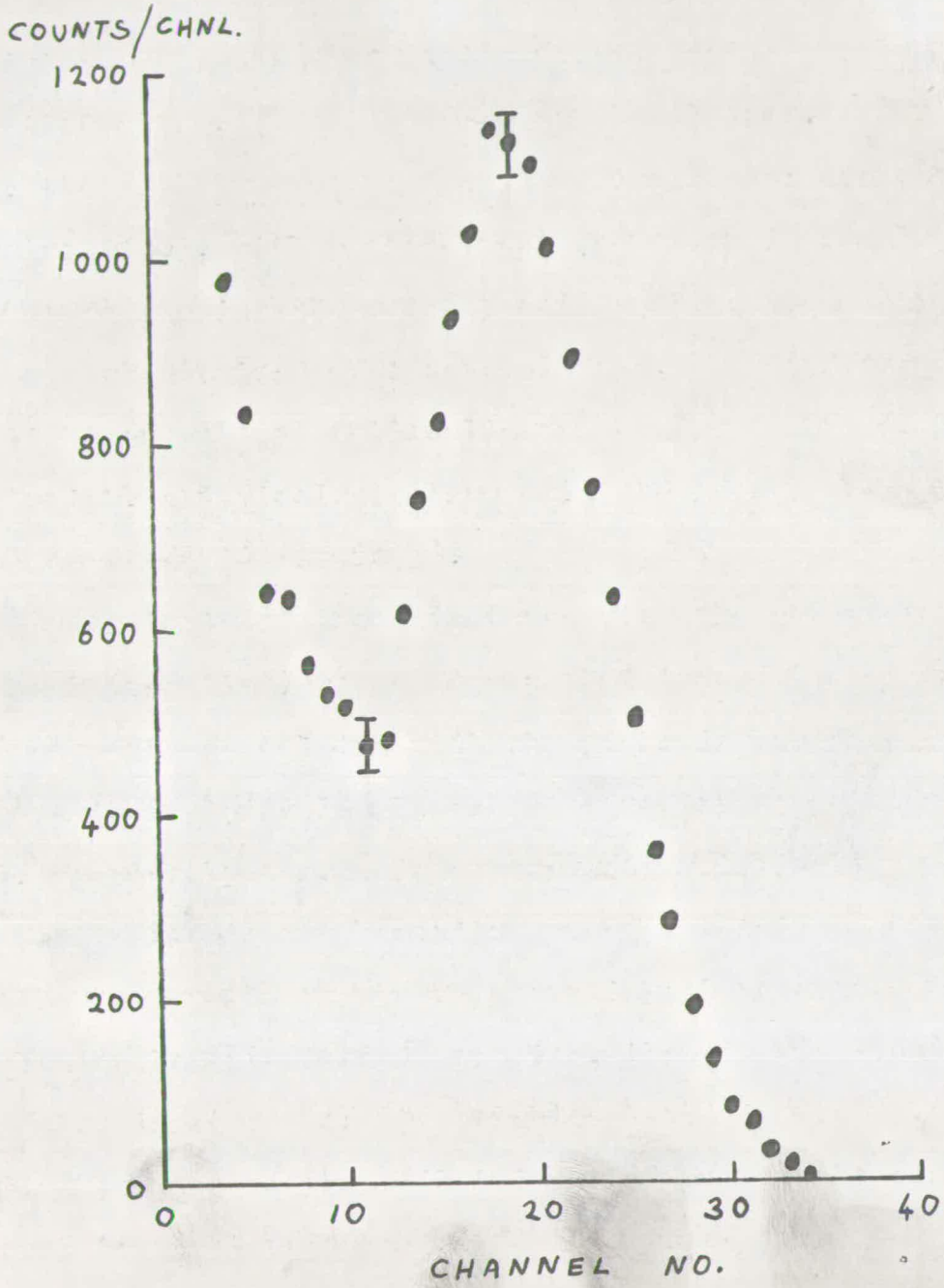

FIG. 36 HELIUM RECOIL SPECTRUM RECORDED DURING PRELIMINARY MEASUREMENTS

recoil spectra) with a light output as large as or greater than those associated with the summit of the peak. An analysis of results will be presented in a later chapter, however, briefly these preliminary results analysed in this fashion indicated a polarization of -0.13 and -0.14 with nominal accelerating potentials of 350kV and 800kV respectively.

This first sequence of polarization measurements led to the following thoughts on further possible measurements: Although these first measurements indicated little variation of the neutron polarization with incident deuteron energy, it was felt desirable to investigate any possible energy variation with a somewhat thinner target. It was also felt important to obtain a good evaluation of the 'tail' effects, and hence good resolution spectra also seemed desirable. This indicated that in the taking of such results a freshly filled gas scintillator would be appropriate as would any technique to reduce the data collection time by, for example, cutting down the dead time in each measurement cycle associated with the print out of data from the pulse height analyser.

Further during this first measurement sequence the data collected during one measurement could amount to ~ 50 sheets of output from the pulse height analyser, each sheet containing 512 channels of information. Even allowing for the fact that the data was usually spread over less than half of these channels, the summation of the data from the individual sheets to produce the desired total recoil spectra was a long and

tedious task, as was the further summation and manipulation of those parts of the recoil spectra from which the polarization information was extracted. Thus in any further series of measurements an automated data analysis system seemed desirable which might allow a 'same day' processing of measurements so giving a quick indication of the quality of the data (i.e. the absence or presence of horizontal asymmetries, the statistical accuracy of the result, the resolution of the spectra etc.).

4.4 The Calibration of the Cockcroft-Walton Accelerator

The thin target material selected for use in the final polarization measurements to be outlined in a following section was ~100keV thick, thus a knowledge of the deuteron accelerating voltage to within some tens of kilovolts seemed desirable. Now the Cockcroft-Walton accelerator's potential is measured by a meter which records the current flowing through an oil cooled resistor chain connected between the high voltage terminal and earth. Since the measuring resistor chain was installed with the accelerator around 1950, it was felt that some check on the voltage calibration would be appropriate, and thus before the final measurements were performed, such a calibration was attempted by studying p, γ resonances.

The γ-ray detector available and thus employed was a cylindrical sodium iodide crystal scintillator of 5inch diameter and 4inch height, mounted on a 58AVP photomultiplier. The information on the proton induced reactions used was taken

from 'Energy Levels of Light Nuclei' by Ajzenberg-Selove and Lauritsen.[49]

With a solid piece of carbon mounted on the target stalk, and the γ-ray detector placed nearby, the $^{12}C\ (p,\gamma)^{13}N$ resonance which occurs at a proton bombarding energy of 457keV was first studied. The output from the photomultiplier after amplification was fed to a pulse height analyser and spectra were recorded at various proton accelerating voltages. The γ-rays emitted in this 40keV wide resonance are of 2.36MeV energy and the step in the yield from the corresponding photo-peak recorded in the pulse height analyser was used to mark the resonance.

A similar procedure was carried out with a thick evaporated layer of zinc fluoride as a target, the group of 6-7 MeV γ-rays from the $^{19}F\ (p,\alpha\gamma)^{16}O$ reaction being observed. This produces a resonance of 160 millibarn cross-section and 3.3keV width at a proton energy of 341keV, and this was used as a further reference point. This reaction has another very strong resonance at a proton bombarding energy of 874keV, the cross-section being 540 millibarns, and the width 5keV. Thus a further step in the yield of 6-7MeV γ-rays from the target was easily observable at this energy, and so provided a third calibration point.

Figure 37 shows in its top section a plot of the observed γ-ray yield on passing through these three resonances (with a different yield scale for each resonance). The error bars on

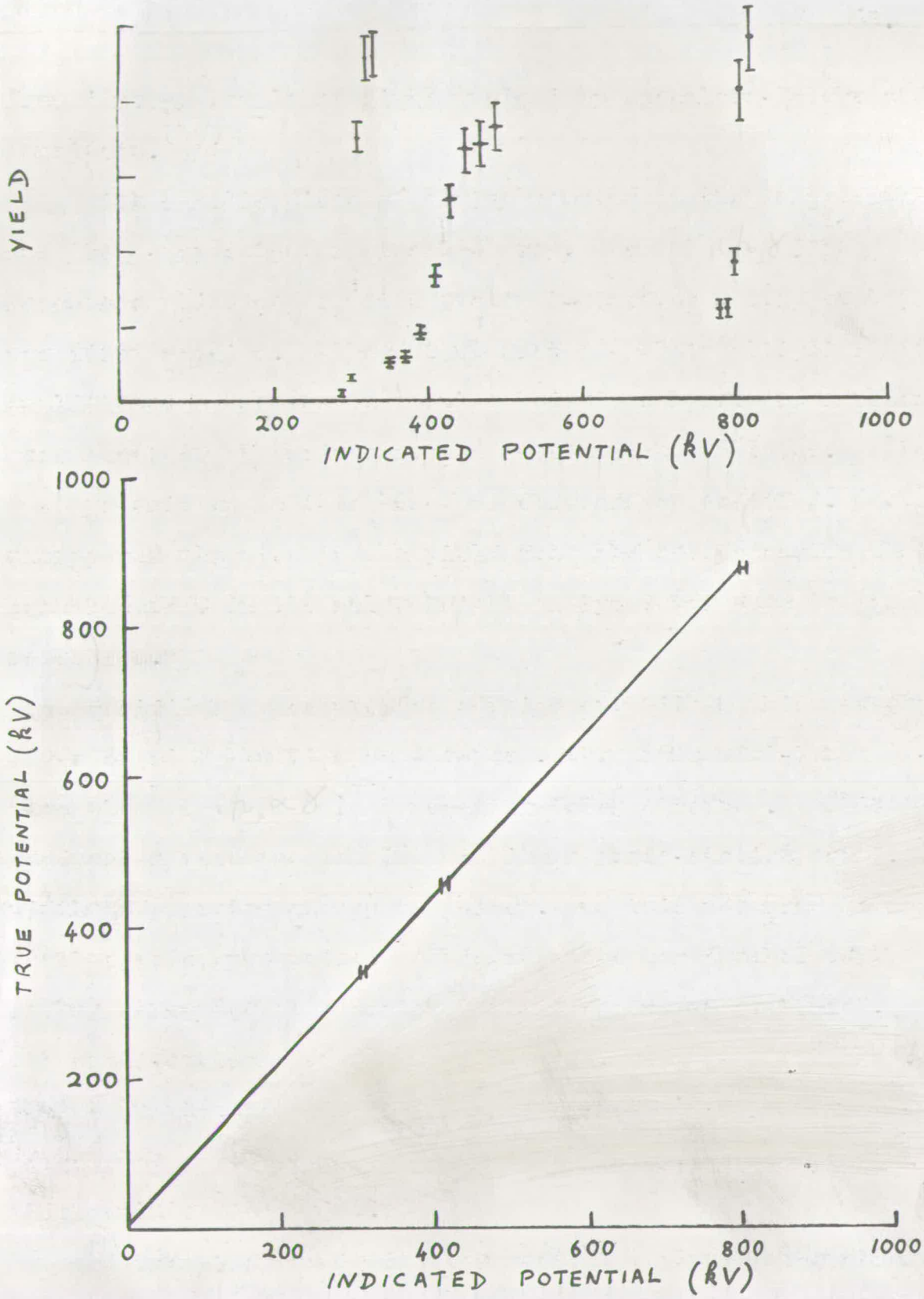

FIG. 37 ACCELERATOR CALIBRATION

I $^{19}F(h,\alpha\gamma)^{16}O$ REACTION, YIELD PLOTTED IN 10kV STEPS

I $^{12}C(h,\gamma)^{13}N$ REACTION, YIELD PLOTTED IN 20kV STEPS

the yields are an estimate of the effect of the uncertainty in the beam current used in the normalisation of these results, the largest errors being present in the measurements at the 874keV resonance, at which energy the beam current was least stable.

The lower part of figure 37 is a plot of the accelerating potential recorded on the meter versus the true accelerating potential, the three points with their plausible uncertainties being taken from the three above yield steps, and the straight line shown drawn through these points was used subsequently as a calibration chart. This shows the meter recorded potential to be consistently 10% too low, confirming the value of a re-calibration. Further the fluorine resonances also show by their sharpness that the ripple voltage on the high voltage terminal must be 10kV or less.

4.5 Data Handling Techniques

To allow some automation in the analysis of the data obtained from the polarimeter the recording of the recoil spectra was changed from the 512 channel Laben analyser to a more modern 400 channel Laben analyser (when this became available), this analyser being provided with a tele-type print out which provides, in addition to typed sheets containing the data stored in its memory, a punched paper tape with this same data stored thereon in ASCII code.

A Digital Equipment Corporation PDP-8 computer was

available within the Department of Physics, it being used in a shared real-time access mode to control several experiments. In such a mode the computer runs under control of a supervisor programme, the system having been developed by Dr. G. Burns and Mr. S.T. Hayes. Thus to use this system to perform a desired task (e.g. to analyse the data tapes from the polarimeter) requires that a programme of instructions is written in a modified form of 'Imp' - a language similar to 'Algol' and serviced by the Edinburgh Regional Computing Centre (E.R.C.C.). This programme is then sent to E.R.C.C. where it is 'translated' by an I.B.M. 360/50 computer into an efficient machine code to operate the PDP-8 under 'supervisor', this translated programme being returned in the form of a paper tape to be fed into the PDP-8 when required.

This system was used to handle the data tapes produced by the 400 channel analyser coupled to the polarimeter. Since the PDP-8 used possessed only 8K of core storage the data handling programme written was split into three sections, only one at a time being fed to the computer in order to minimise the amount of core storage used and so allow as many other simultaneous users as practicable. Even with this subdivision, a memory location was allocated which did not allow simultaneous operation with all of the experiments controlled by the PDP-8. These three data handling programmes operate as described below.

The first programme allows a paper tape produced by the 400 channel Laben analyser to be read into the PDP-8 through

its high speed paper tape reader, and then checks that this tape's format is correct, and stores the number of counts from each of the 400 channels in 400 separate stores. i.e. it stores the number of counts in channel i (say) in store A (i) (say), i running from 1 to 400. Then when a further paper tape produced by the pulse height analyser is fed in, it once more checks the format and adds the number in channel i of this current tape to the contents of the store A (i), this being performed for all 400 channels. One may continue in this fashion until the desired number of tapes has been summed, and then the contents of the 400 locations A(i) may be punched out on the high speed paper tape punch coupled to the PDP-8, the format of this master tape being similar to that of the individual tapes fed in.

Thus the above programme was used to sum all the data tapes produced at one polarimeter orientation during a particular measurement, a facility being provided in the programme to punch an identifier onto the master tape so produced indicating the cradle position and the particular measurement. In the analysis of the data collected in one measurement, this procedure is executed four times, so producing four master tapes each corresponding to a particular cradle position, and these tapes were commonly joined together to provide convenient storage and handling.

The second data analysis programme merely reads in four such master tapes, checks that their identifiers show these to be a 'set', and stores the data thereon on magnetic 'Dectape',

a keyword being introduced at this stage to allow this data to be called down from the Dectape in the following programme for further analysis. Now this data is contained in four elements of four hundred channels, each element corresponding to a particular cradle position. Further each such element contains four one hundred channel spectra, each spectrum corresponding to helium recoils associated with one of the four gating outputs as described in section 3.1. Thus we have 16 one hundred channel spectra stored on Dectape for each measurement.

The third data handling programme calls the appropriate keyword to obtain access to the data stored as above (and related to one measurement), and then on the selection of two channel numbers from the keyboard, the programme sums the counts between the selected channel limits in each of the 16 spectra. It prints out these totals then calculates and prints out the measured asymmetry with its associated statistical accuracy for this selected part of the spectra, this being performed for the scintillators lying in both the horizontal and vertical planes. A fresh pair of channel limits may then be selected, and the programme will repeat the above calculations for these new limits until termination by the operator.

These three programmes were used with the PDP-8 computer to process the data from the measurements reported in section 4.7. In one such measurement typically ~ 50 data tapes might be obtained, and these could be summed by the first programme

in ~2 hours, the manual effort involved in feeding these tapes to the computer absorbing most of this time. The execution of the second programme takes only a few minutes, and once the data is stored on Dectape it remains so even after analysis by programme 3. Thus separate keywords were given to each complete measurement, a single Dectape providing more than adequate storage for all the results analysed in this fashion. The final programme as described above allowed an evaluation of the asymmetry corresponding to any selected part of the gated recoil spectra, the results being returned within a few seconds of the selection of the desired limits. Thus one could with ease study the variation of the asymmetry through the peak and tail areas of the recoil spectra.

4.6 Reliability of the Polarimeter and Accelerator

Before reporting the final sequence of measurements, the reliability of the system and such limitations as this imposed on polarization measurements will be considered.

The electronic units employed with the polarimeter and designed as described in chapter 3 proved very reliable. Thus the author can recall but one operational failure in these units, the open circuit capacitor causing it being speedily replaced.

The 512 channel Laben pulse height analyser also proved extremely reliable, however the more modern 400 channel Laben analyser, to which data collection was transferred to allow

paper tape production, gave considerable trouble and required much attention by its service engineers. Among the troubles experienced with it were that its analogue to digital converter drifted and was non linear, and for no apparent reason it would lose the contents of its memory. This analyser has now been replaced by its manufacturer, (Laben).

The 'bubble free' liquid scintillators also gave trouble, both of these leaking shortly after purchase. On being refilled and re-sealed one once more broke down as described in section 4.3, and this experience was further repeated several times, thus requiring the polarimeter to be stripped down and the cells checked after each sequence of measurements.

As previously recorded, the gas scintillator light output (and pressure) declined markedly over a period of some months, the rate of decline increasing with the frequency of useage in taking polarization measurements, however, refilling was a standard procedure customarily taking little more than a day.

The major source of trouble in the taking of the final measurements was the Cockcroft-Walton accelerator. Although this trouble was on occasion due to obvious component failures which could be remedied, most of the time the problem was merely the inability to produce a useable ion beam. After the first sequence of measurements, recorded in section 4.3, the accelerator deteriorated further and 50/uA beams on target could only be obtained infrequently and at selected energies in spite of considerable attention to and replacement of ion source parts.

Thus when a combination of a fully working polarimeter system and a functioning accelerator finally allowed a sequence of thin target measurements to take place, these results were restricted to deuteron energies above 600keV, since a useable target current ($\sim$50/uA) could not be reliably obtained at lower energies. Above an $\sim$850kV accelerating potential frequent discharges from the high voltage terminal caused overloading of the accelerator and its consequent automatic switch off. The difficulties of continually attempting to bring back the deuteron beam after such events combined with the occasional loss of data in the memory of the pulse height analyser during such discharges effectively made measurements impracticable above such a voltage.

To obtain thin target measurements at deuteron energies below 600keV, considerable modifications were made to the ion source and its associated focussing lens, the result being that a $\sim$100/uA beam current was attainable at energies down to $\sim$300keV, albeit that the beam spot was badly focussed, being $\sim$1cm. in diameter, and consequently not all of this current could be obtained on the target strip. While these conditions remained, further thin target measurements were made at deuteron energies down to $\sim$300keV.

4.7 Final Measurements.

With the data collection transferred to the 400 channel Laben analyser, measurements re-commenced. Initially a fresh

target strip of ~850keV thickness was fitted, and this it was hoped would allow a quick check on the system operation. However the combination of a freshly filled gas scintillator, two truly 'bubble free' liquid scintillators, and reliable operation from both the pulse height analyser and the Cockcroft-Walton accelerator proved difficult to obtain. When a measurement was performed under difficult beam conditions, a horizontal asymmetry of a few per cent was recorded, and some time was spent before this was traced to overcritical collimation of the neutron beam. Thus the deuteron beam which was striking the edge of the target could not quite 'see' all of the gas scintillator active volume. This was easily remedied by adjusting the collimator inserts, and successful measurements were thereafter obtained with this thick target and for accelerating voltages of ~660kV and ~880kV.

Now to obtain an asymmetry measurement to within a statistical uncertainty of $\pm$ 0.01, one requires to record more than 10,000 real coincidences between the gas scintillator and the side neutron detectors. Since the asymmetry one wishes to measure to obtain a polarization estimate is associated with the peak in the gated recoil spectrum, only ~ $\frac{1}{2}$ of the counts contained in such a spectrum as figure 35 will be useable. Further as described in section 4.3 horizontal asymmetry measurements were interspersed with vertical ones to maintain a constant check on the quality of the data, and also ~ $\frac{1}{3}$ of the measurement cycle is taken up by data print out. Thus a

polarization measurement taken with a 50 μA beam of 600keV deuterons on a thick Ti-D target continues for a few hours (with the present polarimeter) until a statistical accuracy of ± .01 is achieved.

On going to thin targets an obvious drop in count rate results, this being further exacerbated on going to low energies by the fall off in the reaction cross-section and in the loss of focus of the deuteron beam resulting in a loss of deuteron beam striking the target strip. Thus should a 50 μA beam of 300keV deuterons be maintained on a 50keV thick Ti-D target strip, several tens of hours would be required to obtain a polarization measurement to within a statistical accuracy of ±0.01 using the adopted procedure, yet as reported in section 4.3 such results should be taken over as short a period as possible to maintain good resolution spectra.

Fortunately the acquisition of a high speed paper tape punch for the 400 channel analyser (which allowed its stored data to be punched out in less than one minute) produced a substantial reduction in the dead time during each measurement cycle (and further allowed shorter measurement cycles to be sensibly employed). Also the 'thin' Ti-D target now fitted was ~340 μgm/cm^2 thick to the incident deuteron beam, the deuteron energy loss therein being 90keV for 800keV deuterons and 120keV for 300keV deuterons, it being thought that the apparent slow variation in the polarization with energy did not justify the use of considerably thinner targets with their

associated longer data collection times.

With this target fitted and when a suitable deuteron beam became available, measurements re-commenced. Since at this stage the 400 channel Laben analyser became unuseable due to sporadic memory loss, it was returned to Nuclear Enterprises for a thorough overhaul, and the first thin target measurements were made with a borrowed (400 channel Laben) analyser. A result was obtained at a mean deuteron energy of 840keV, this being achieved in one days running. A result at a mean deuteron energy of 620keV was also obtained, but the deuteron beam was badly displaced at this energy and required to be magnetically steered into the main bending magnet. Further loss of beam current required ion source parts to be replaced, and so this result took 5 days to complete. Encouraged by the 80 uA on target obtainable at this stage, the gas scintillator was refilled and a result taken on the day following the refill for a mean deuteron energy of 730keV, this being the best resolution thin target result obtained.

However on reducing the accelerating potential below 600kV, the deuteron beam current could not be maintained, and a number of modifications were made to parts associated with the ion source as recorded in the previous section. With these made, and with the original overhauled 400 channel analyser once more in use, measurements were performed at mean deuteron energies of 500keV, 385keV, and 275keV, the 500keV result taking one day, the other two requiring two days each. As some check on the possible ageing of targets, the result

at 385keV was taken with a fresh strip of target material cut from the same piece of material as was that strip used for the 840, 730, 620keV results, this material having been stored for several years in the laboratory, while the results at 500keV and 275keV were taken with a strip cut from a freshly supplied piece of target material. No significant difference in neutron yield was observed in these three samples, nor was there any significant fluctuations in the measured asymmetry.

Thus ended the final sequence of measurement of the polarization of the neutrons emitted in the $^{2}H(d,n)^{3}He$ reaction at a lab angle of 46^{o}. The results obtained will be presented in chapter 6.

CHAPTER 5.

ANALYSING POWER CALCULATIONS

As reported in section 1.3, the measured asymmetry ε is related to the polarization P by the relation

$$\varepsilon = \langle A \rangle P$$

where $\langle A \rangle$ is the mean analysing power of the polarimeter, conventionally calculated by 'averaging' the analysing power of the scatterer, in this case helium, over the neutron scattering angles employed in the measurement.

Early workers have performed this 'averaging' process by an approximate analytical technique outlined by Meier et al.[19] and McCormac et al.[12]. Boersma et al.[10] have indicated that the dimensions of a typical helium polarimeter are too large for this technique to be used with success, but merely indicate that they 'numerically computed' their mean analysing power. More recently Aspelund and Gustafsson[50] and Miller et al.[51] have tackled the corrections required to fast neutron polarization data due to the effects of finite geometry and of multiple scattering within the analyser by using Monte-Carlo type computer programmes to trace the scattering histories of 'simulated' neutrons. Now as will be seen in the following sections, the mean analysing power (i.e. corrected for finite geometry, multiple scattering etc.) may be formulated in terms of multi-dimensional integrals evaluated over the volumes of the scattering sample and the neutron detectors. Stinson et al.[52]

have reported the evaluation of such integrals by a regular sub-division of both the scattering sample volume and the solid angle sub-tended by a neutron detector at the scattering sample.

In the present chapter, the analysing power calculations will be presented in terms of multi-dimensional integrals of a somewhat similar form to those employed by Stinson et al.[52]. With simplifications assumed to the experimental geometry, certain such integrals were initially evaluated by regular sub-division of the neutron detector and scatterer volumes, but the presently reported treatment uses random Monte-Carlo type sampling of these volumes, thus imposing no constraints on the geometrical shapes employed.

Now the present study has shown up the importance of recording the energy spectrum of the helium recoils associated with neutrons detected in coincidence between the gas scintillator and the neutron detectors. To obtain a reliable polarization measurement, only a portion of the 'peak' in such recoil spectra will be utilised, and thus the variation of the analysing power across such peaks will also be considered.

Further, routes involving double scattering of the neutrons (with at least one of the scatters being due to the helium) before they are detected in the liquid scintillators will be considered in order to plausibly account for a 'tail' in the gated recoil spectra, and also to obtain some lower estimate of such double scattering effects which produce contributions to the peaks in the gated recoil spectra.

Figure 38, which represents a cross section taken through the polarimeter in the vertical (reaction) plane, shows the co-ordinate system which will be employed in the following discussion. Thus the origin of co-ordinates is the centre of the rear face of the gas scintillator, $\hat{\underline{y}}$ and $\hat{\underline{z}}$ being unit vectors in the directions shown, and $\hat{\underline{x}}$ being a further unit vector projecting vertically out from the plane of the paper.

5.1 The Mean Analysing Power - A Simplified Case

Consider initially the following simplified case:

Let a uniform monoenergetic neutron flux N, with polarization $P\hat{\underline{x}}$, travelling in the $\hat{\underline{z}}$ direction be incident upon the gas scintillator. Let attenuation of this neutron flux in the helium gas and its container be ignored and further let attenuation of the scattered neutron flux in the liquid scintillators and their containers be ignored. Let the detection efficiency of the liquid scintillators remain constant over the spread in neutron energies in the scattered beam.

Hence the number of neutrons per second detected by a small volume element dv' of liquid scintillator 'X'(shown in figure 38) after having been scattered by a small volume element dv of gas scintillator will be

$$\frac{N E_x n' \sigma(\theta) \{1 + A(\theta) P \cos\phi\} dv dv'}{r^2}$$

where θ, ϕ are the scattering and azimuthal angles as defined in section 1.2 for the incident neutrons scattered by dv into dv', these small volume elements being a distance r apart. $\sigma(\theta)$ and

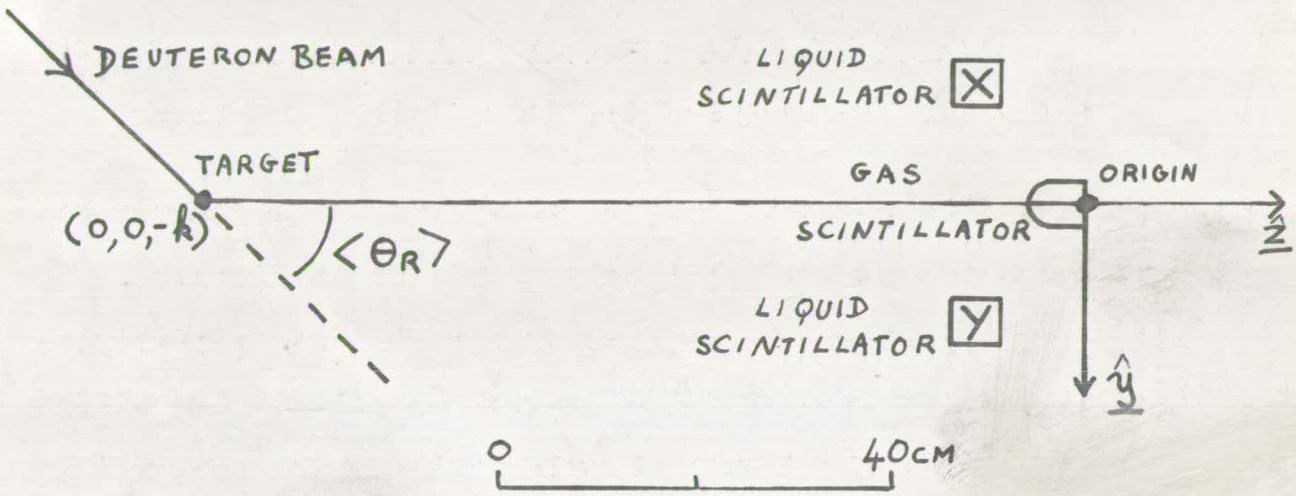

FIG. 38 SKETCH OF POLARIMETER GEOMETRY

$A(\theta)$ are respectively the (nuclear) laboratory differential cross section and the analysing power for the neutrons scattered in the helium, n' is the number of helium nuclei per unit volume of the gas scintillator, and E_x is the probability of a scattered neutron being detected in the 'X' liquid scintillator per unit distance travelled therein.

Thus the total number of neutrons per second detected by the liquid scintillator 'X' after being scattered (once) by the gas scintillator will be

$$N E_x n' \int \frac{\sigma(\theta)\{1 + A(\theta) P \cos\phi\}}{r^2} \, dv \, dv'$$

$= N E_x n' \mathcal{I}_1$ say, $\mathcal{I}_1$ being a double volume integral evaluated throughout the sensitive volumes of both the gas scintillator and the liquid scintillator 'X'.

Now due to the symmetry of the system, the count rate in liquid scintillator 'Y', located as shown in figure 38, due to neutrons scattered (once) by the gas scintillator active volume will be

$$N E_y n' \int \frac{\sigma(\theta)\{1 - A(\theta) P \cos\phi\}}{r^2} \, dv \, dv'$$

$= N E_y n' \mathcal{I}_2$ say, $\mathcal{I}_2$ being evaluated throughout the same volumes as $\mathcal{I}_1$.

Hence the measured asymmetry $\mathcal{E}$, which is obtained by rotating the polarimeter and so uses the technique described in section 1.3 to eliminate both the efficiency factors (E_x, E_y) and the variations in incident neutron flux, will be

$$\mathcal{E} = \frac{\mathcal{I}_1 - \mathcal{I}_2}{\mathcal{I}_1 + \mathcal{I}_2}$$

$$\varepsilon = P \left\{ \frac{\int \frac{\sigma(\theta) A(\theta) \cos\phi}{r^2} \, dv \, dv'}{\int \frac{\sigma(\theta)}{r^2} \, dv \, dv'} \right\}$$

$$= P\langle A1 \rangle \quad \text{say,}$$

where $\langle A1 \rangle$ is the mean analysing power (to this first approximation) the integrals defining it being evaluated over the same volumes as $\mathcal{I}_1, \mathcal{I}_2$.

To evaluate $\langle A1 \rangle$, a Monte-Carlo technique using a digital computer was employed. Thus the volumes of the gas scintillator and the liquid scintillator (i.e. the limits of integration of the integrals to be evaluated) were sampled in a random manner, the 'rectangular' random number distribution used in this process (and in all other similar calculations outlined in this chapter) being generated by a power residue method.[53] An outline of the calculation of $\langle A1 \rangle$ is as below:

Line 1: Set stores T, W equal to zero

Line 2: Select the co-ordinates of a point from within the active volume of the gas scintillator in a random manner. Select the co-ordinates of a point from within the active volume of the liquid scintillator in a random manner.

Line 3: For this pair of points calculate θ, ϕ, and hence $\sigma(\theta)$, $A(\theta)$, $\cos\phi$, using as required the (given) phase shift angles.

Line 4: Increment the store T by the value $\frac{\sigma(\theta) A(\theta) \cos\phi}{r^2}$.
Increment the store W by the value $\frac{\sigma(\theta)}{r^2}$

Line 5: Return to line 2 and continue in this cycle until the desired number of samples has been taken, then proceed to line 6

Line 6: Print out T/W, which is an estimate of $\langle A \rangle$

The results of such a calculation are shown in figure 39, the phase shift angles for neutron-helium scattering employed in these calculations (and in all other results reported in the present chapter unless otherwise stated) being those of Austin et al.[17] extrapolated to an incident neutron energy of 3.3MeV, neutrons of such an energy being produced in the $^{2}H(d,n)^{3}He$ reaction for an incident deuteron energy of $\sim$ 600keV and a lab. reaction angle of 46°.

Thus the set of points labelled $\langle A \rangle$ in figure 39 represents a set of values of $\langle A \rangle$ calculated as above, and plotted as a function of the number of times the computational cycle was performed to obtain the result (labelled 'no. of sub-divisions'). These results show that $\langle A \rangle$ rapidly converges with an increasing number of computational cycles to an accuracy of an order of magnitude better than that to which the analysing power of helium is known (see section 2.1). Further the straight line labelled 'A'_{MAX} in figure 39, represents the maximum value of the analysing power of helium ($A(\theta)$) evaluated with the set of phase shift angles as employed in the calculation of $\langle A \rangle$ above, and we note that $\langle A \rangle$ differs from this maximum value of $A(\theta)$ by $\sim 6\%$.

These observations might lead one to expect that the mean analysing power is a slowly varying function of detector and analyser size, and is thus uncritical of exact symmetry in the

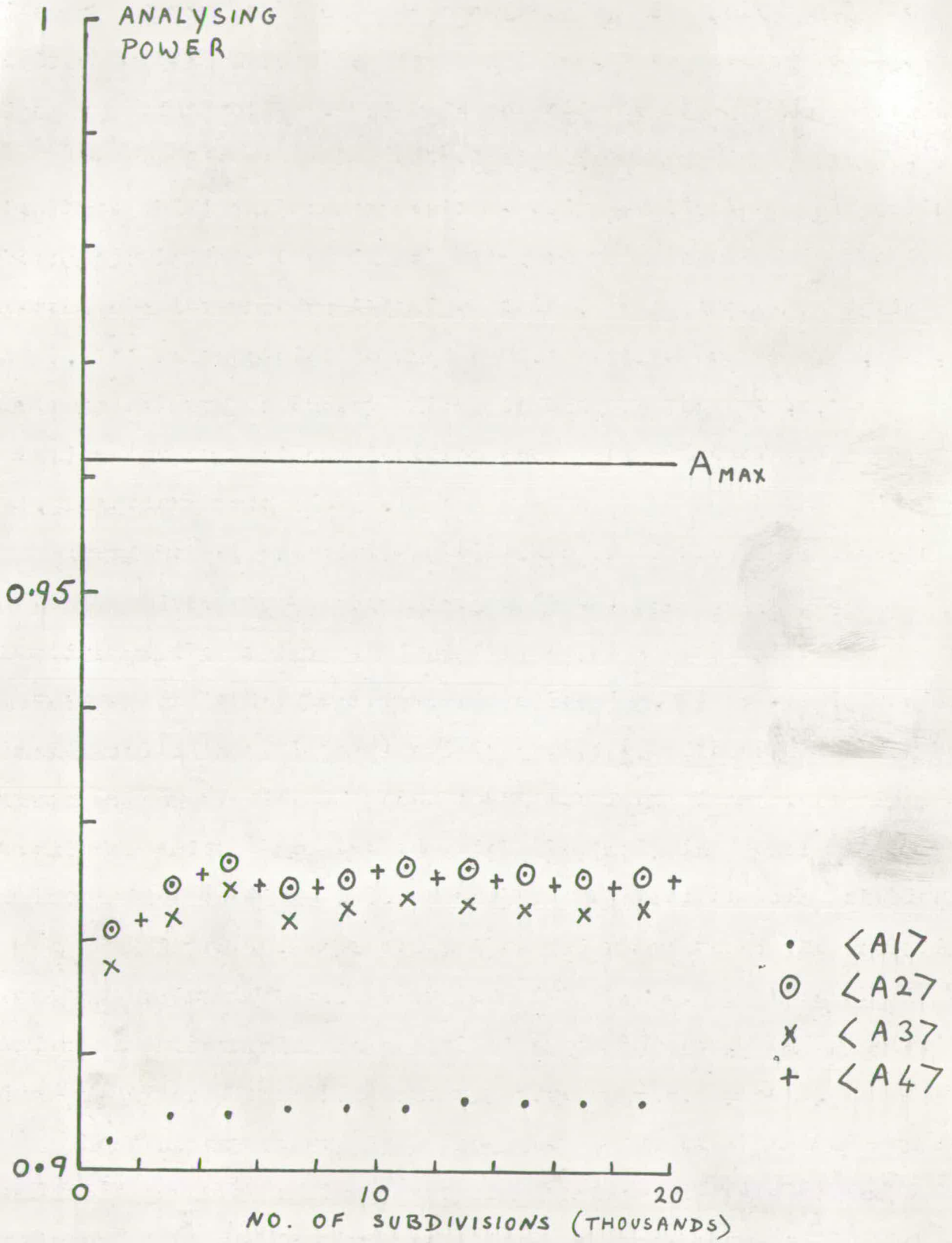

FIG. 39 POLARIMETER ANALYSING POWER CALCULATIONS

neutron detector positions, a conclusion supported by further computations made with varying geometries.

5.2 A Correction for the Asymmetry Introduced by the Variation with Reaction Angle of the Neutron Producing Reaction Cross Section.

In the evaluation of $\langle A_1 \rangle$ a parallel uniform flux of incident neutrons has been assumed, i.e. effectively the target has been considered to be located at an infinite distance from the gas scintillator. Consider now the experimental arrangement of figure 38, with the target located a distance k from the origin, and thus consider the corrections required due to the finite angle subtended by the scatterer at the target. This will introduce changes in the spread of scattering angle which will be considered in the following section, but a more serious effect will be introduced due to the variation of the $^2H(d,n)^3He$ reaction cross section over the spread in reaction angle.

If one traverses along a curve through the gas scintillator at a constant radius from the target, keeping the 'x' co-ordinate constant, then the neutron flux will increase monotonically with the 'y' co-ordinate due to the accompanying increase of the differential cross section for the $^2H(d,n)^3He$ reaction with decreasing reaction angle at the chosen mean reaction angle of 46°. Thus the neutron scattering centre of the gas scintillator will not lie along the Z axis, but will have a slightly positive 'y' co-ordinate. Hence, with the present polarimeter one must expect an asymmetry in scattering in the vertical ($\phi=0$) plane

due to this effect, for which a correction is required.

A scrutiny of the work listed in table 1 which employed a 'conventional' polarimeter with a helium gas scintillator as scatterer-analyser shows that Pasma[13] believed the correction required due to this reaction cross section variation to be trivial, and hence ignored it, while Boersma et al.[10] utilised a magnetic spin inversion type of polarimeter which does not record this 'false' asymmetry. It is not clear from the published papers of Behof et al.[8] and of Roding and Scholermann[7] how these authors made their analysing power corrections, although the former reports that they employed the $^{2}H(d,n)^{3}He$ reaction differential cross section in their computations. The formulation of the reaction cross section correction developed for the present study is as below.

To a first order, the reaction angle θ_R corresponding to a neutron originating at the target (0, 0, k) and scattered at a point (AH, BH, CH) in the gas scintillator is

$$\theta_R = \langle\theta_R\rangle - \frac{BH}{CH+k} \quad \text{radians,}$$

where $\langle\theta_R\rangle$ is the mean reaction angle shown in figure 38. Further, the fractional variation of the differential cross section for the $^{2}H(d,n)^{3}He$ reaction with reaction angle may be considered a constant, α say, for small deviations from the mean reaction angle. Hence the neutron flux at a point (AH, BH, CH) within the gas scintillator will be of the form

$$N = \frac{N'}{AH^2+BH^2+CH^2}\left\{1 - \frac{\alpha\, BH}{CH+k}\right\} \quad \text{-- eqn 5.1}$$

and since $k \gg |AH|, |BH|, |CH|$

this may be approximated to a parallel neutron flux varying as

$$N = N''\{1 + \gamma BH\}$$

where γ is the fractional variation of the $^2H(d,n)^3He$ differential cross section per unit length traversed in the y direction in the gas scintillator, and is evaluated at its volume centre. Clearly γ is deuteron energy and polarimeter geometry dependent. Now the number of neutrons per second detected by the liquid scintillator 'X' after having been scattered by the gas scintillator becomes

$$N'' E_x n' \int \frac{\sigma(\theta)\{1+\gamma BH\}\{1 + A(\theta) P \cos\phi\}}{r^2} d\omega d\omega'$$

and similarly by liquid scintillator 'Y'

$$N'' E_y n' \int \frac{\sigma(\theta)\{1-\gamma BH\}\{1 - A(\theta) P \cos\phi\}}{r^2} d\omega d\omega'$$

Thus the measured asymmetry ε now becomes

$$\varepsilon = P\left\{ \frac{\int \frac{\sigma(\theta) A(\theta) \cos\phi}{r^2} d\omega d\omega' + \frac{\gamma}{P}\int \frac{BH\,\sigma(\theta)}{r^2} d\omega d\omega'}{\int \frac{\sigma(\theta)}{r^2} d\omega d\omega' + \gamma P \int \frac{BH\,\sigma(\theta) A(\theta)\cos\phi}{r^2} d\omega d\omega'} \right\}$$

$$= P\left\{ \frac{T + \frac{\gamma}{P} T'}{W + \gamma P W'} \right\} \quad - - - - \text{eqn } 5.2$$

$$= P \langle A2 \rangle$$

Now $\langle A2 \rangle$ is the second approximation to the analysing power of the polarimeter, since it includes both the finite geometry corrections evaluated in $\langle A1 \rangle$, and also a correction for the effect of the $^2H(d,n)^3He$ cross section variation with angle. The integrals defining $\langle A2 \rangle$ have been labelled in an obvious fashion T, T', W, W' in eqn. 5.2, all being evaluated over the

same volumes as g_1 .

The computation of $\langle A2 \rangle$ proceeds in an analogous fashion to that of $\langle A1 \rangle$, but with obvious additional quantities to be evaluated and stored during each cycle. The results of such a computation are shown plotted as points $\langle A2 \rangle$ in figure 39, using the same set of phase shift angles and random co-ordinates as were employed in the evaluation of points $\langle A1 \rangle$. An estimate of the polarization $P = -0.15$ was supplied to the programme as was a γ evaluated at a deuteron energy of 600keV, using the differential cross section data for the $^2H(d,n)^3He$ reaction compiled by Brolley and Fowler[54].

Once more there is a rapid convergence of the calculation to a more than acceptable degree of accuracy, and further it may be noted that $\langle A2 \rangle$ differs from $\langle A1 \rangle$ by ~ 0.02, this being of a similar magnitude to the uncertainty in the analysing power of helium for a 120° (lab.) neutron scattering angle. It also represents a correction to the measured polarization of $\sim$ one sixth of the statistical standard deviation associated with such a measurement in the present study, and thus is clearly not of major importance.

Should the polarimeter be employed in the measurement of small unknown neutron polarizations, (e.g. the neutrons from the $^3H(d,n)^4He$ reaction at deuteron energies < 1 MeV) then a more convenient evaluation of the correction required due to the angular variation of the reaction cross section appears when it is realised that with reference to eqn. 5.2, the integral T is

of a similar size to the integral W, but the correction term $\frac{\gamma}{P} T' \gg \gamma P W'$ (a factor of $\sim 1/P^2$). Hence $\gamma P W'$ may be safely ignored, and thus eqn. 5.2 becomes

$$\begin{aligned} \varepsilon &= P\frac{I}{W} + \gamma\frac{I'}{W} \\ &= P\langle A1\rangle + \chi \end{aligned}$$

where

$$\chi = \frac{\gamma \int \frac{BH\, G(\theta)}{T^2}\, d\upsilon\, d\upsilon'}{\int \frac{G(\theta)}{T^2}\, d\upsilon\, d\upsilon'}$$

is the 'false' asymmetry due to the angular variation of the reaction cross section, and is calculable without assumptions as to P.

5.3 The Mean Analysing Power - Removal of the Simplifications.

Let the effects of removing certain of the simplifying assumptions utilised in obtaining expressions for $\langle A1\rangle$ and $\langle A2\rangle$ now be examined.

A full treatment of the effect of absorbtion of the scattered neutron flux within the liquid scintillators would involve following the multiple scattering trajectories inside the liquid scintillator of a sample of neutrons until they had an energy less than that which might be detected. Let the effect be treated approximately by defining λ as the mean free unscattered path of a neutron in the liquid scintillator, and consider it to be independent of the spread in incident neutron energies.

Then $$\frac{1}{\lambda} = \hbar\rho \left\{ \frac{\tau' G_H + G_C}{\tau' A_H + A_C} \right\}$$

where h is Avogadro's number, ρ is the density of Ne 213 liquid scintillator, τ' is the ratio of hydrogen to carbon atoms in Ne 213, $\sigma_{H(C)}$ is the total cross section for neutron-hydrogen (carbon) scattering at a neutron energy of 1.5MeV, and $A_{H(C)}$ is the atomic weight of hydrogen (carbon). Then λ so evaluated is approximately 4cm, of the same order as the liquid scintillator dimensions.

Now proceeding as previously, but introducing an attenuation factor of exp $(-S/\lambda)$ where S is the distance the neutron travels in the liquid scintillator after having been scattered by $d\omega$ and before being detected by $d\omega'$, a further corrected mean analysing power $\langle A3 \rangle$ is obtained where

$$\langle A3 \rangle = \frac{\int \frac{\sigma(\theta)\, exp(-S/\lambda)}{\tau^2} \left\{ A(\theta)\cos\phi + \frac{\gamma}{P} BH \right\} d\omega d\omega'}{\int \frac{\sigma(\theta)\, exp(-S/\lambda)}{\tau^2} \left\{ 1 + \gamma P BH\, A(\theta)\cos\phi \right\} d\omega d\omega'}$$

Further let the approximation of an incident flux of neutrons travelling parallel to the Z axis be removed, and consider the neutron flux to originate from the target (0,0,-k) and take the form of eqn. 5.1. Thus $\langle A4 \rangle$, which is as $\langle A3 \rangle$ but is further corrected for the effects of finite target distance, becomes

$$\langle A4 \rangle = \frac{\int \frac{\sigma(\theta)\, exp(-S/\lambda)}{\ell^2 \tau^2} \left\{ A(\theta)\cos\phi - \frac{\alpha BH}{P(CH+k)} \right\} d\omega d\omega'}{\int \frac{\sigma(\theta)\, exp(-S/\lambda)}{\ell^2 \tau^2} \left\{ 1 - \frac{\alpha P BH}{CH+k} A(\theta)\cos\phi \right\} d\omega d\omega'}$$

where $\ell^2 = AH^2 + BH^2 + (CH+k)^2$

These integrals defining $\langle A3 \rangle$, $\langle A4 \rangle$ are to be evaluated over the

same limits as ϑ_1 , and thus $\langle A3 \rangle$, $\langle A4 \rangle$ may be calculated using programmes similar to those used in the evaluation of $\langle A1 \rangle$, $\langle A2 \rangle$.

Values of $\langle A3 \rangle$, $\langle A4 \rangle$ computed for the present polarimeter are plotted in figure 39, these calculations using the same set of common parameters and randomly chosen points as were used in the calculation of $\langle A1 \rangle$ and $\langle A2 \rangle$ also displayed in figure 39. From this figure it may be seen that $\langle A3 \rangle$, which contains a correction due to absorption in the liquid scintillator, differs from $\langle A2 \rangle$ which has no such correction by ~ 0.003, while the addition of a further correction to $\langle A3 \rangle$ for the effects of finite target distance, so producing $\langle A4 \rangle$, reduces this difference to ~ 0.0005 and necessitated the plotting of $\langle A4 \rangle$ at sub-divisions intermediate to those chosen for $\langle A2 \rangle$ to avoid coincidence on the scale chosen. A consideration of the comments made in the previous section concerning both the statistical accuracy of the measured asymmetries and the uncertainty in the analysing power of helium will clearly indicate that these last two corrections may be safely ignored, hence saving considerable computer time.

Attenuation of the incident neutron flux in the gas scintillator has not been corrected for, as this effect ought to be an order of magnitude down on that for the liquid scintillator. In the following section it will be shown that the mean energy of the (singly) scattered neutron flux is ~ 1.5MeV with a spread (F.W.H.M.) of $\sim 15\%$ for monoenergetic incident neutrons.

The assumption of constancy of detection efficiency of the liquid scintillator over such an energy range is supported by Batchelor et al.[55].

Thus ignoring all but singly scattered neutrons, and assuming that all of the helium recoil spectrum from the gas scintillator associated with such events is accepted, then a calculation of $\langle A2 \rangle$ (or $\langle A1 \rangle$ and χ) would seem to provide an adequate evaluation of the mean analysing power at a selected incident neutron energy.

5.4 The Helium Recoil Spectrum

The observed helium recoil energy spectrum corresponding to monoenergetic neutrons emitted by the target and singly scattered by the helium before being detected in a liquid scintillator, should exhibit a single peak whose width is a function of the spread in neutron scattering angles and of the resolution of the helium gas scintillator.

With an unpolarized incident neutron beam, but with conditions otherwise as assumed in the calculation of $\langle A1 \rangle$, we have

$$\frac{\Delta N_H(E)}{N_H} = \frac{\int \frac{\sigma(\theta)}{\tau^2} \delta(E)\, d\omega\, d\omega'}{\int \frac{\sigma(\theta)}{\tau^2}\, d\omega\, d\omega'}$$

where N_H is the number of neutrons per second detected in liquid scintillator 'X' after having been scattered once by the helium gas, and $\Delta N_H(E)$ is the no of such events per second

corresponding to a helium recoil energy in the range E to $E+\Delta E$, $\delta(E)$ equalling unity if the helium recoil energy lies within this range, and being zero otherwise.

Thus $\frac{\Delta N_H(E)}{\Delta E\ N_H}$ plotted as a function of E is the required helium recoil energy spectrum uncorrected for the vagaries of the light collection process in the gas scintillator. An outline of a programme to calculate this quantity for a ΔE = one fiftieth of the incident neutron energy E_n, is as follows:

Line 1: Set all elements of an array $D(J)$ equal to zero for J ranging from 1 to 50. Set store $W = 0$.

Line 2: Set $J = 0$

Line 3: Select the co-ordinates of a point from within the active volume of the gas scintillator in a random manner. Select the co-ordinates of a point from within the active volume of the liquid scintillator in a random manner.

Line 4: Calculate θ, τ, and hence $\sigma(\theta)$, and $E(\theta)$

Line 5: Increment store W by an amount $\frac{\sigma(\theta)}{\tau^2}$

Line 6: If $J < 50$, increment J by one, otherwise jump to line 9

Line 7: If $J-\frac{1}{2} < \frac{50E}{E_n} < J+\frac{1}{2}$, then proceed otherwise jump back to line 6

Line 8: Increment store $D(J)$ by an amount $\sigma(\theta)/\tau^2$

Line 9: Return to line 2 and continue in this cycle until the desired no. of samples has been taken, then proceed to line 10

Line 10: Print out $D(J)/W$ which is an estimate of $\frac{\Delta N_H(E)}{N_H}$ for $E = \frac{(J-\frac{1}{2})E_n}{50}$ and $\Delta E = \frac{E_n}{50}$.

Such a calculation was performed (for 3.3MeV neutrons and the phase shifts of Austin et al.[17]), the computational cycle

being executed 2,000 times, no substantial modifications arising from the use of a greater number of cycles. The simulated helium recoil energy spectrum so produced is shown in figure 40, the title 'Counts/Chnl.' representing $2{,}000\,D(J)/W$, while the 'Channel No.' represents J. Thus the simulated spectrum contains 2,000 counts, and channel zero corresponds to zero energy, while channel 50 corresponds to the energy of the incident neutrons.

Now with polarized incident neutrons, the count rate in each channel of the recoil spectrum will vary according to the azimuthal angle of the associated neutron detector. Hence one may consider a mean analysing power to be associated with each such channel, and this, defined to the same degree of approximation as $\langle A2 \rangle$ is given by

$$\frac{\int \frac{\epsilon(\theta)\,\delta(E)}{r^2} \left\{ A(\theta)\cos\phi + \frac{\gamma}{P} BH \right\} d\omega\, d\omega'}{\int \frac{\epsilon(\theta)\,\delta(E)}{r^2} \left\{ 1 + \gamma P BH A(\theta)\cos\phi \right\} d\omega\, d\omega'}$$

This was calculated in a similar fashion to ΔN_H, and is also shown plotted in figure 40.

The recoil spectrum shown calculated in figure 40, exhibits a full width half maximum resolution of ~15%, thus rendering unimportant the ~3% spread in neutron energy present during the thin target polarization measurements. However since even the best resolution thin target measurements obtained in the present study show a F.W.H.M. resolution of ~35%, clearly the intrinsic resolution of the gas scintillator is of major importance. Thus to plausibly represent the effects of the resolution of the gas

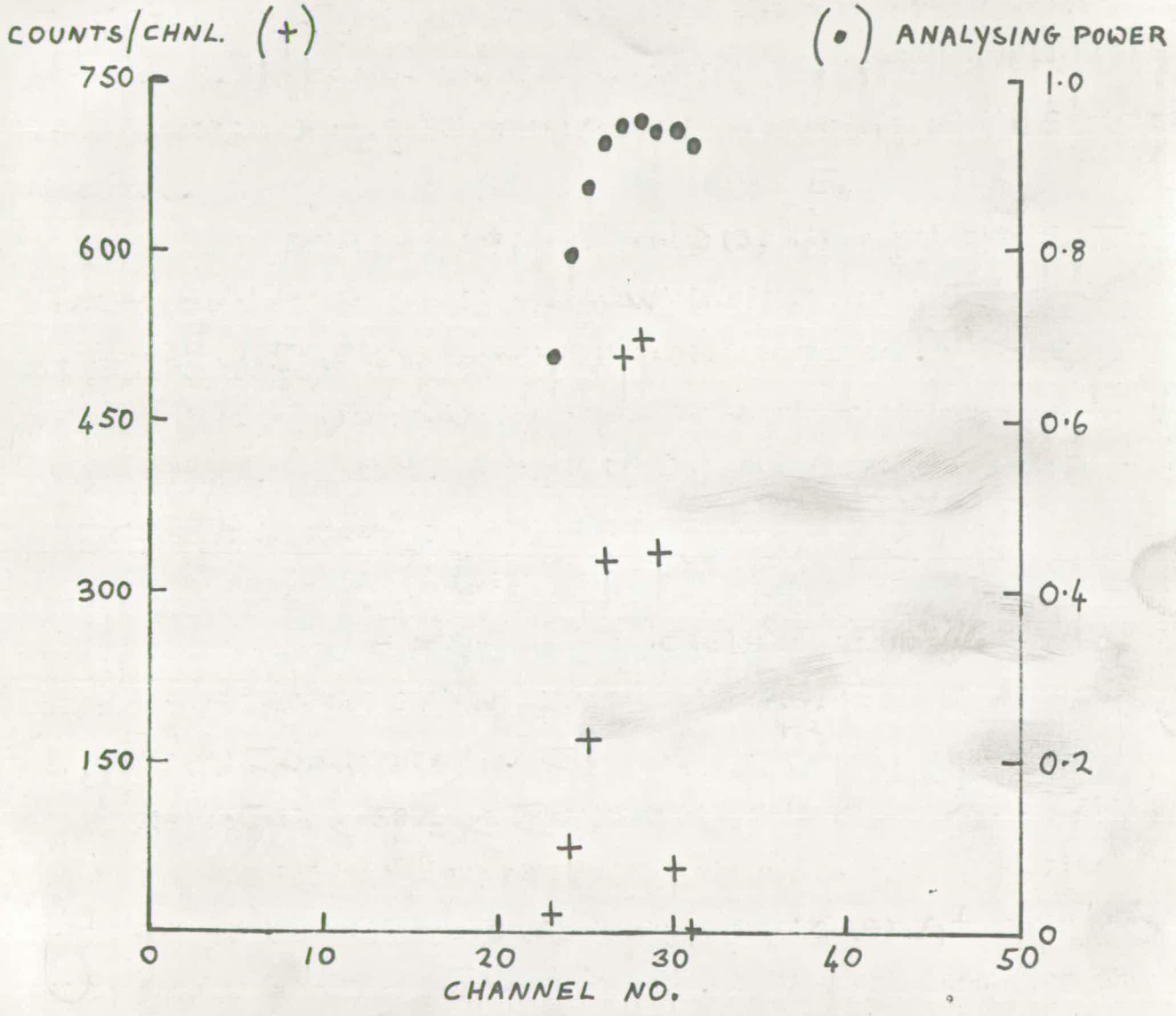

FIG. 40 SIMULATED HELIUM RECOIL ENERGY SPECTRUM WITH ASSOCIATED ANALYSING POWER

scintillator, the calculated recoil spectrum of figure 40 was given a gaussian smear as follows:

Let a gaussian curve with channel J as its mean, R as its F.W.H.M., and with an area proportional to the contents of channel J of the recoil spectrum of figure 40 be produced for each channel J making up this spectrum. Now let such a curve with J as mean have an area G_{IJ} beneath it and between the channel limits $I-\frac{1}{2}$ and $I+\frac{1}{2}$. Then the contents of channel I of the smeared spectrum shown in figure 41 is given by $\sum_J G_{IJ}$, the summation being over all channels J making up the non-smeared spectrum of figure 40. And if the mean analysing power shown associated with channel of the non-smeared spectrum is given by $\langle \Delta A2J \rangle$, then the mean analysing power shown associated with each channel of the smeared spectrum of figure 41 is given by $\frac{\sum G_{IJ} \langle \Delta A2J \rangle}{\sum G_{IJ}}$.

Now the intrinsic resolution of the gas scintillator will include a contribution from the statistical nature of the light production processes which might be expected to vary as one over the square root of the energy deposited in the scintillator, while non uniformities in the light collection process from different parts of the sensitive volume might be expected to contribute an energy independent term to the resolution. Thus the resolution employed in the gaussian smear was

$$R = 15\sqrt{2 + \frac{50}{J}}\ \%$$

where J is the number of the channel in the recoil spectrum of figure 40 to be smeared. R is therefore $\sim 30\%$ around the peak

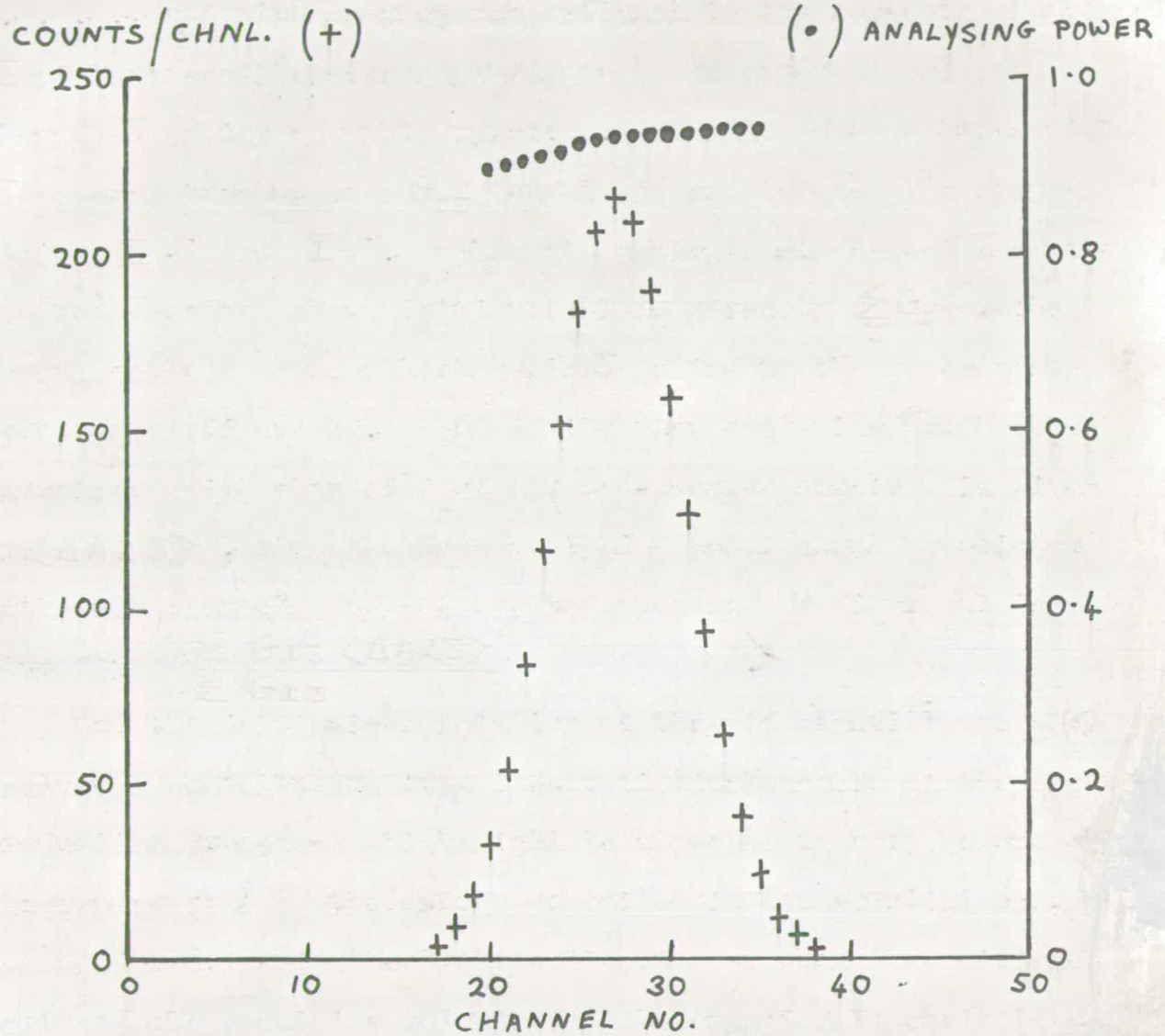

FIG. 41 SIMULATED HELIUM RECOIL ENERGY SPECTRUM WITH ASSOCIATED ANALYSING POWER.
A GAUSSIAN SMEAR HAS BEEN EMPLOYED TO REPRESENT THE EFFECT OF THE GAS SCINTILLATOR RESOLUTION.

of the recoil spectrum where the resolution is chosen to be equally shared between the energy dependent and independent terms. The use of a constant 30% resolution was also tried and made little difference.

An examination of the mean analysing power plotted as a function of channel number in figure 41 shows that it remains near constant, falling slightly to the lower side of the recoil spectrum peak as a greater proportion of neutrons with a scattering angle remote from the mean of $\sim 120^{\circ}$ are included. While one might expect a similar fall off on the upper side of the peak, this does not occur due to the corrections for the angular variation in the $^{2}H(d,n)^{3}He$ reaction cross section which are largest over this portion of the spectrum.

However these variations are small, thus little change in the effective analysing power occurs if only a (convenient) selected portion of the spectrum is used.

Thus the mean analysing power including all of the recoil spectrum is 0.927

The mean analysing power including only those channels within the full width at half maximum of the recoil spectrum is 0.928

The mean analysing power including only three channels around the summit of the peak in the recoil spectrum is 0.930

The mean analysing power including all of the channels on the upper side of the peak in the recoil spectrum is 0.936.

Clearly these variations are trivial in their effect when compared to the statistical uncertainties in the polarization

measurements to be reported, and also when compared to the uncertainties in our knowledge of the analysing power of helium. Thus if it is accepted that the construction of a recoil spectrum and its associated analysing power as outlined above is a reasonable representation of those observed, then it would seem that one may select parts of the peak in the observed spectra and after correction for any double scattering effects present, one may apply the analysing power $\langle A_2 \rangle$ computed for the full peak without a significant loss in accuracy.

5.5 The Tail in the Helium Recoil Spectrum.

Immediately to the rear (i.e. in the positive Z direction) of the active volume of the gas scintillator lies a quartz window with a stainless steel surround, and behind this stands a brass saddle, all with dimensions comparable to the mean free path for the incident neutrons in these materials. Thus one might expect a substantial number of neutrons to be scattered by both the helium gas and by this volume of solid material before entering the liquid scintillators.

A detailed evaluation of this effect is beyond the scope of the present study, but consider the following very approximate treatment which might plausibly indicate whether this effect can account for the observed 'tails' in the experimental gated helium recoil spectra.

Consider first neutrons scattered by the helium (ν) then by the quartz or its stainless steel surround (ν'') before being

detected by the liquid scintillator (v'). Let the probability (μ) of a scatter per unit distance travelled in the solid (v'') by a neutron be considered a constant, independent of the incident neutron energy, the angle of scatter or the scattering material. Then with an unpolarized incident neutron beam, and ignoring attenuation of the neutrons in the solid (v''), the conditions being otherwise as assumed in section 5.1, we have that the number of neutrons per second detected by this double scattering route is given by

$$\frac{N n' E_x \mu}{4\pi} \int \frac{\sigma(\theta')}{h^2 q^2} \, dv \, dv' dv''$$

where θ' is the angle through which a neutron, incident along the Z direction, is scattered by dv into dv'', h is the distance between dv and dv'' and q is the distance between dv'' and dv', the terminology being otherwise that of section 5.1. The integral is to be evaluated over the three volumes v, v', v''.

Now consider neutrons scattered first by the quartz and stainless steel surround (v'') before being scattered by the helium (v) into a liquid scintillator. Let all of the simplifications assumed above be adopted, and in addition assume that no energy loss occurs on the neutrons being scattered by the solid (v'') into the helium (v). Then the number of neutrons per second recorded as following this second route will be

$$\frac{N n' E_x \mu}{4\pi} \int \frac{\sigma(\theta'')}{h^2 r^2} \, dv \, dv' dv''$$

where θ'' is now the angle through which a neutron, incident from dv'' is scattered by dv into dv', the notation being

otherwise as above or in section 5.1. The integration is over the volumes of the gas scintillator v, and the liquid scintillator v' as in the previous integral, but the integration w.r.t. the solid v'' takes place only over that portion of the solid which is irradiated by the target.

Now proceeding as in the previous section, one may introduce the function $\delta(E)$ into the above integrals, and after their evaluation smear the result with a gaussian also as described in section 5.4. Thus one may obtain simulated helium recoil spectra corresponding to the two above considered double scattering routes.

Such computations were performed, and the results are shown plotted in figure 42. The set of points 'a' represents the route $v \rightarrow v'' \rightarrow v'$, while 'b' represents the route $v'' \rightarrow v \rightarrow v'$. The set of points 'c' represents a summation of 'a', 'b', and the single scattered peak as calculated in the previous section. The magnitude of the tail thus shown corresponds to a μ computed assuming a ~ 0.15 barn per steradian nuclear scattering differential cross section in the solid material, and this seems a not unreasonable value at the large backward scattering angles occurring, when both elastic and inelastic processes are considered. The evaluation of nine-fold integrals of the type shown above and in later sections was performed by a random sampling Monte-Carlo type process. Typically, estimates were made at multiples of 500 samples, the final result involving 2,000 samples by which stage the main features of the distribution

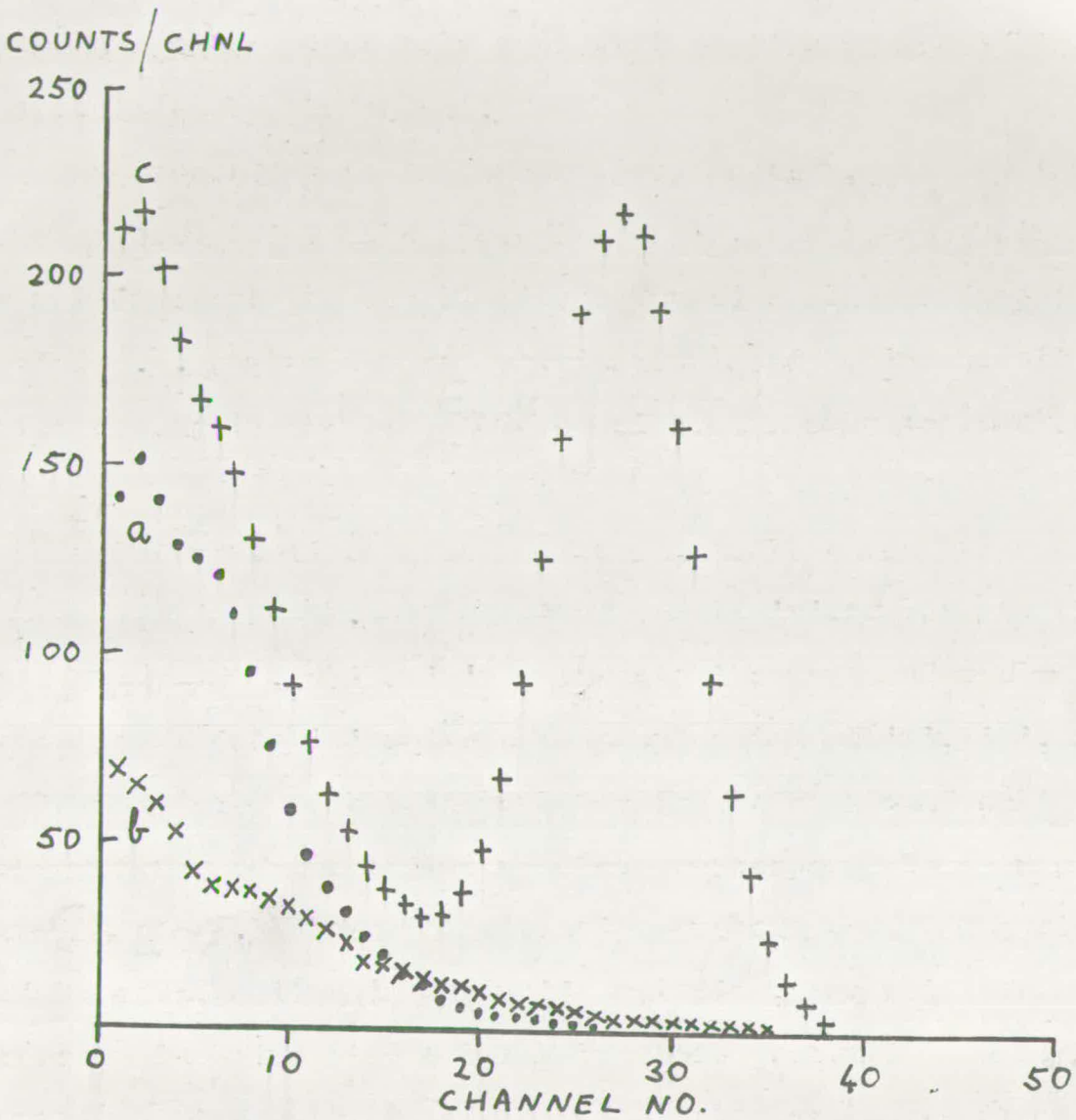

FIG. 42 SIMULATED HELIUM RECOIL ENERGY SPECTRUM SHOWING 'TAIL' DUE TO MULTIPLE SCATTERING.

were acceptably stable.

Figure 42 thus shows that indeed double scattering involving the solid material to the rear of the gas scintillator is a plausible source of a major portion of the tails in the observed gated recoil spectra, although considering the approximations assumed no great trust may be placed in it as an accurate representation of these tails. For example, if the energy lost during the scatter in the solid material is considered, then clearly there would be a shift of the events under curve 'b' of figure 42 to a lower recoil energy, which would deepen the valley region of curve 'c' and heighten the low energy end of this spectrum. Conversly if small angle scattering of neutrons by the stainless steel shell containing the helium gas is considered, then this should tend to fill up the valley of curve 'c'. Further contributions to double scattering processes might be expected from the routes involving the aluminium mounting plate, the liquid scintillator photomultiplier and its brass container etc., and further calculations confirmed that these also tended to fill up the valley.

Now experimentally the tails in the gated recoil spectra were observed to exhibit a near zero scattering asymmetry, thus indicating that the mean analysing power corresponding to the above considered double scattering routes should be near zero. To check this by computation would involve a formulation of the spin dependent scattering processes in both the helium gas and in the solid scatterer, this being beyond the scope of the

present treatment. However if the scattering route $v \rightarrow v'' \rightarrow v'$, which seems to be a major contributor to the tail, is considered and if the assumptions used in the computation of its associated recoil spectrum are made with the addition that μ is independent of the spin orientation of the incident neutrons, then the mean analysing power corresponding to this route is given by

$$\frac{\int \frac{\sigma(\theta') A(\theta') \cos\phi'}{k^2 q^2} dv\, dv'\, dv''}{\int \frac{\sigma(\theta')}{k^2 q^2} dv\, dv'\, dv''}$$

where ϕ' is the azimuthal angle associated with the scattering angle θ', the notation being otherwise as previously indicated, and the integrals being taken over the volumes v, v', and v''. These when evaluated gave a mean analysing power of -0.05, in fair agreement with the experimental near zero tail asymmetries.

5.6 Contributions to the Recoil Spectrum Peak from Double Scattering Processes.

In the following chapter an analysis of the data collected as recorded in chapter four will be presented. Although only a portion of the peak in the observed recoil spectra will be selected for analysis in order to minimise the inclusion of events corresponding to doubly scattered neutrons (i.e. the events responsible for the tail), some correction will still be necessary for the inclusion of such events. Clearly it is impracticable to accurately compute this correction by a consideration of all possible double scattering routes (involving at best one scatter

in the helium), however let those routes which might be expected to produce a significant contribution lying under the peak in the recoil spectrum and whose effect is amenable to calculation be considered.

Clearly such a contribution might be expected from neutrons scattered by the helium, then by the front plate of the polarimeter cradle before being detected in the liquid scintillators, since this steel plate is $\sim$2.5cm thick and lies $\sim$1cm to the front of the active volumes of the liquid scintillators. This process was examined in an analagous fashion to the route $\upsilon \rightarrow \upsilon'' \rightarrow \upsilon'$ as described in the previous section, but since the mean energy of the neutrons involved as they scatter from the iron proved to be 1.4MeV (for 3.3MeV neutrons incident upon the gas scintillator), then it was felt that an inelastic scatter from the 0.85MeV level in ^{56}Fe would significantly reduce their chances of being detected in the liquid scintillator. Thus the computations were performed assuming that these neutrons were elastically scattered in the front plate without a loss in their ability to be detected by the liquid scintillators and with the nuclear differential cross section for the process being chosen as a constant 0.15 barns per steradian, corresponding to the elastic differential scattering cross section of iron at this neutron energy and these backward angles. However an attenuation term $\exp(-s'/\lambda')$ was introduced into the calculations in order to take account of the inelastic scatter from the iron, s' being the total distance travelled by the neutron

in the front plate, and λ' being the mean free path of the neutron in the plate before an inelastic scatter occurs, calculated assuming a ~ 0.6 barn total nuclear inelastic scattering cross section for the iron. The simulated recoil spectrum so produced contains $\sim 9\%$ of the events in the simulated single scatter peak shown in figure 41, and further it is of a similar shape to figure 41, albeit that its mean lies at a slightly ($\sim 8\%$) higher recoil energy. Thus a selection of say only those events lying within the limits of the full width at half maximum of the single scatter peak will not substantially alter this 9% contribution. However associated with this double scatter peak is a substantial analysing power, the scattering angles in the helium being near 120°. This analysing power may be calculated in a similar fashion to that for the route $v \rightarrow v'' \rightarrow v'$ in the previous section, assuming the analysing power of iron to be zero (a reasonable approximation, see reference 5). The mean analysing power so computed for neutrons detected in the liquid scintillator after being scattered both by the helium and the cradle front plate is $\sim 2/3$ of that due to neutrons once scattered in the helium before detection in the liquid scintillator. Now as recorded these double scatters amount to $\sim 9\%$ of the single scatters, thus if these were the only routes that need be considered, then the measured asymmetry would require to be multiplied by ~ 1.03 (i.e. a 3% correction) before the analysing power $\langle A2 \rangle$ is applied to obtain the polarization of the incident neutrons.

Double scattering routes involving a scatter in the helium then in either the aluminium mounting plate or the brass liquid scintillator photomultiplier containers are much less simple to treat due to the considerable spread in both the energy of the neutrons incident upon these metals and their associated scattering angles, thus rendering unreasonable the assumption of a constant scattering cross section in these metals. Further the recoil spectra when computed with such approximations tended to fall off beneath the single scatter peak, thus the overlap was considerably sensitive to both the assumed resolution and the portion of the spectrum selected for analysis. With the above reservations in mind, and selecting only events lying within the full width at half maximum of the single scatter recoil peak, a computation (similar to that for the steel plate at the front of the cradle) gave that a $\sim$1.5% correction was required to the measured asymmetry for the sum of the effects due to double scattering routes involving the aluminium mounting plate and the brass photomultiplier containers.

Double scattering routes which involve neutrons scattered in the helium and in its container (in either order) before their detection in the liquid scintillators are extremely difficult to treat theoretically, the reasons being as advanced in the preceeding discussion, only 'more so', since all neutron scattering angles are possible in the container materials (quartz, steel, magnesium oxide), and a very large tail is present falling off beneath the peak. Further any accurate treatment of the

routes involving scatters first in the container material would require to introduce the energy lost in this process and the new orientation of the neutron spin w.r.t. the momentum vector of the recoiling neutrons. Thus only crude estimates of the effects of double scattering involving both the helium and its container (i.e. including the quartz window and its steel surround) were performed, these being based on the recoil spectrum of the tail as developed in section 5.5 and on further computations to a similar degree of simplification involving neutron scatters from the 2mm thick stainless steel shell containing the forward portion of the helium gas, and these crude estimates suggested that a correction of more than a few per cent might be appropriate to the asymmetry measured for events lying between the full width at half maximum of the single scatter peak.

Finally in this section consider the neutrons double scattered by the helium itself before being detected in the liquid scintillators, taking into account the mean analysing power for this process. Then accepting the assumptions listed in section 5.1 and used in the computation of $\langle A_1 \rangle$, let this double scattering route be:

The neutrons of polarization $\underline{P}$ ($P\hat{\underline{z}}$)
incident in a direction $\underline{k}_1$ ($\hat{\underline{z}}$)
are scattered by a small volume element dv_1 of helium gas along a direction $\underline{k}_2$ to a similar small volume element of helium gas dv_2, a distance r_1 away. Thence they are scattered along a direction $\underline{k}_3$ into a small volume element dv' of the liquid scintillator,

a distance τ_2 from dv_2. Then with $\underline{k}_1$, $\underline{k}_2$, $\underline{k}_3$ unit vectors, the two scattering angles θ_1, θ_2 are defined by

$\cos\theta_1 = \underline{k}_1 \cdot \underline{k}_2$; $\cos\theta_2 = \underline{k}_2 \cdot \underline{k}_3$, with θ_1, θ_2 taking values between 0 and π. Now let

$$\underline{n}_1 = \frac{\underline{k}_1 \wedge \underline{k}_2}{\sin\theta_1} \quad ; \quad \underline{n}_2 = \frac{\underline{k}_2 \wedge \underline{k}_3}{\sin\theta_2}$$

then the azimuthal angles ϕ_1, ϕ_2 corresponding to θ_1, θ_2 are given by

$$P\cos\phi_1 = \underline{P} \cdot \underline{n}_1 \quad ; \quad \cos\phi_2 = \underline{n}_1 \cdot \underline{n}_2$$
$$P\sin\phi_1 \underline{k}_1 = \underline{P} \wedge \underline{n}_1 \quad ; \quad \sin\phi_2 \underline{k}_2 = \underline{n}_1 \wedge \underline{n}_2$$

Then one may obtain that the number of neutrons per second double scattered by the gas scintillator and then detected by the liquid scintillator 'X' is given by $N(n')^2 E_x \int \frac{\sigma_1(\theta_1)\,\sigma_2(\theta_2)}{\tau_1^2\,\tau_2^2}\, dv_1\, dv_2\, dv'$ where $\sigma_1(\theta_1)$ is the differential cross section for the scattering of (monoenergetic) neutrons through an angle θ_1, while $\sigma_2(\theta_2)$ is the differential cross section for the second scatter in the helium, and clearly a knowledge of the phase shift angles for n-^{4}He scattering at all neutron energies in the once scattered flux are required for its evaluation in the integration process. For the present series of calculations, a fit was made in the neutron energy range of interest ($\sim$1.2 $\rightarrow$ 3.5MeV) to the compilations of Satchler et al.[35]. The triple volume integration is over the active volume of the gas scintillator (twice) and over the active volume of the liquid scintillator. N, n', E_x are as recorded in section 5.1.

Now the polarization of the incident neutron beam changes to

$\underline{P}_f$ (say) on being once scattered by $d\nu_1$, where

$$\underline{P}_f \left\{ 1 + A_1(\theta_1)\, \underline{P} \cdot \underline{n}_1 \right\}$$

$$= \underline{P} + A_1(\theta_1)\underline{n}_1 - \frac{(g^x h + h^x g)}{|g|^2 + |h|^2} \underline{P} \wedge \underline{n}_1 + \frac{2|h|^2}{|g|^2 + |h|^2} \left\{ (\underline{P} \cdot \underline{n}_1)\underline{n}_1 - \underline{P} \right\}$$

and g, h are the non spin flip and spin flip wave amplitudes for this first scatter as defined in reference 5.

Hence taking into account this change in polarization, the mean analysing power for neutrons double scattered in the helium before detection in a liquid scintillator becomes

$$\frac{\int \frac{\sigma_1(\theta_1)\,\sigma_2(\theta_2)}{\tau_1^2\,\tau_2^2} \left\{ \alpha + \beta + \gamma \right\} d\nu_1\, d\nu_2\, d\nu'}{\int \frac{\sigma_1(\theta_1)\,\sigma_2(\theta_2)}{\tau_1^2\,\tau_2^2} \left\{ 1 + \delta \right\} d\nu_1\, d\nu_2\, d\nu'}$$

with

$$\alpha = A_1(\theta_1)\cos\phi_1$$

$$\beta = A_2(\theta_2)\cos\phi_1\cos\phi_2$$

$$\gamma = \frac{A_2(\theta_2)\sin\phi_1\sin\phi_2}{|g|^2 + |h|^2} \left\{ -(g^x h + h^x g)\sin\theta_1 + (|h|^2 - |g|^2)\cos\theta_1 \right\}$$

$$\delta = A_1(\theta_1)\, A_2(\theta_2)\cos\phi_2$$

The analysing power $A_1(\theta_1)$ is calculated for the first scatter of monoenergetic neutrons (as are σ_1, g, h) while $A_2(\theta_2)$ is calculated as $\sigma(\theta_2)$, using the phase shift angles corresponding to the scattered neutron flux.

Now using the above relations, and proceeding in an analogous fashion to that outlined in section 5.4, the recoil spectrum associated with neutrons double scattered in helium

was computed along with its associated analysing power. These are plotted in figure 43, a helium gas pressure of 65 atmospheres in the gas scintillator being assumed. These calculations show that the neutrons double scattered in the helium amount to $\sim 3\%$ of the single scatters, and they have associated with them an overall mean analysing power of 0.2. Thus one might expect a $\sim 2.3\%$ correction to be required to the measured asymmetry to account for this effect. However if only those events falling within the full width at half maximum of the single scatter spectrum are selected, then the required correction reduces to $\sim 1\%$ due to the recoil spectrum for double scatters in helium being flatter than that due to single scatters and further the double scatter analysing power peaks in the region of the recoil spectrum selected.

Now bringing together the double scattering processes discussed in the present section, and accepting that in the analysis of the results to be presented in the following chapter the measured asymmetry will be taken from a portion of the observed recoil spectra within limits similar to the full width at half maximum limits employed extensively in the present section, then these computations show that a $\sim 5\%$ correction is required to this measured asymmetry when the (not easily calculable) double scattering routes involving the gas scintillator container are ignored. Thus in the following result analysis, this value will be taken as a lower limit to the correction required for double scattering effects, although such

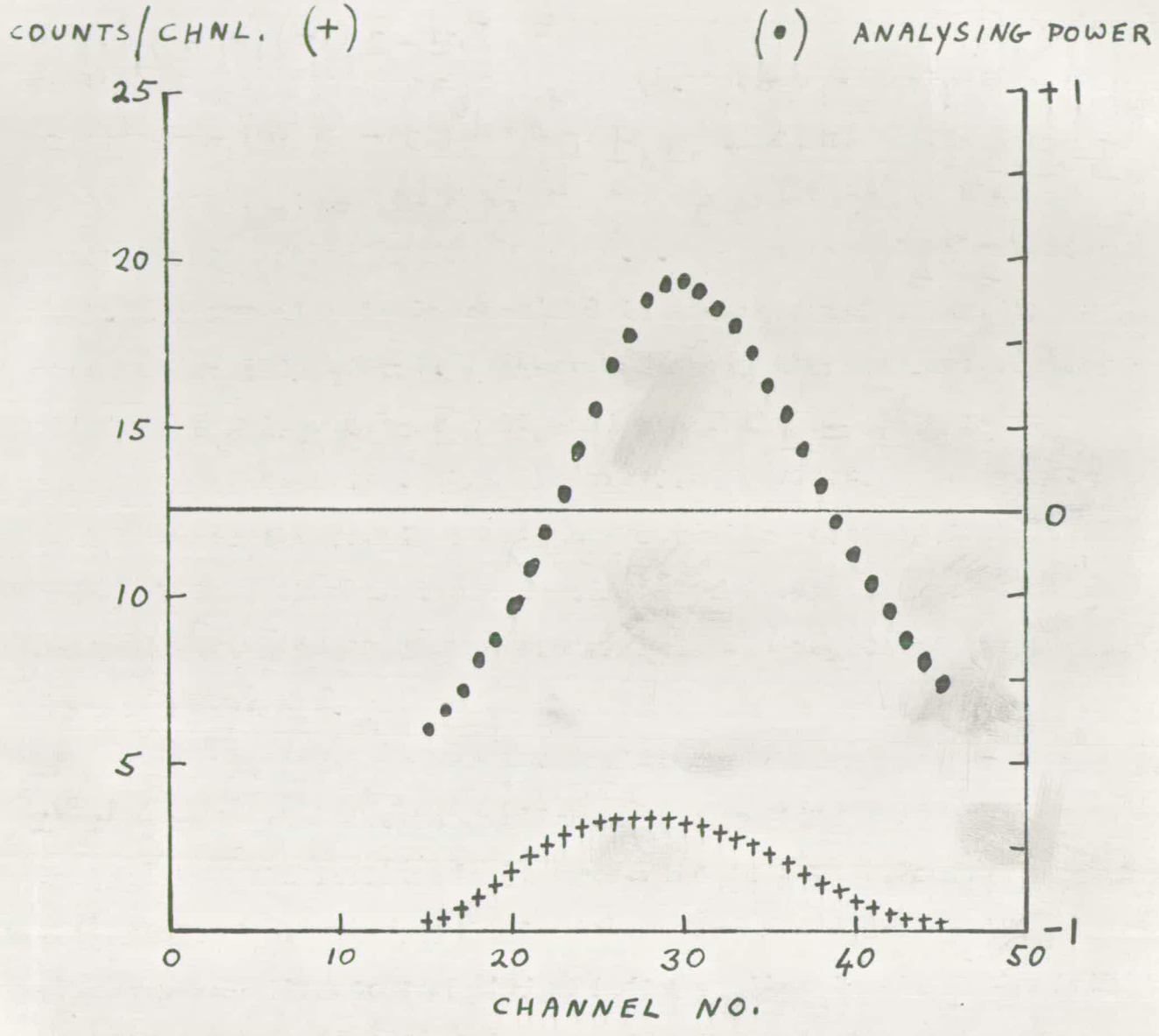

FIG. 43 SIMULATED PULSE HEIGHT SPECTRUM OF THE OUTPUT FROM THE GAS SCINTILLATOR DUE TO NEUTRONS SCATTERED TWICE IN THE HELIUM BEFORE DETECTION IN A LIQUID SCINTILLATOR. CO-ORDINATES AS IN FIGS. 40 → 42

computations as were made on the effects due to the gas scintillator container suggest that this might possibly require doubling.

Before concluding the present chapter, consider as a by-product of the present computations the following comments on the corrections required to the observed asymmetry for neutrons double scattered in liquid helium, this having approximately ten times the density of helium gas at a pressure of 65 atmospheres, and thus has a corresponding increase in the double scatter to single scatter ratio. Computations of the corrections due for double scattering in liquid helium polarimeters have been published by Stinson et al.[52] and Miller et al.[51], neither of these discussing the associated helium recoil energy spectrum or the possibility of some selection being made from this. Clearly the results quoted above for the present polarimeter indicate that should the selection of a portion of the (liquid) helium recoil spectrum be employed, then such published computations are inadequate, and a treatment involving simulated recoil spectra as developed in the present chapter is more appropriate.

CHAPTER 6.

MEASUREMENTS OF THE POLARIZATION OF THE NEUTRONS EMITTED IN THE $^{2}H(d,n)^{3}He$ REACTION.

In the present chapter, the asymmetries measured as indicated in chapter 4 will be processed using the techniques outlined in chapter 5, thus producing the desired neutron polarization estimates. These will be compared with the results of the workers listed in table 1, and the experimental techniques of these workers will be critically examined.

6.1 Tail Corrections

As previously noted it is important to obtain an estimate of the extent to which the (unpolarized) tails of the gated helium recoil spectra extend beneath their respective peaks and so allow a correction to be applied to the measured asymmetry in the peak area.

In the previous chapter, some computations were presented which indicate that the source of the tail is various double scattering processes, the main contribution involving a scatter in the solid surrounds of the gas scintillator. Such a contribution falls off beneath the peak as do contributions from scattering in the aluminium mounting plate and the brass photomultiplier containers. Further, these latter contributions become partially polarized beneath the peak as are the contributions (which lie beneath the peak) from scattering involving the cradle front plate and double scattering in the helium itself. Thus if

one represents the effect of all these processes by a single unpolarized contribution to the gated recoil spectrum, the curve representing this follows the initial downward fall of the experimentally observed tail and might be expected to so continue beneath the peak with a reduced gradient (due to the contributions from the cradle front plate and double scattering in the helium).

An examination of the measured asymmetry for events occurring around (a) the mid point of the lower edge of the peak, (b) the summit of the peak, and (c) the mid point of the upper edge of the peak showed consistently throughout the thin target results fair agreement (within statistical uncertainties) between (b) and (c), with (a) being significantly lower, thus supporting the idea of a fall off in the unpolarized contribution beneath the peak.

Thus the experimentally recorded data was analysed by drawing smooth curves through the tails continuing beneath their associated peaks in a fashion as shown in figure 44, and such curves were taken to be the unpolarized contributions to be corrected for. Support for such extrapolations was obtained by examining (for each one of the thin target results) the asymmetry so corrected for groups of channels throughout the peak region, this showing reasonable agreement with an expected constant value, although the statistical uncertainties due to the limited number of events sampled did not allow this technique to accurately define the required correction.

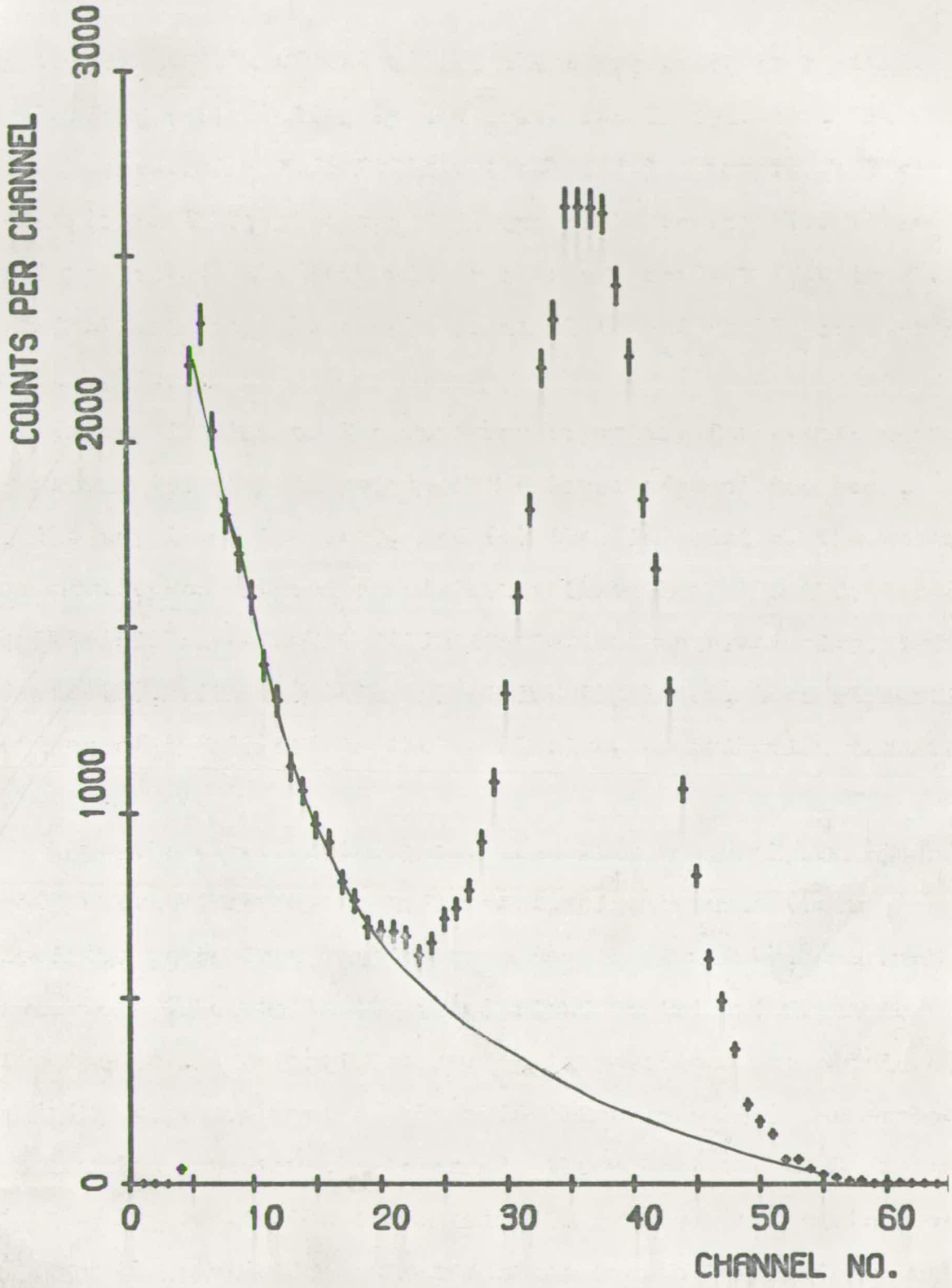

FIG. 44 THE TAIL EXTRAPOLATION

Now to minimise the inclusion of the unpolarized contribution in a polarization estimate (and so reduce the correction required with its accompanying uncertainty), clearly it is desirable to sample only events around the summit of the peak, at the same time taking care not to select so few channels as to introduce a statistical uncertainty considerably larger than the uncertainty in the unpolarized contribution. Further, since the unpolarized contribution is observed to fall off with increasing pulse height, the optimum selected channel limits should lie slightly asymmetric about the summit of the peak, incorporating more of the upper edge than of the lower.

With these criteria in mind, the lower limit selected lay between the mid point of the lower edge and the summit of the peak, while the upper limit lay a few channels from the mid point of the upper edge, but on the side remote from the summit. The selection of narrower limits was not found significantly to alter the correction required for the proposed unpolarized tail, it merely serving to reduce the statistical accuracy of the result.

The asymmetries so measured between the selected limits in the thin target data recorded as indicated in chapter 4 were found to require multiplication by factors of from 1.10 to 1.14 to correct for the unpolarized contribution evaluated as above, the lower corrections corresponding to the better resolution spectra. These proposed corrections are listed with the results in table 2.

It is difficult to determine the accuracy to which these

corrections are known. The discussion in the final section of the preceeding chapter suggested that a correction factor of at least 1.05 was required for spectra of a resolution similar to the best attained. Thus a lower limit to the experimentally required correction might reasonably be taken as one half of the proposed correction. Further the trial of other smoothly varying tail extrapolations monotonically decreasing with pulse height indicated that an unpolarized contribution greater than ~50% up on the proposed contribution was unlikely. Thus a correction factor of $1.\alpha$ say may be plausibly quoted to an accuracy of $\pm \frac{\alpha}{20}$, and a consideration of the results listed in table 2 and described in more detail in the following section will show that the uncertainty so produced in the final results was consistently less than the statistical accuracy to which these are quoted.

6.2(a) Thin Target Measurements

The results of the six thin target measurements taken as described in chapter 4 are shown in table 2, and in figures 45 to 50 are shown six gated helium recoil spectra, each corresponding to one of these measurements, and representing the sum of the real coincidences recorded between the gas scintillator and the neutron detectors for all four cradle positions.

The incident deuteron energy was obtained using the meter indicated accelerating voltage and the calibration chart prepared as indicated in section 4.4. The target stopping

TABLE 2 THIN TARGET RESULTS

1	2	3	4	5	6	7	8	9	10
Ed (keV)	Δ Ed (keV)					$\langle A_2 \rangle$	P		
275	± 60	− 0.077 ± 0.007	− 0.115 ± 0.010	1.12	− 0.129 ± 0.012	0.89	− 0.145 ± 0.013	+ 0.004 ± 0.007	− 0.002 ± 0.010
385	± 55	− 0.085 ± 0.006	− 0.133 ± 0.009	1.12	− 0.149 ± 0.010	0.90	− 0.165 ± 0.011	− 0.008 ± 0.006	− 0.006 ± 0.009
500	± 55	− 0.081 ± 0.007	− 0.127 ± 0.010	1.12	− 0.142 ± 0.011	0.92	− 0.155 ± 0.012	− 0.005 ± 0.007	− 0.001 ± 0.010
620	± 50	− 0.071 ± 0.007	− 0.119 ± 0.009	1.14	− 0.136 ± 0.011	0.93	− 0.147 ± 0.012	+ 0.005 ± 0.007	+ 0.002 ± 0.010
730	± 50	− 0.074 ± 0.006	− 0.135 ± 0.090	1.10	− 0.149 ± 0.099	0.93	− 0.159 ± 0.011	0.000 ± 0.006	+ 0.007 ± 0.009
840	± 45	− 0.080 ± 0.008	− 0.124 ± 0.011	1.14	− 0.141 ± 0.013	0.94	− 0.150 ± 0.013	− 0.005 ± 0.008	+ 0.009 ± 0.011

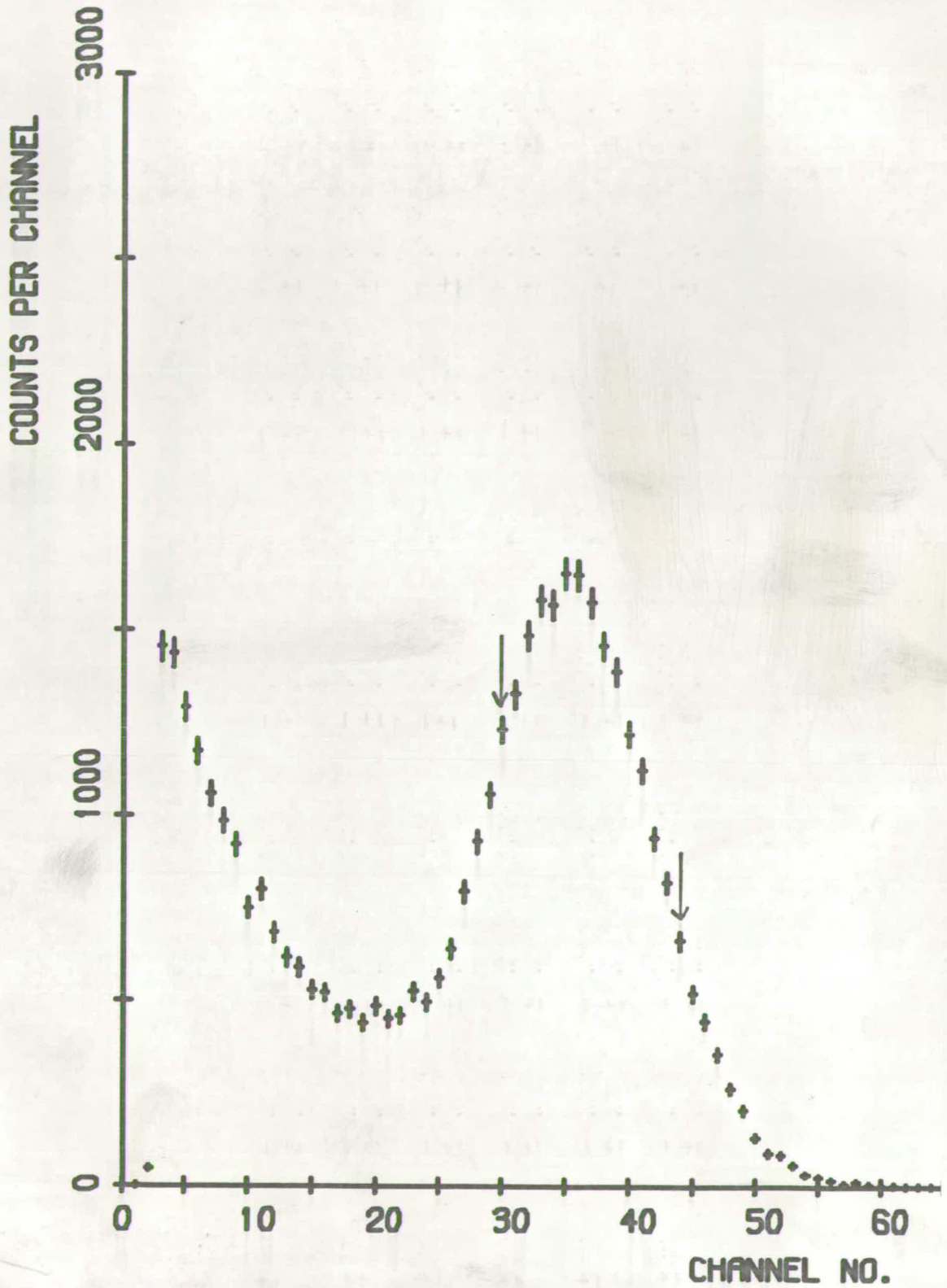

FIG. 45 THE GATED HELIUM RECOIL SPECTRUM FOR $\overline{E_d} = 275\,keV$

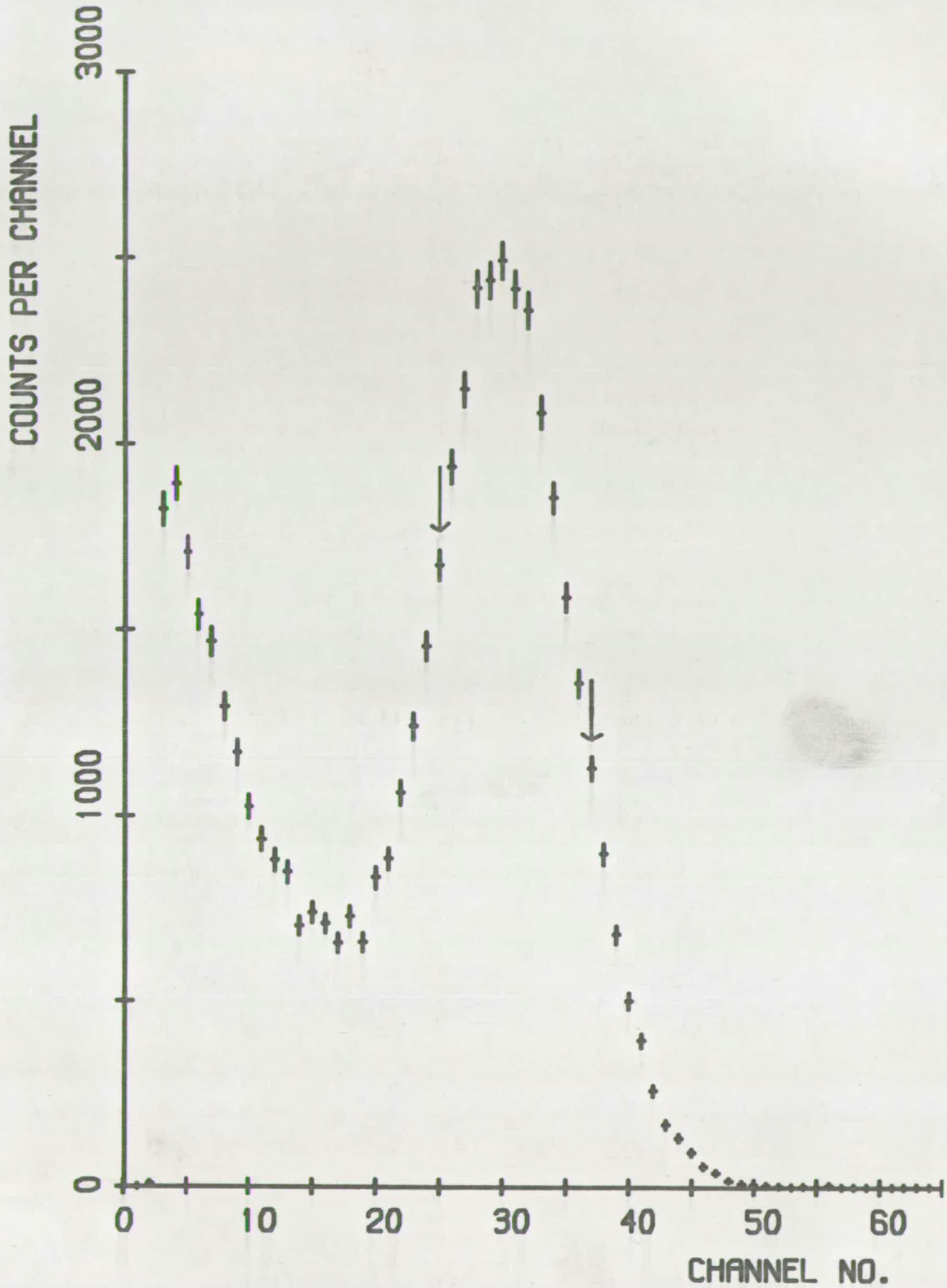

FIG. 46 THE GATED HELIUM RECOIL SPECTRUM FOR $\overline{E_d} = 385\,keV$

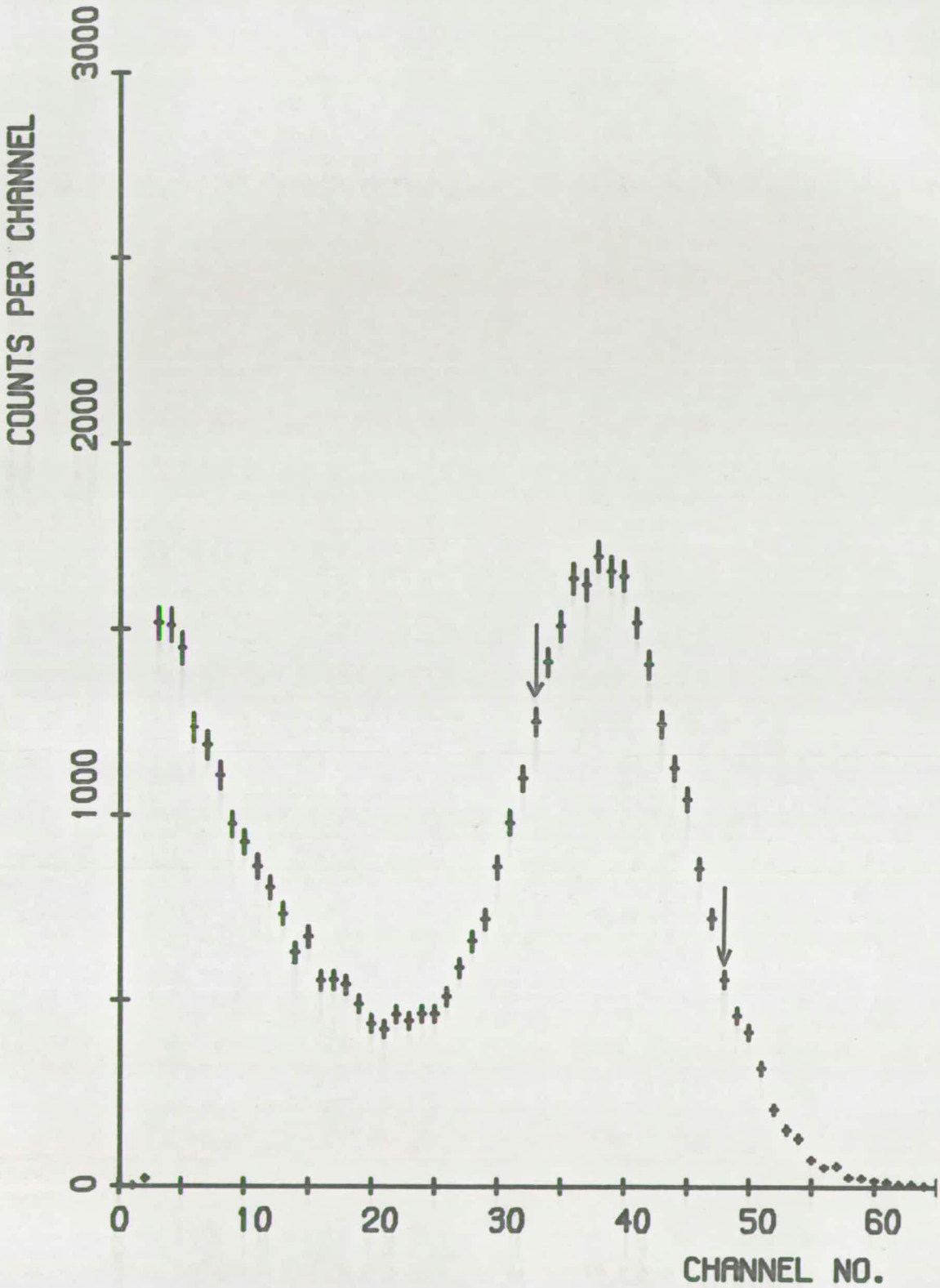

FIG. 47 THE GATED HELIUM RECOIL SPECTRUM FOR $\overline{E_d}$ = 500 keV

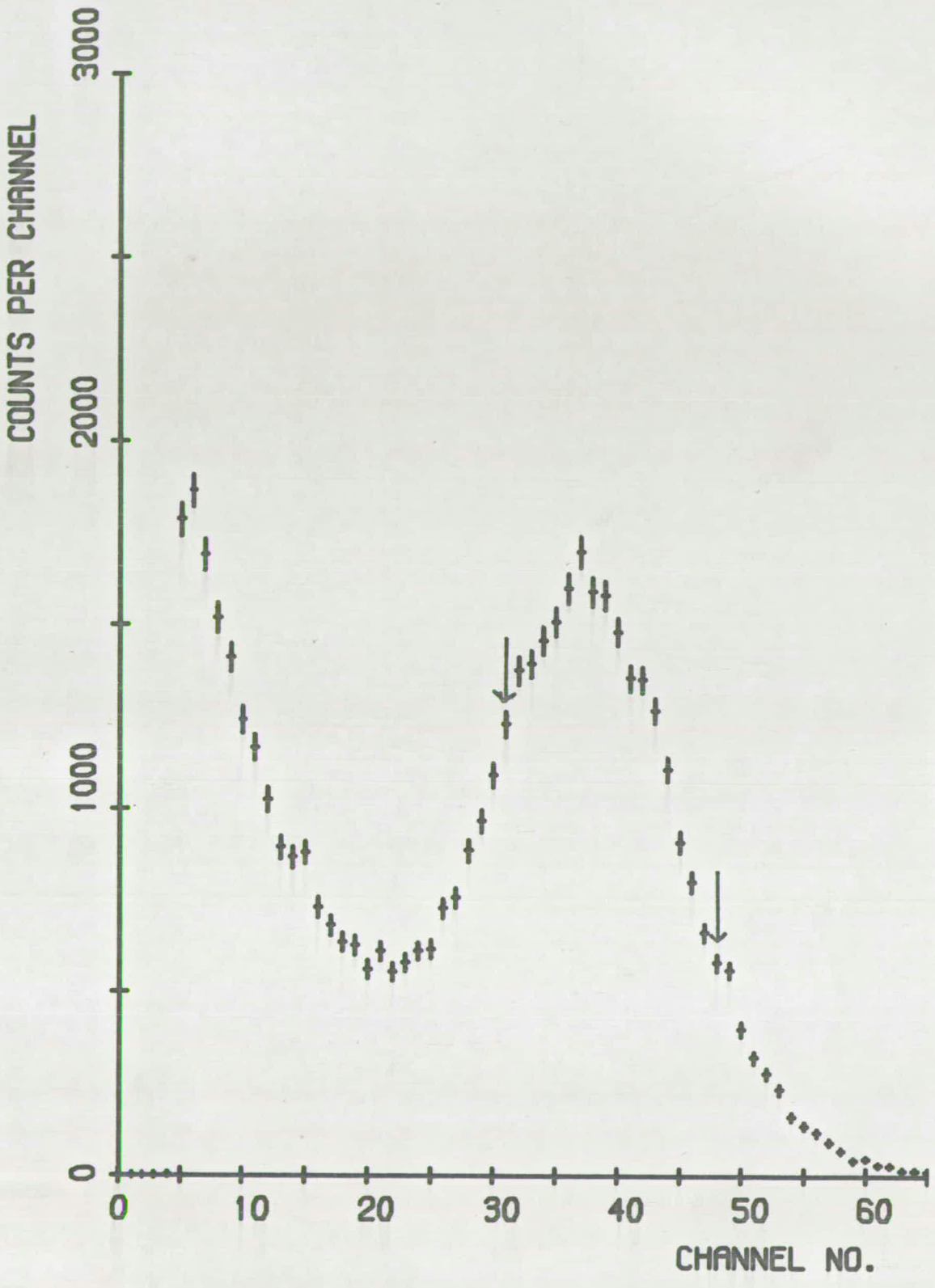

FIG. 48 THE GATED HELIUM RECOIL SPECTRUM FOR $\overline{E_d} = 620\ keV$

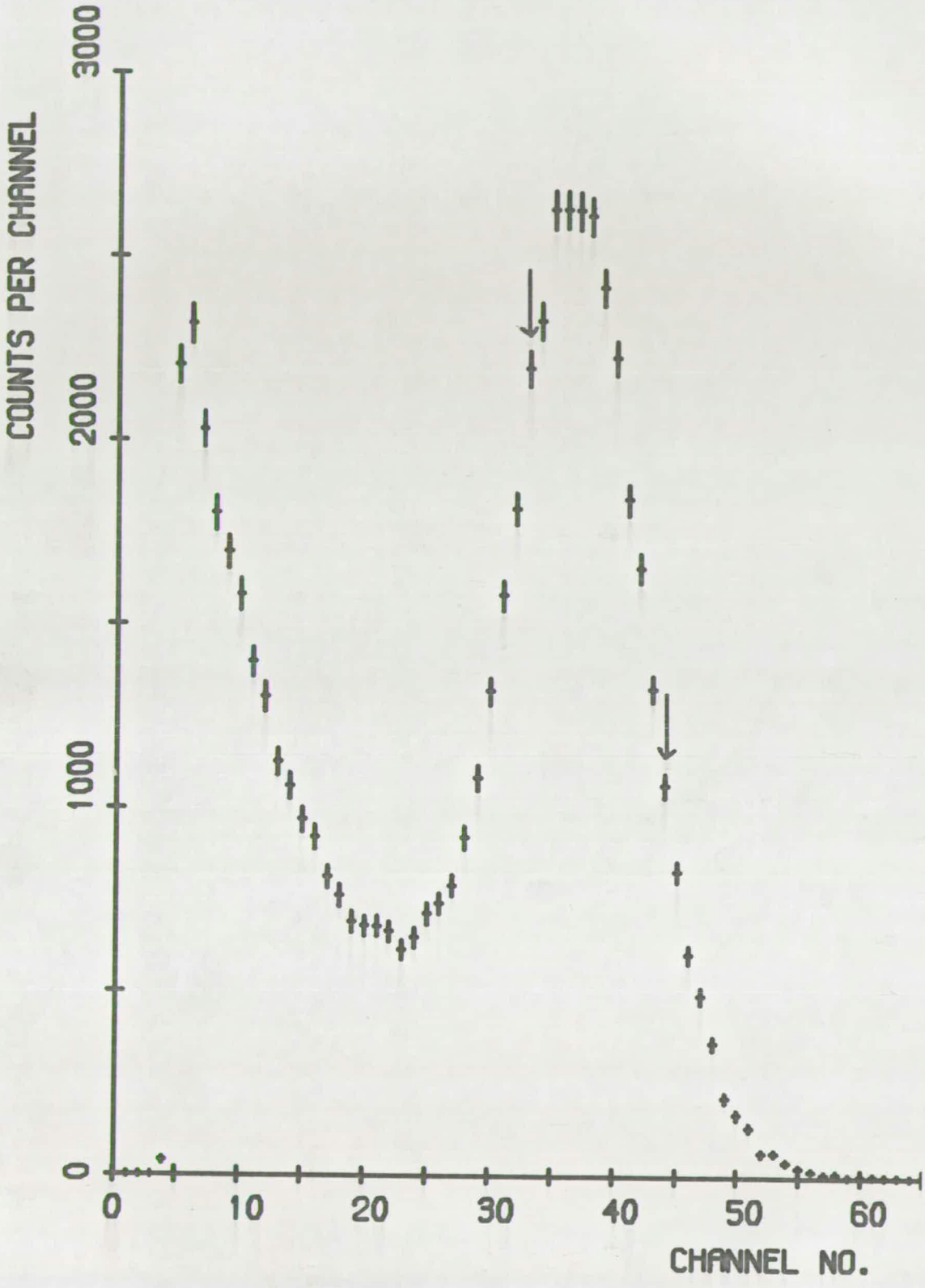

FIG. 49 THE GATED HELIUM RECOIL SPECTRUM FOR $\overline{E_d}$ = 730 keV

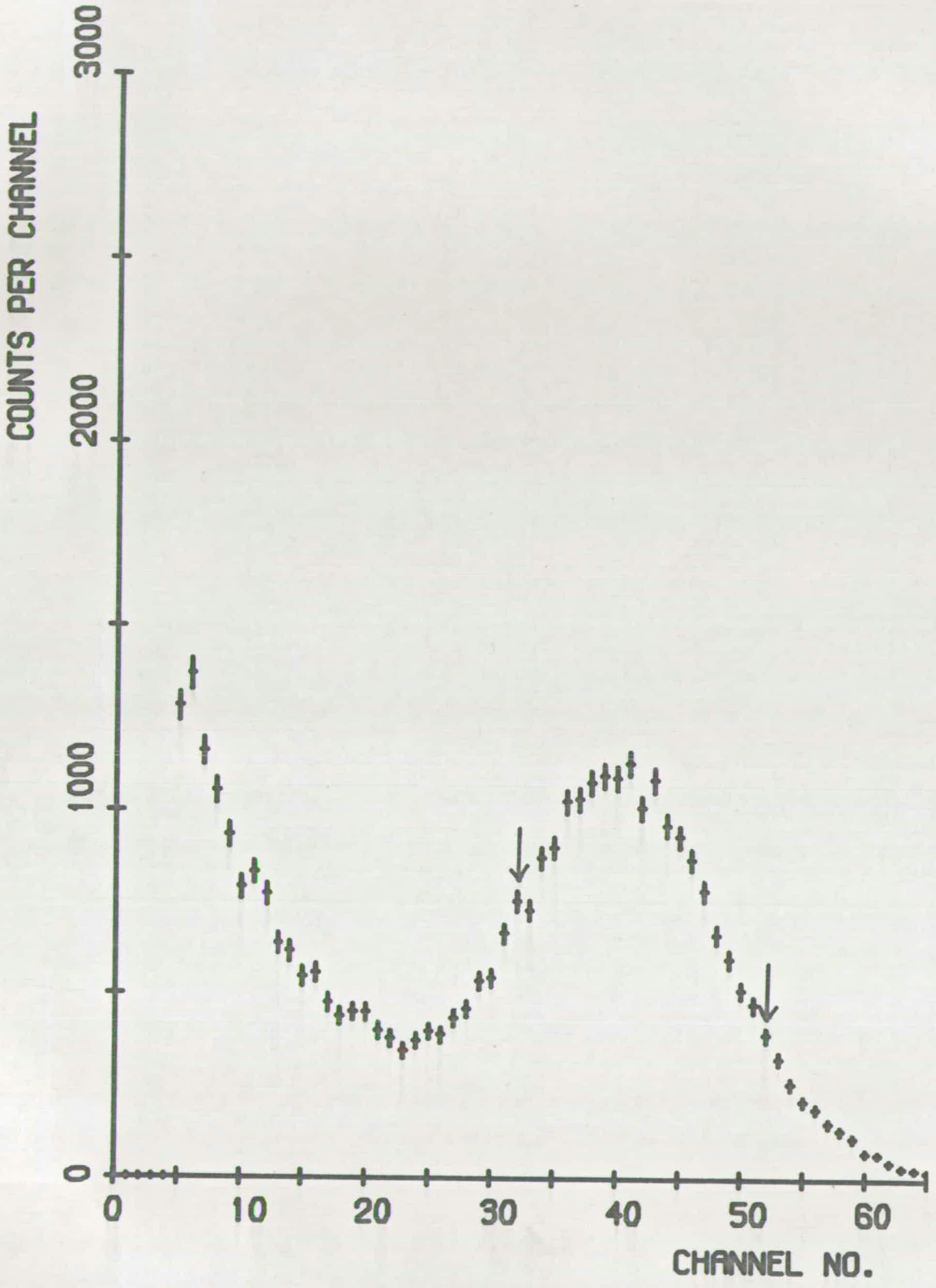

FIG. 50 THE GATED HELIUM RECOIL SPECTRUM FOR $\overline{E_d}$ = 840 keV

powers used in the present work were taken from the compilations of Northcliffe and Schilling,[56] assuming a Ti to D atomic ratio of one to one. These compilations are based on extrapolations of theoretical predictions and experimental results. An indication of the accuracy to which these stopping powers are known may be obtained by considering the tabulations, also based on extrapolation, of Coon[57], these giving stopping powers ranging from 40% to 10% higher than the values of Northcliffe and Schilling[56] for deuterons ranging in energy from 0.2 to 1MeV incident upon Ti-D targets.

Column one of table 2 shows the median deuteron energies at which the measurements were taken, and column 2 gives ± one half the target stopping powers at these energies, all of these figures being rounded to the nearest 5 keV. The third column of table 2 shows the measured asymmetry in the reaction plane with no energy selection (i.e. accepting both the peak and tail of the associated recoil spectrum), the uncertainties quoted in this and in all other columns being purely statistical. In the fourth column is shown the measured reaction plane asymmetry for events selected between the limits as described in the previous section (and as shown between the arrows in the corresponding spectra of figures 45 to 50). Column five shows the correction factor for the presence of an unpolarized tail estimated as indicated in the previous section, and the following column contains the corrected (energy selected) asymmetry. In chapter 5, $\langle A2 \rangle$ as defined in section 5.2 was shown to be an adequate representation

of the analysing power of the polarimeter (after 'tail' effects have been corrected for) even when selection of a part of the gated recoil spectrum peak is employed. Thus $\langle A_2 \rangle$ was computed for incident neutron energies as produced in the $^{2}H(d,n)^{3}He$ reaction for a laboratory reaction angle of 46° at each of the six listed median deuteron energies, the results being shown in column seven of table 2. These computations used the $n-^{4}He$ scattering phase shift angles of Austin et al.[17], the $^{2}H(d,n)^{3}He$ differential cross section data of Brolley and Fowler[54], and a (non-critical) polarization estimate of -0.15. Hence column eight lists the neutron polarizations calculated from the corrected asymmetries of column six and these computed analysing powers.

The final two columns of table 2 merely list the asymmetries observed in the horizontal plane (i.e. vertical to the reaction plane) during their associated polarization measurements, the first of these including the whole of the recorded recoil spectra, the second selecting events between the same limits as used to obtain the associated polarization values. A combination of the horizontal asymmetries listed in column nine gives a result of -0.0014 ± 0.0028. A combination of the asymmetries recorded in the vertical plane for the above thin target results, but associated with the 'tails' of the recoil spectra gives a result of -0.015 ± 0.005.

All of these thin target results were taken with a mean laboratory reaction angle of 46°, the geometrical spread in this angle due to the finite size of the gas scintillator being $\pm 1.75^{\circ}$.

However Rutherford scattering of the incident deuterons by the titanium nuclei in the target material gives rise to a further spread in the reaction angles of the neutrons observed. Thus the probability that a deuteron of energy E will be scattered through an angle between θ and $\theta+d\theta$ during its passage through a thin titanium foil of thickness t is given by $\frac{ntZ^2e^4d\theta}{8\pi\varepsilon_0^2E^2\theta^3}$ for small θ, where n is the number of titanium atoms (of nuclear charge Ze) per unit volume of the foil. Thus considering the case of the lowest mean deuteron energy result listed in table 2, and noting that the mean distance travelled in the target material by the deuterons producing the neutrons is one half of the target thickness, then we find that there is only a 10% probability of such 'mean' deuterons having been single scattered through an angle greater than 5°. Further this 10% probability angle is inversly proportional to the deuteron energy and thus reduces to $\sim 1.7^\circ$ for the highest energy measurement listed in table 2. However the probability of scattering rises sharply with decreasing angle, and thus multiple Rutherford scattering should be considered. Following the treatment of Williams[58], the root mean square angular deviation of the deuterons multiple scattered by the titanium after traversing one half of the target thickness was also calculated, and this turned out to be $\sim 4.2^\circ$ in the case of the 275keV measurement listed in table 2. Once more this angle varied inversly with deuteron energy, and so is $\sim 1.5^\circ$ for the 840keV measurement listed in table 2.

6.2(b) Thick Target Measurements

Associated with the neutrons emitted (in the $^{2}H(d,n)^{3}He$ reaction) from a target in a particular direction will be a spread in deuteron energies (due to deuteron energy loss within the target) and a spread in the laboratory reaction angle (due to deuteron scattering within the target), both of these increasing with target thickness. Thus the unfolding of polarization data from thick target measurements will require to take account of this.

However the thin target polarization measurements listed in table 2 show little sign of a marked polarization dependence on deuteron energy. Further as indicated in section 1.1, the polarization angular distribution is both theoretically predicted and experimentally observed to exhibit a broad maximum close to the chosen mean angle, thus one might expect our thick target polarization measurements to be in reasonable agreement with the thin target results.

As recorded in chapter 4, two measurements were performed, prior to the thin target measurements, at incident deuteron energies of 880keV and 660keV, with a Ti-D target thick for deuterons of up to 850keV. These two results were analysed in a similar fashion to the thin target measurements, except that the 'mean' deuteron energy, at which the analysing power was evaluated, was computed by fitting the yield curve (i.e. the differential cross section for the $^{2}H(d,n)^{3}He$ reaction divided by the stopping power per unit distance travelled in a Ti-D

target) to a quadratic function of deuteron energy.

Thus with an incident deuteron energy of 660keV, the mean deuteron energy was $\sim$430keV, a correction factor of 1.12 was applied to account for the presence of an unpolarized tail, and the resultant polarization was found to be -0.15, with a statistical uncertainty of $\pm$0.0125. With an incident deuteron energy of 880keV, the mean deuteron energy was $\sim$ 570keV, a correction factor of 1.12 was applied to account for the presence of an unpolarized tail, and the resultant polarization was found to be -0.158 with a statistical accuracy of $\pm$0.0124. Clearly these results show good agreement with the thin target measurements listed in table 2.

Now in the preliminary measurement sequence, two measurements were also performed with the complete polarimeter, these being recorded at incident deuteron energies of 390keV and 880keV, with a Ti-D target which was thick for deuterons up to $\sim$400keV. However, as recorded, the rapid downward drift of the light output from the gas scintillator at this stage so spoiled the resolution of the recorded spectra as to make the evaluation of a contribution due to an unpolarized tail difficult. As previously indicated, this data was initially analysed by considering only events in the gated spectra with pulse heights greater or equal to those occurring around the summits of the peaks, and no correction was applied to account for the presence of an unpolarized contribution. In this fashion a polarization of -0.129 with a statistical accuracy of $\pm$0.007 was recorded for a mean

deuteron energy of 255keV, as was a polarization of - 0.14 with a statistical accuracy of ±0.007 at a mean deuteron energy of 690keV. Once more these are in reasonable agreement with the thin target results of section 6.2a when account is taken of the correction factors of ~ 1.12 these included.

6.3 Scattering in the Target Assembly.

The preceeding results report the measurement of the polarization of the neutrons viewed by the gas scintillator and originating from the target assembly. These neutrons will in the main arrive directly from the target strip, but a contribution may arise from neutrons scattered in that part of the target assembly seen by the gas scintillator through the collimator, this scattering taking place mainly from the brass stalk or the cooling water flowing therein. Consider the following simplified evaluation of this contribution recorded during a polarization measurement.

A point in the centre of the gas scintillator volume views through the collimator a portion of the target stalk as sketched in figure 51. Let a deuteron beam be incidentupon the centre spot of the top surface of this target, thereby producing N neutrons per second equally distributed throughout 4π. Let the probability of such a neutron being scattered per unit distance travelled within the volume (v) of the portion of the target stalk shown be a constant μ. Then ignoring attenuation, the number of neutrons per second once scattered in v is $\frac{N\mu}{4\pi}\int\frac{dv}{r^2}$,

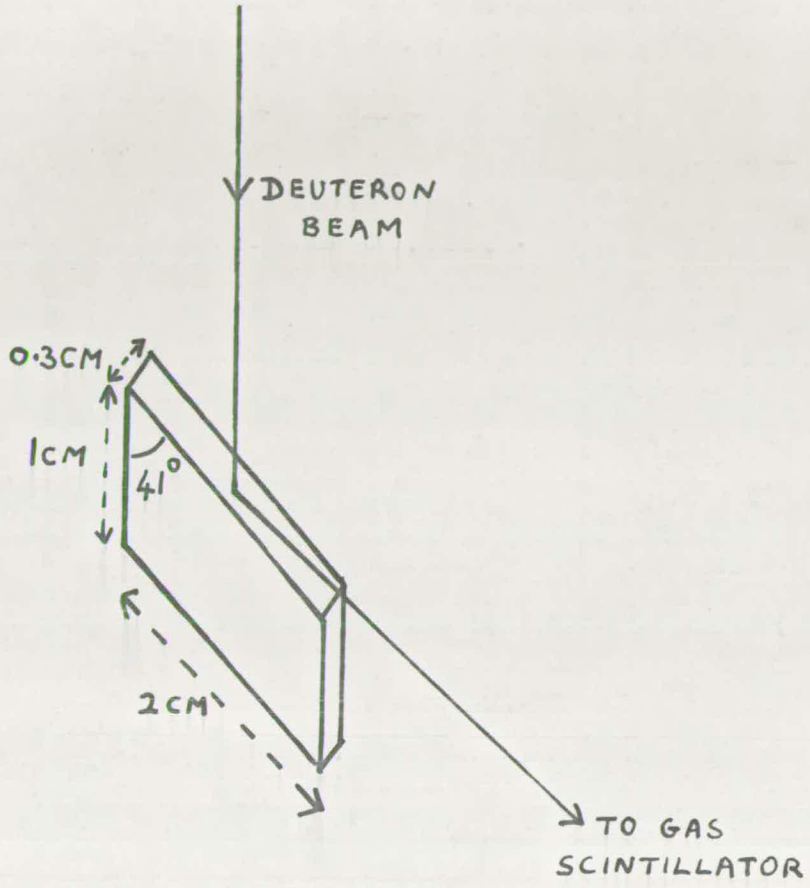

FIG. 51 SKETCH OF PORTION OF TARGET STALK VIEWED FROM THE CENTRE OF THE GAS SCINTILLATOR

where τ is the distance from the deuteron beam spot to a point within the volume v throughout which the integration takes place. And thus if once more this scattered flux is distributed evenly throughout 4π , then the ratio (R) of this once scattered flux to the direct flux as seen at the centre of the gas scintillator is $\frac{\mu}{4\pi}\int\frac{dv}{\tau^2}$.

Now to obtain the polarization measurements listed in the previous section, pulse amplitude selection of the gated helium recoil spectra was employed, thus significantly reducing the probability of inclusion of neutrons inelastically scattered in the brass of the target stalk, hence only the elastically scattered contribution will be considered. Now both brass and water have $\sim 10^{23}$ atoms per cc, and their constituent nuclei (H,O,Cu,Zn) exhibit near 2.25 barn total elastic scattering cross sections for neutrons in the 3 to 3.5MeV range. Hence these values were used to compute μ and so gave $R \sim 0.05$, i.e. there is a $\sim 5\%$ contamination of the direct neutron flux with neutrons arising from elastic scattering in the target assembly.

Now the $^2H(d,n)^3He$ reaction differential cross section is not, as assumed in the preceeding discussion, isotropic in the laboratory frame. (e.g. for 600keV incident deuterons, the differential cross section at a neutron emission angle of zero degrees is approximately three times the value at 46°.) Thus a consideration of the geometry of the target might suggest that this factor might raise R slightly. However operating in the opposite direction (i.e. to reduce R) is the loss in energy

of the neutrons elastically scattered by the hydrogen in the cooling water, this reaching 50% for 45° scattering, by which stage there will be little probability of these neutrons being recorded between the selected limits in the helium recoil spectra.

Further, if one considers the angular variation of the differential cross sections for neutrons scattered in the target assembly materials, it may be noted that these peak sharply at small (neutron) scattering angles, especially in the case of the Zn and Cu . Thus much of the target scattered flux detected by the gas scintillator will be associated with neutrons emitted close to the mean reaction angle of 46° before being small angle scattered. Hence these neutrons will be produced with a polarization near to that of the studied direct flux, and this will not change significantly on their being small angle elastically scattered. This will further reduce the correction required to the measured polarization due to the presence of neutrons scattered by the target, and suggests that 5% is an upper limit to the correction required, this lying well inside the statistical uncertainties.

6.4 Discussion of Measurements

In comparing the present measurements of table 2 with those displayed in figure 1, consider first the results and techniques of Pasma[13], Boersma[10] et al, Behof[8] et al, and Roding and Scholermann,[7] all of whom used a polarimeter employing a helium gas scintillator as scatterer-analyser.

A feature of the present study was the presence of a tail (with near zero polarization) in the gated helium recoil spectrum which in chapter 5 has been attributed to various double scattering routes. Yet none of the four groups of workers listed above have reported their recoil spectra, and indeed only Behof et al.[8] have apparently recorded it. Thus there is no indication as to the amount of tail that Pasma[13], Boersma et al.[10], and Roding and Scholermann[7] might have included in their measurements, nor do Behof et al.[8] mention whether they observed unpolarized tail contributions and what steps (i.e. tail extrapolations) they took to account for these.

Unpolarized tails have been reported by a group associated with Duke University[59,60]. Thus in reference 59 they show small near horizontal tails in their gated helium recoil spectra produced by $\sim$2.5MeV neutrons from the $^{12}C(d,n)^{13}N$ reaction and these tails they have arbitrarily extrapolated as continuing beneath their associated peaks with straight line fits. As in the present case these workers have selected only a portion of their peaks for analysis and between their selected limits the extrapolated unpolarized contribution amounts to 9% of the recorded events. They indicate that they have considered γ-rays and neutron inelastic and elastic scattering in the walls of their gas scintillator as possible sources of tails, but maintain that these processes could not account for the magnitude of the effect they observed. They thus arbitrarily placed an error of $\pm$ 25% on the magnitude of their extrapolated

background estimates. A more recent paper by this group[60] shows gated helium recoil spectra for ~7MeV neutrons from the $^{6}Li(d,n)^{7}Be$ reaction which exhibit larger tails than in their previous paper, albeit still smaller than reported in the present work. These tails, referred to as 'background' exhibit a slope similar to those in the present work and have been arbitrarily extrapolated with smooth curves falling to zero beneath their respective peaks.

Clearly if we accept that a major source of such tails arises from scattering of the neutrons in the material of the gas scintillator viewing window and its bulky surrounds, then the size of the tail will depend on the amount of this material present, on its orientation with respect to the neutron beam, and on the collimation of the neutron beam. Thus one might expect it to be considerably less than in the present polarimeter for a gas scintillator mounted transverse to the neutron beam with only that part of the sensitive volume remote from the viewing window being irradiated by the neutron beam. Such an arrangement would appear to have been employed in the polarimeters used by the Duke University group[59,60].

A further complication in regard to the amount of tail that may erroneously be included in polarization measurements arises from the use by certain workers (e.g. Behof et al.[8], Roding and Scholermann[7] and the Duke University Group[59,60],) of the difference in the time of flight of the neutrons and γ-rays between the gas scintillator and the side neutron detectors to

reject the γ-rays. Should the time that an event is recorded in a scintillator be determined by a fast discriminator set to trigger on the leading edge of the associated pulse from the scintillator, then a time jitter will be introduced of the same order as the rise time of the input pulses. In the case of the neutron detectors, usually organic scintillators, the main component of the scintillations has a decay time of a few nanoseconds, thus should these pulses be integrated before reaching the fast discriminator, they will still have a rise time of this order. However the scintillation decay time observed with the present helium gas scintillator was $\sim$ one microsecond, and hence unless considerable care is taken to avoid integration of these pulses, and/or use is made of very low fast discriminator levels, then a time jitter of the same order as the typical flight time difference ($\sim$20 ns) between the γ-rays and neutrons will easily result. Hence the apparent flight time of neutrons producing low energy helium recoils (i.e. associated with tail contributions) might easily be $\sim$ 20 ns less than that due to neutrons producing the higher energy helium recoils associated with the single scattering peak. Thus the use of a $\sim$ 20 ns resolving time in coincidences recorded between the gas scintillator and the neutron detectors (e.g. by Behof et al.[8]) might result not only in a rejection of γ-rays but also in a substantial reduction in the tail remote from the peak. This effect was simulated in the present polarimeter, albeit on a much longer time scale, by increasing the delay on the discriminator

connected to the gas scintillator amplifier by $\sim 0.5/\mu s$. The resultant recoil spectrum is shown in figure 52, along with a 'non-delayed' spectrum recorded for $\sim$ one half of the incident neutron flux employed for the 'delayed' spectrum. Clearly the tail events trigger the discriminator later in time than the peak events due to the $\sim 0.5/\mu s$ rise time of the pulses coming from the gas scintillator amplifier, thus these are hardest hit by the delay.

Should a worker fail to record the gated helium recoil spectra, and merely record the number of coincidences between the gas scintillator and the neutron detectors, then such a loss of tail resulting from the use of fast timing to reject γ-rays will reduce the error in his measurement. However should these recoil spectra be recorded, then the modified tail resulting from fast timing to reject γ-rays might lead to a false extrapolation (e.g. a horizontal line in figure 52), and a consequent introduction of error.

Returning now to the polarization measurements published by the workers listed in table 1 who employed gas scintillators as scatterers-analysers, we see that the pioneering work of Pasma[13] may easily be in error, since he employed a polarimeter similar to the present one, yet failed to record the gated helium recoil spectra or to discriminate in any way against γ-rays. Thus it is not surprising that the magnitude of the polarization which he indicates (after re-interpretation, using the analysing power of Austin et al[17], by Boersma et al.[10]) lies well

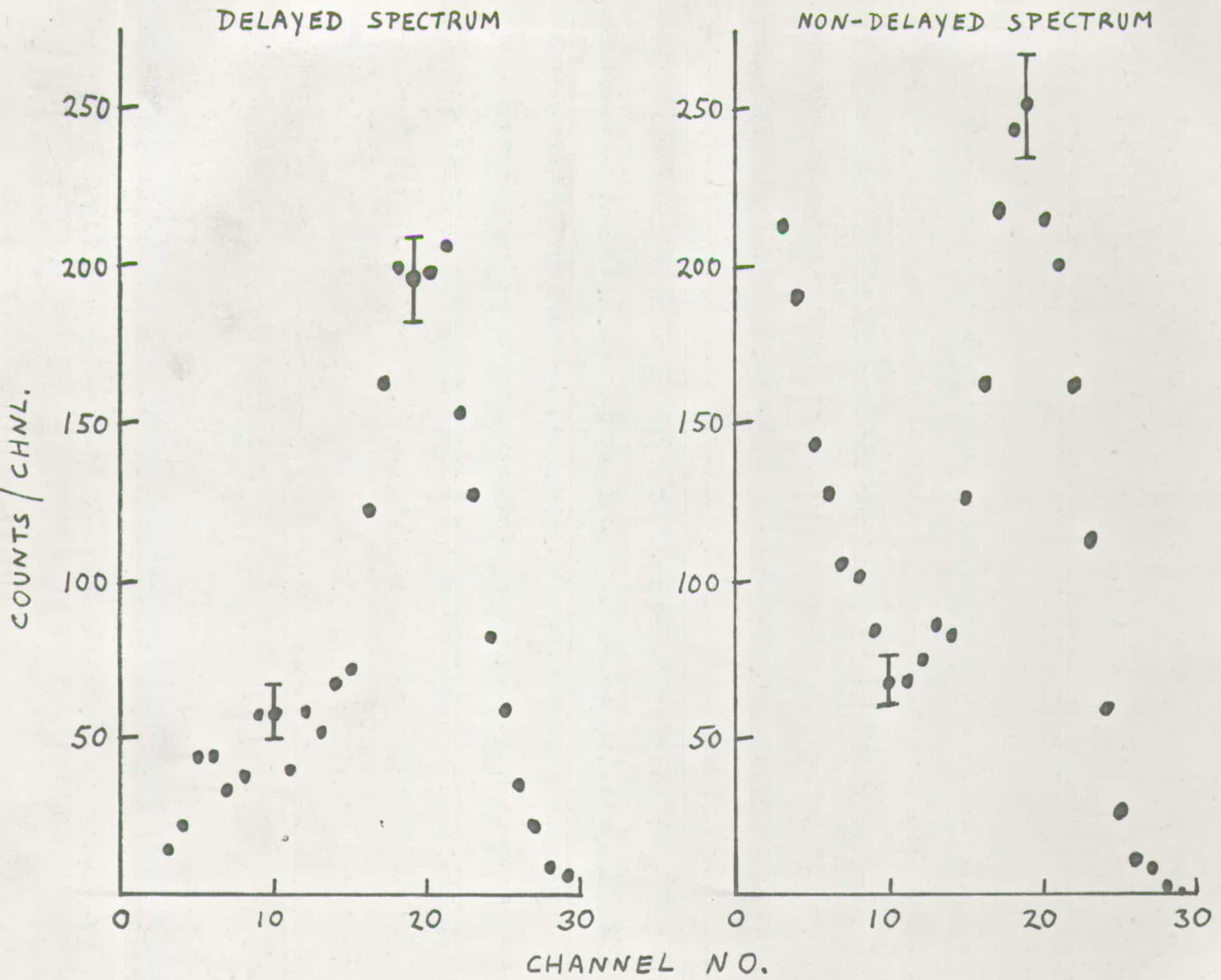

FIG. 52 EFFECT OF DELAYING THE OUTPUT FROM THE GAS SCINTILLATOR

below the present results.

Boersma et al.[10] also used a gas scintillator oriented as in the present polarimeter, and although they failed to record the helium recoil spectra associated with the coincident neutrons, they did employ a pulse shape discrimination technique to reject γ-rays. They considered that a 15% contamination of their thin target (Ti-D) neutrons arose from neutrons generated in the copper backing of the target material, and in the belief that these lower energy neutrons should have a lower polarization, they multiplied their measured asymmetries by 1.055 to account for this contamination. Further they employed what to the present author appears rather low mean analysing powers, yet in spite of this their reported polarizations are consistently less than the presently measured ones, probably due to their unwitting inclusion of unpolarized tail. Their results show a sharp drop in the magnitude of the polarization on proceeding from a mean deuteron energy of 350keV to 250keV, but this is not reflected in the present results, albeit that they were taken with a somewhat thicker target and at slightly different deuteron energies. Should the level above which pulses were accepted from the gas scintillator in the apparatus of Boersma et al.[10] have been altered between the measurements at 350keV and 250keV mean deuteron energies, then this fluctuation in their results could be attributed to the amount of unpolarized tail recorded being thereby changed.

Behof et al.[8] employed a gas scintillator mounted

tranversly to the neutron beam, but their sketch of their polarimeter suggests that little collimation of the neutron beam was employed, thus apparently the whole active volume of the gas scintillator plus its window and surrounds would appear to have been irradiated, so discarding the benefit of this orientation. They indicate that they used an electronic arrangement as described in a previous paper [61], this system using fast timing to reject γ-ray events, and also recording the gated helium recoil spectra. However no mention is made of such spectra recorded during their $^{2}H(d,n)^{3}He$ reaction measurements nor are corrections for unpolarized tails referred to. Their results were taken for thick heavy ice targets at incident deuteron energies from 60keV to 380keV, and show little variation with deuteron energy, in agreement with the present results at higher deuteron energies. Further, the magnitude of the polarization they record, although somewhat larger at the top end of their deuteron energy range than that presently reported at these deuteron energies with thin Ti-D targets is yet in fair agreement within the statistical uncertainty limits.

Roding and Scholermann[7] employed a helium gas scintillator with a cylindrical active volume viewed through windows at either end by a pair of photomultipliers. Thus it would appear to have been mounted with its cylindrical axis tranverse to the incident neutron beam, but there is no sketch of the polarimeter to show this or to show the degree of collimation employed or the mean angle through which the neutrons were scattered by the

helium into the side neutron detectors, although this would appear from the analysing powers quoted to have been a forward angle, in distinction to the ~120° angle used by Pasma[13], Boersma et al.[10], Behof et al.[8] and the present worker. Roding and Scholermann's results,[7] the most recently published of those listed in table 1, were taken with a thin (50keV stopping power) Ti-D target over the range of deuteron energies from 0.5MeV to 2MeV, and at a selection of laboratory reaction angles. Those plotted in figure 1 were taken with a laboratory reaction angle of 40°, however their results at 60° Lab. at each of the three deuteron energies plotted do not differ significantly from these 40° results, and their fitted angular distributions of polarization show a peaking between 40° and 60°, indicating that in a comparison with the present work (46° reaction angle), the results of Roding and Scholermann[7] plotted in figure 1 are if anything an underestimate of the polarization they claim to exist around a 45° laboratory reaction angle. This consistent measurement at both 40° and 60° reaction angles of considerably larger polarizations than were recorded in the present series of measurements shows clear disagreement with the present work which cannot be accounted for by the large statistical error limits on the individual measurements of Roding and Scholermann[7] shown in figure 1. At a deuteron energy of 0.5MeV the magnitude of the polarization they record is ~50% greater than that observed in the present study, however their results indicate that this value falls off with increasing

deuteron energy until at 2MeV they record a polarization of -0.14, in fair agreement with the work of Dubbeldam et al.[62] and Purser et al.[63]

Now in chapter 2 of the present work the analysing power of helium was considered, and it was seen that only small ($\sim$3%) uncertainties appeared to exist for neutrons scattered through angles around 120° (Lab.). However for forward scattering of neutrons from helium, as appears to have been employed by Roding and Scholermann,[7] there exist $\sim$ 20% variations in the analysing power at neutron energies around 3MeV, depending on the phase shift angles selected, this uncertainty tending to decrease with increasing neutron energy. Roding and Scholermann[7] employed the phase shift angles of Hoop and Barschall[15], these giving for 3 MeV neutrons an analysing power similar to the curve of Austin et al.[17] shown in figure 4a. Thus if the analysing power computed using the phase shift angles of Morgan and Walter[36], also shown in figure 4a, is the more correct representation, then it would appear that the polarization values recorded by Roding and Scholermann[7] at the lower end of their deuteron energy range require to be reduced by $\sim$20% in magnitude, so bringing them closer to the presently reported results.

No gated helium recoil spectra were reported (or apparently recorded) by Roding and Scholermann[7], the coincidences observed being recorded in the form of time of flight spectra taken between the gas scintillator and each side neutron detector. One such spectrum is shown in their paper and is

reproduced in figure 53, where the peaks attributed to neutrons and γ-rays are shown. No slow linear biases were employed to gate these spectra and so remove pulses occurring just above the fast bias levels with their accompanying large time jitter. Thus it is difficult to decide whether the (apparently sloping) background in this spectrum is due to such time jitter or is the result of random coincidences. Roding and Scholermann[7] make no comment as to how they treated this background, but should they have, for instance, believed that it was unpolarized and due to random coincidences, and hence have selected events between the channel limits shown with the background extrapolation shown (both added by the present author), then their background would amount to $\sim 30\%$ of their peak, and would introduce an overestimate of the asymmetry of this order if it in fact corresponded to real (polarized) coincidences.

Turning now to the results listed in table 1 as obtained using polarimeters not employing helium gas scintillators, we note that Levintov et al.[14] published in 1957 a series of measurements taken with long helium filled proportional counters. The magnitude of these results tends to be somewhat less than the presently recorded values, however, Levintov et al.[14] applied no corrections for neutrons detected after having been scattered in the metal surrounds of their proportional counters, merely indicating from tests with lead jackets that such a correction should be less than their statistical uncertainties. When this is considered, the agreement with the present results

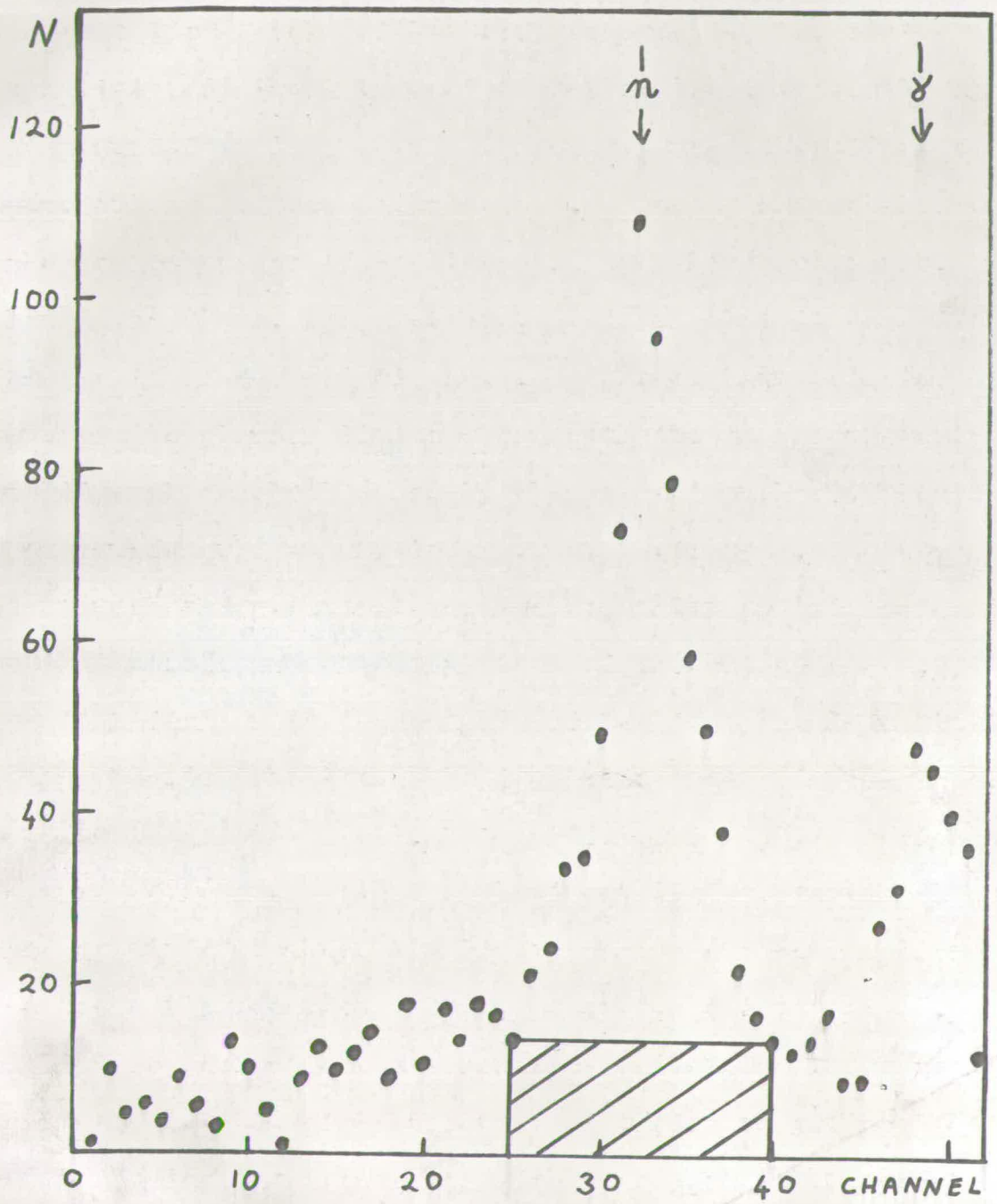

FIG. 53 TIME OF FLIGHT SPECTRUM OF RODING AND SCHOLERMANN

would appear to be fair. Similarly the single result of Mulder[9], taken with a helium filled cloud chamber is in fair agreement with the present results, although once more its magnitude lies to the low side of these. Mulder[9] provides no sketch of his apparatus and makes no mention of the possibility of having detected neutrons once scattered in the walls of his cloud chamber.

Finally, the result of Steuer et al.[11], interpreted on the basis of the carbon phase shifts of Wills et al.[18] would appear to provide better agreement with the present results than when interpreted using the phase shifts of Meier et al.[19]

CHAPTER 7.

PROPOSED FURTHER STUDIES

7.1 Polarimeter Developments

The orientation and mounting of the helium gas scintillator in the present polarimeter allowed convenient and accurately reproduceable alignment of this apparatus. However, the irradiation of the full sensitive volume of this scintillator and also its viewing window with its metal surrounds, leads to considerable tails being observed in the gated recoil spectra as described in previous chapters. These tails required extrapolation beneath their accompanying peaks to allow a correction to be applied to the measured asymmetries, albeit that in the present series of measurements this commonly amounted to no more than the statistical uncertainties in the results.

However, should more measurements of a greater fractional accuracy than the present be desired, then clearly some reduction in the tail size and/or some improvement in the gas scintillator resolution (so separating the tail from the peak) would be of value. Such improvements would also prove useful should the polarimeter be employed to study reactions producing neutrons associated with both the ground state and an excited state of the product nucleus, or to study reactions where competing three body break up would produce a background neutron spectrum (e.g. the $^{2}H(d,n)^{3}He$ reaction above a deuteron energy of 4.5MeV, the threshold of $^{2}H+^{2}H \rightarrow p + n + {}^{2}H$), since in both of these types

of reaction, the lower energy neutrons will sit upon the tail of the higher energy group, so making estimates of corrections difficult.

Considering first a reduction in the size of the tail, yet still maintaining the present orientation of the gas scintillator, then clearly a reduction is required in the volume of the solid material around the rear of the active volume of the gas scintillator. Figure 6 shows a sketch of the present gas scintillator, the considerable volume of stainless steel near the window having been left to allow both ease of manufacture and more than adequate safety margins in the containment of the helium. Other designs (e.g. that of Jenkin and Shamu[37]) show much less material around the window, and a new gas scintillator constructed to such a standard could result in a considerable tail reduction, or alternatively some of the metal could be removed from the present design. For example, the $\sim$1.25cm thick neck around the gas scintillator container which extends $\sim$1.5cm forward from the rear of the active volume was left to allow a good thickness of stainless steel into which the gas filling pipe could be conveniently tapped and gas-proof welded (after several attempts!). This neck contributes approximately one quarter of the counts in the simulated tail of figure 42, and more seriously much of this contribution lies around the valley region between the falling tail and the rising peak. Thus on repeating the calculation of section 5.5, but ignoring contributions from this neck, an improvement in the

simulated peak to valley ratio of ~50% was found to result. Although the complete removal of this neck is impracticable, it is obviously allowable to mill away much of the metal (down to a 2mm wall thickness) around most of its circumference, leaving only an island containing the gas filling pipe. Further the flanges around the viewing window into which the retaining bolts are tapped could be reduced and tapered, and some metal could be milled out between the individual bolts as in [37].
A reduction in the amount of metal contained in the mounting saddle would also prove of value.

Turning attention to the intrinsic resolution of the gas scintillator, this would appear to have been when freshly filled ~ 30% F.W.H.M. for 1.6MeVα recoils resulting from the 120° scattering of 3MeV neutrons. Donoghue et al.[40] reported that considerably improved resolution resulted on their increasing their thickness of diphenyl stilbene wavelength shifter. Thus they obtained ~10% resolution with 5MeV incident neutrons and a diphenyl stilbene layer up to ten times the thickness of the present one. Clearly there exist grounds for experimentation in this area.

Morgan and Walter[38] reported a gas scintillator whose resolution they measured by considering the upper edge in the pulse height spectrum due to irradiation by near monoenergetic neutrons, and this they performed over a range of incident neutron energies of from 0.8MeV to 7MeV. They used a diphenyl stilbene coating, different in distribution to and approximately

twice as thick as in the present gas scintillator, and reported a resolution of 11% for 1.6MeV α recoils resulting from 180° scattering of neutrons. On filling this gas scintillator, they employed a 'research' grade of xenon, whilst their grade 'A' helium they first passed through filtering material at liquid nitrogen temperatures. Babenko et al.(39) also record their use of 'especially pure' helium and xenon, and claim a 6% resolution for 5MeV α particles from a polonium source within their gas scintillator.

In the present work it was found that small amounts of contaminant entering the gas scintillator during filling due to improperly evacuated filling lines resulted in a markedly inferior light output, thus supporting the desirability of using high purity gas. The gases used in the present scintillator were supplied by the British Oxygen Company, the xenon being a grade 'x', quoted as being 99.99% (min) pure, while the helium was a grade 'A' quoted as being 99.95% (min) pure, all purity levels being w.r.t. volume. A (more expensive) cylinder of helium quoted as being 99.995% (min) pure, but also classed as grade 'A', is available from British Oxygen, and the use of this might improve the light output and resolution of the gas scintillator, and possibly reduce the rate of loss of light output.

Thus such suggested experimentation to improve the resolution of the gas scintillator might achieve worthwhile increases in the peak to valley ratios in the gated recoil spectra,

however, it should be noted that the continued reduction in this intrinsic resolution below 15% will progressively become less fruitful, as this corresponds to the energy resolution of the peak in the gated recoil spectrum due to finite geometry effects alone.

7.2 Further Measurements

The statement in chapter one to the effect that disagreements exist in published polarization measurements over the whole range at which more than one set of measurements have been recorded may be extended to cover more than the $^{2}H(d,n)^{3}He$ reaction. Indeed such is the confusion that one author[64,65] has twice published results on the $^{12}C(d,n)^{13}N$ reaction at a deuteron energy of $\sim$6.4MeV with no explanation offered as to why they differ by a factor of approximately two. Thus confirmatory (or non-confirmatory) measurements are required in many reactions.

However a Van de Graaff type accelerator is to be installed in the Physics Department at Edinburgh University, with a maximum terminal voltage of 500kV, thus it would seem attractive to use this (hopefully more reliable) machine to continue the present measurements on the $^{2}H(d,n)^{3}He$ reaction to lower deuteron energies. At such low deuteron energies various theoretical predictions of the energy dependence of the neutron polarization expected in the $^{2}H(d,n)^{3}He$ reaction exist. These include extensions of the work of Knnopinski and Teller[66] as proposed by Blin-Stoyle[21] and Rook and Goldfarb.[67] Boersma[68] has

recently criticized this model of Konopinski and Teller and has formulated an alternative description of the reaction. Briefly the work of Blin-Stoyle[21] and Rook and Goldfarb[67] predicts a neutron polarization of zero at zero deuteron energy, the former indicating that it will thereafter rise monotonically with deuteron energy, the latter allowing the possibility of a rise to a broad maximum, followed thereafter by a slow decline. Boersma[68] favours a slow monotonic increase in the polarization with deuteron energy, but predicts a non-zero polarization at zero deuteron energy.

Experimental measurements of the polarization of the neutrons emitted from the $^{2}H(d,n)^{3}He$ reaction at deuteron energies below a few hundred keV are also in considerable disagreement as may be seen from the review of Galloway.[6] These fall into two main groupings, one observing a strong narrow (10keV to 60keV wide) peaking of the polarization as a function of deuteron energy and at mean deuteron energies around 75keV, the other group reporting no such peaking. To add further to the confusion, Hansgen who formerly reported such a peak[69] has since published results[27] reported in chapter 2 which purport to explain his observations on the basis of a resonance in his carbon scatterer-analyser. However Thomas and Hoffman[70] also report a peak $\sim$10keV wide using a helium scatter-analyser, and suggest that this apparent resonance in the polarization of the neutrons emitted in the $^{2}H(d,n)^{3}He$ reaction is evidence for a level at 23.9MeV in ^{4}He. This work may be criticized in a similar

manner to the latter paper of Hansgen et al.[27], namely that resonances are reported with widths of an order of magnitude less than the spread of the deuteron and neutron energies involved.

Clearly a continuation of the present measurements, on the Van de Graaff accelerator, to lower deuteron energies would be valuable, possibly using the molecular beam to get down to incident deuteron energies below 100keV, the lowest practicable terminal voltage obtainable with this machine. Further, as reported in section 6.4, the experimental results of Boersma et al.[10] are suspect, thus there exist no good thin target polarization angular distribution measurements for the $^{2}H(d,n)^{3}He$ reaction at low deuteron energies, and such a distribution could conveniently be measured in a horizontal reaction plane using the Van de Graaff accelerator.

REFERENCES

(1) L. WOLFENSTEIN: Phys. Rev. 75 (1949) 342

(2) J. SCHWINGER: Phys. Rev. 69 (1946) 681

(3) P. HUBER and E. BAUMGARTNER: Helv. Phys. Acta 26 (1953)420

(4) R. RICAMO: Helv. Phys. Acta 26 (1953) 423
R. RICAMO: Nuovo Cimento 10 (1953) 1607

(5) W. HAEBERLI: Fast Neutron Physics 2 (Interscience, New York 1963) ch. VG

(6) R.B. GALLOWAY: Nucl. Instr. and Meth. 92 (1971) 537.
Errata: Nucl. Instr. and Meth. 95 (1971) 393

(7) P. RODING and H. SCHOLERMANN: Nucl. Phys. A125 (1969) 585

(8) A.F. BEHOF, T.H. MAY and W.I. McGARRY: Nucl. Phys. A108 (1968) 250

(9) J.P.F. MULDER: Phys. Lett. 23 (1966) 589

(10) H.J. BOERSMA, C.C. JONKER, J.G. NIJENHUIS, and P.J. VAN HALL: Nucl. Phys. 46 (1963) 660

(11) M.F. STEUER, W.P. BUCHER, and F.L. HEREFORD: Compt. Rend. Congres Intern. Phys. Nucl. (Dunod, Paris, 1959) pg.545

(12) B.M. McCORMAC, M.F. STEUER, C.D. BOND, and F.L. HEREFORD: Phys. Rev. 104 (1956) 718 and Phys. Rev. 108 (1957) 116.

(13) P.J. PASMA: Nucl. Phys. 6 (1958) 141

(14) I.I. LEVINTOV, A.V. MILLER, E.Z. TARUMOV and V.N. SHAMSHEV: Nucl. Phys. 3 (1957) 237

(15) B. HOOP and H.H. BARSCHALL: Nucl. Phys. 83 (1966) 65

(16) D.C. DODDER and J.L. GAMMEL: Phys. Rev. 88 (1952) 520
J.D. SEAGRAVE: Phys. Rev. 92 (1953) 1222

(17) S.M. AUSTIN, H.H. BARSCHALL and R.E. SHAMU: Phys. Rev. 126 (1962) 1532

(18) J.E. WILLS, J.K. BAIR, H.O. COHN and H.B. WILLARD: Phys. Rev. 109 (1958) 891

(19) R.W. MEIER, P. SCHERRER and G. TRUMPY: Helv. Phys. Acta 27 (1954) 577

REFERENCES: (Continued)

(20) I.I. LEVINTOV, A.V. MILLER and V.N. SHAMSHEV: Nucl. Phys. 3 (1957) 221

(21) R.J. BLIN-STOYLE: Proc. Phys. Soc. A64 (1951) 700, and Proc. Phys. Soc. A65 (1952) 949

(22) J. SCHWINGER: Phys. Rev. 73 (1948) 407

(23) H.H. BARSCHALL: Helv. Phys. Acta 29 (1956) 145

(24) B.E. WENZEL and M.F. STEUER: Phys. Rev. 137 (1965) 80

(25) T.G. MILLER and J.A. BIGGERSTAFF: Nucl. Phys. A124 (1969) 637

(26) G.L. MORGAN, R.W. WALTER, C.S. SOLTESZ, and T.R. DONOGHUE: Phys. Rev. 150 (1966) 836

(27) H. HANSGEN and M. NITSCHE: Nucl. Phys. A165 (1971) 401

(28) T.G. MILLER: Nucl. Instr. and Meth. 43 (1966) 338

(29) M.F. STEUER and B.E. WENZEL: Nucl. Instr. and Meth. 33 (1965) 131

(30) R.W. FINLAY: Nuclear Research with Low Energy Accelerators (Academic Press, New York, 1968) pg. 311.

(31) P. HILLMAN, G.H. STAFFORD and C. WHITEHEAD: Nuovo Cimento 4 (1956) 67

(32) J. ATKINSON and J.E. SHERWOOD: Nucl. Instr. and Meth. 34 (1965) 137

(33) T.G. MILLER: Nucl. Instr. and Meth. 40 (1966) 93

(34) H. DAVIE and R.B. GALLOWAY: Nucl. Instr. and Meth. 92 (1971) 547

(35) G.R. SATCHLER, L.W. OWEN, A.J. ELWYN, G.L. MORGAN and R.L. WALTER: Nucl. Phys. A112 (1968) 1

(36) G.L. MORGAN and R.L. WALTER: Phys. Rev. 168 (1968) 1114

(37) J.G. JENKIN and R.E. SHAMU: Nucl. Instr. and Meth. 34 (1965) 116

(38) G.L. MORGAN and R.L. WALTER: Nucl. Instr. and Meth. 58 (1968) 277

REFERENCES: (Continued)

(39) N.P. BABENKO, I.O. KONSTANTINOV and Yu. A. NEMILOV: Pribory i Techn. Eksperim. 2 (1964) 164; Instr. and Exp. Techn. 2 (1964) 432

(40) T.R. DONOGHUE, W.L. BAKER, P.L. PEACH, D.C. DeMARTINI and C.R. SOLTESZ: Phys. Rev. 173 (1968) 952

(41) P.A. TEILEX and J.R. WALDRON: Journ. Opt. Soc. Am. 45 (1955) 19

(42) R.B. OWEN: Nucleonics 17 (1959)92

(43) M.L. ROUSH, M.A. WILSON and W.F. HORNYAK: Nucl. Instr. and Meth. 31 (1964) 112

(44) K. MASOOD ALI, R.B. GALLOWAY and D.G. VASS: Nucl. Instr. and Meth. 92 (1971) 553

(45) K. PEUCKERT: Nucl. Instr. and Meth. 15 (1962) 257

(46) E. NADAV and B. KAUFMAN: Nucl. Instr. and Meth. 33 (1965) 289

(47) W. SCHWEIMER: Nucl. Instr. and Meth. 39 (1966) 343

(48) A. LANGSDORF, Jr.: Fast Neutron Physics 1 (Interscience, New York, 1960) ch. 1VE

(49) F. AJZENBERG-SELOVE and T. LAURITSEN: Nucl. Phys. 11 (1959) 1

(50) O. ASPELUND and B. GUSTAFSSON: Nucl. Instr. and Meth. 57 (1967) 197

(51) T.G. MILLER, F.B. GIBSON and G.W. MORRISON: Nucl. Instr. and Meth. 80 (1970) 325

(52) G.M. STINSON, S.M. TANG and J.T. SAMPLE: Nucl. Instr. and Meth 62 (1968) 13

(53) I.B.M. MANUAL C20-8011, Random Number Generation and Testing.

(54) J.E. BROLLEY and J.L. FOWLER: Fast Neutron Physics 1 (Interscience, New York, 1960) ch. IC

(55) R. BATCHELOR, W.B. GILBOY, J.B. PARKER and J.H. TOWLE: Nucl. Instr. and Meth. 13 (1961) 70

REFERENCES: (Continued)

(56) L.C. NORTHCLIFFE and R.F. SCHILLING: Nucl. Data A7 (1970) 233

(57) J.H. COON: Fast Neutron Physics 1 (Interscience, New York, 1960) ch. IVD

(58) E.J. WILLIAMS: Rev. Mod. Phys. 17 (1945) 217

(59) J.R. SAWERS, Jr., G.L. MORGAN, L.A. SCHALLER and R.L. WALTER: Phys. Rev. 168 (1968) 1102

(60) R.S. THOMASON, G. SPALEK and R.L. WALTER: Nucl. Phys. A155 (1970) 659

(61) G.P. LIETZ, S.F. TREVINO, A.F. BEHOF and S.E. DARDEN: Nucl. Phys. 67 (1965) 193

(62) P.S. DUBBELDAM and R.L. WALTER: Nucl. Phys. 28 (1961) 414

(63) F.O. PURSER, J.R. SAWERS and R.L. WALTER: Phys. Rev. 140 (1965) 870

(64) N.P. BABENKO, B.A. BIBICHEV, I.O. KONSTANTINOV and Yu. A. NEMILOV: Zh. Eksperim. Teor. Fiz. 44 (1963) 135; Soviet Phys. JETP 17 (1963) 92

(65) N.P. BABENKO and V.D. DOMKIN: Yad. Fiz. 12 (1970) 692; Soviet Journ. Nucl. Phys. 12 (1971) 375

(66) E.J. KONOPINSKI and E. TELLER: Phys. Rev. 73 (1948) 822

(67) R.J. ROOK and L.J.B. GOLDFARB: Nucl. Phys. 27 (1961) 79

(68) H.J. BOERSMA: Nucl. Phys. A135 (1969) 609

(69) H. HANSGEN, H. POSE, G. SCHIRMER and D. SEELIGER: Nucl. Phys. 76 (1965) 417.

(70) K. THOMAS and A. HOFMANN: Z. Physik 217 (1968) 128

ACKNOWLEDGEMENTS

I thank Professor N. Feather for the facilities provided for this experiment. During the first eighteen months of my research I held an S.R.C. Studentship, and I thank the Science Research Council for this financial assistance.

The advice, encouragement and help of Dr. R.B. Galloway, Dr. G. Bradford and Dr. D.G. Vass, throughout the present study is gratefully acknowledged. I thank Dr. G. Burns and Mr. S.T. Hayes for their advice and help in matters connected with computers.

I am grateful to Mr. H.J. Napier, Mr. G. Turnbull and Mr. D. Green, the technical staff of the H.T. Laboratory, for their willing assistance often at inconvenient hours. I thank the staff of the Electronic Workshop for their willing co-operation.

ABSTRACT OF THESIS

Name of Candidate HENRY DAVIE

Address 131 CARRICK KNOWE DRIVE, EDINBURGH

Degree DOCTOR OF PHILOSOPHY *Date* SEPTEMBER 1971

Title of Thesis FAST NEUTRON POLARIZATION STUDIES

The design, construction and operation of a fast neutron polarimeter employed to study the neutrons emitted in the $^{2}H(d,n)^{3}He$ reaction at deuteron energies less than 1MeV is described. The polarimeter employs neutron scattering from a high pressure helium gas scintillator into two liquid scintillator neutron detectors, all three scintillators being mounted on a rotatable cradle to allow an interchange of the roles of the two neutron detectors and hence eliminate instrumental error arising from differences in their detection efficiences. In selecting an appropriate scattering angle consideration is given to the speed of data collection and the accuracy to which the analysing power of helium is known. A series of electronic units designed to operate with the polarimeter is described. Considerable use is made of both linear and digital integrated circuits in these units, and a modular racking system is used for their construction. The importance of recording the helium recoil spectra associated with the neutrons detected in coincidence between the neutron detectors and the gas scintillator is emphasised, experimental measurements and Monte-Carlo type calculations being performed to account for background tails present in these spectra. Measurements of the polarization of the neutrons emitted in the $^{2}H(d,n)^{3}He$ reaction at a mean laboratory reaction angle of 46° are reported for six mean deuteron energies in the range from 300 keV to 800 keV using a Ti-D target of 100 keV stopping power. Programmes

Use other side if necessary.

to allow semi-automated data handling by a small computer are described, as are Monte-Carlo type computations of the mean analysing power of the polarimeter. The results and experimental techniques of previous workers are critically examined, and proposals are made for the possible improvement of the polarimeter and for its use in further studies.